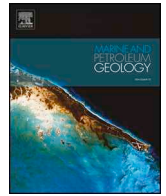




ELSEVIER

Contents lists available at ScienceDirect

## Marine and Petroleum Geology

journal homepage: [www.elsevier.com/locate/marpetgeo](http://www.elsevier.com/locate/marpetgeo)

Research paper

# From quantitative 3D seismic stratigraphy to sequence stratigraphy: Insights into the vertical and lateral variability of shelf-margin depositional systems at different stratigraphic orders

Victorien Paumard<sup>a,\*</sup>, Julien Bourget<sup>a</sup>, Tobi Payenberg<sup>b</sup>, Annette D. George<sup>a</sup>,  
R. Bruce Ainsworth<sup>b</sup>, Simon Lang<sup>a</sup>

<sup>a</sup> Centre for Energy Geoscience, School of Earth Sciences, The University of Western Australia, 35 Stirling Highway, Perth WA 6009, Australia

<sup>b</sup> Chevron Australia Pty. Ltd., 250 St Georges Terrace, Perth WA 6000, Australia

## ARTICLE INFO

## Keywords:

Quantitative 3D seismic stratigraphy  
Sequence stratigraphy  
Shelf-margin clinoforms  
Clinothems  
Shelf-edge trajectory  
Lateral and vertical variability  
Allogenic and autogenic controls  
Lower Barrow Group

## ABSTRACT

A major challenge in sequence stratigraphy is objectively identifying stratigraphic surfaces and sequences across multiple scales of observation. Identification is commonly dependent on the resolution of the data used (i.e., seismic vs. well data), its dimension (i.e., 1D vs. 2D vs. 3D) or the criteria chosen to select sequence boundaries. Through shelf-edge trajectory analysis, the clinothem (i.e., highest order seismic sequence identified on seismic data) can constitute the elementary building block of an observation-based and data-driven quantitative workflow to develop sequence stratigraphic frameworks across different orders and ranks of hierarchy. Here, we use high-quality 3D seismic data to interpret a Late Tithonian–Early Cretaceous shelf margin, the Lower Barrow Group (LBG), developed in the Northern Carnarvon Basin on the North West Shelf of Australia. Based on full-volume seismic interpretation techniques that integrate the 3D variability of the data when identifying seismic unconformities, a high-resolution seismic stratigraphic framework was built (73 interpreted clinothems with an average time duration of ~63,000 yrs). The computation of high-frequency shelf-edge trajectory angle ( $T_{se}$ ) curves on selected seismic cross-sections is used to objectively pick sequence stratigraphic surfaces based on the accommodation succession method, thereby highlighting small changes in trajectory and proposing a method reproducible by interpreters based on the same quantitative data. Within the *D. lobispinosum* interval (142.3–140.9 Ma), the definition of stratigraphic sequences and composite stratigraphic sequences through this workflow is used to discriminate the controls at high and low temporal frequency on the vertical and lateral variability (which is here quantified) of this shelf-slope-basin system. The results show that the high-frequency interplay between short-term glacio-eustasy (i.e., Milankovitch eccentricity cycles of ~100,000 yrs) and sediment supply (locus of fluvial input along the margin) impacted the three-dimensional stratigraphic architecture of the LBG. In contrast, tectonic subsidence had a significant impact on the stratigraphic architecture of the LBG within the main depocentre at lower temporal frequency by overprinting the eustatic signal and accelerating/decelerating the rates of accommodation creation. However, identification of long-term glacio-eustatic Milankovitch cycles (~400,000 yrs) outside the main depocentre, where the rates of accommodation creation due to rift-related subsidence are moderate, also suggests low-frequency eustatic control. Therefore, the vertical and lateral variability of the LBG results from variations in sediment supply and subsidence regime under local (i.e., process regime, currents), regional (i.e., tectonics) and global (i.e., eustasy, climate) forcing parameters interplaying across timescales. In contrast to standard sequence stratigraphic workflows that are based on model-dependent choices to select sequence boundaries, quantitative 3D seismic stratigraphy constitutes an improved method to interpret 3D seismic data in shelf-margin depositional systems within a sequence stratigraphic framework, which provides an observation-based and model-independent tool allowing the definition of stratigraphic sequences with results that are reproducible across multiple stratigraphers. This work highlights the need for developing new sequence stratigraphic tools and methods that integrate the 4D variability of depositional systems and moves beyond the two-dimensionality inherent to current sequence stratigraphic methods. Quantitative 3D seismic stratigraphy represents a first step towards the creation of 3D sequence stratigraphic workflows that could improve the prediction of stratigraphic patterns and facies relationships (source, reservoir, seal distribution) across shelf margins.

\* Corresponding author.

E-mail address: [victorien.paumard@uwa.edu.au](mailto:victorien.paumard@uwa.edu.au) (V. Paumard).

<https://doi.org/10.1016/j.marpetgeo.2019.07.007>

Received 7 March 2019; Received in revised form 1 July 2019; Accepted 3 July 2019

Available online 17 July 2019

0264-8172/ © 2019 Elsevier Ltd. All rights reserved.

## 1. Introduction

When conducting sequence stratigraphy analyses, there are several widely accepted methods and models that are all theoretically valid, with some being more relevant and useful to a range of specific datasets and/or geological settings than others (Catuneanu et al., 2009; Bhattacharya and Abreu, 2016). The main challenge for stratigraphers is to be flexible and adopt the approach that is the most suitable to the specific scales and methods of observation for the data available (Catuneanu, 2019). It has also been acknowledged for a long time that the strike (i.e., lateral) variability of siliciclastic depositional systems has yet to be fully integrated into sequence stratigraphic models (e.g., Martinsen and Helland-Hansen, 1995; Madof et al., 2016). For instance, the complex lateral variability of shelf–slope–basin systems is typically recognized and expressed qualitatively through different interrelated parameters (e.g., shelf-edge trajectory, process regime, stratal stacking patterns; Sanchez et al., 2012; Jones et al., 2015; Laugier and Plink-Björklund, 2016; Marin et al., 2017). However, despite the fundamental goal of understanding and predicting the distribution of sand bodies between the shelf and basin, no workflow exists to integrate along-strike variability objectively and/or quantitatively into sequence stratigraphic frameworks. This aspect is relevant to the integration of a third dimension in the workflow of sequence stratigraphic analysis (Burgess, 2016).

Important allogenic controls are recognized as playing a key role in the generation of stratal architecture by directly affecting accommodation and sediment supply: e.g., tectonics and climate in the source area (e.g., Castellort and Van Den Driessche, 2003; Armitage et al., 2011); tectonics of the sink (e.g., Martins-Neto and Catuneanu, 2010); sediment dispersal systems and associated processes (e.g., Porebski and Steel, 2006); and basin physiography (e.g., Posamentier and Allen, 1993). Important autogenic parameters may also control the stratigraphic architecture of depositional systems: e.g., hydrodynamic changes along paleoshorelines (e.g., Olariu, 2014); river channel avulsion (e.g., Mohrig et al., 2000; Slingerland and Smith, 2004); delta-lobe switching (e.g., Coleman and Gagliano, 1964; Edmonds et al., 2009); and shoreline autoretreat (e.g., Muto and Steel, 1992, 1997, 2002). The focus on controls led to the development of an integrated “sequence stratigraphic solution set” that acknowledges the role of multiple controls on the development of stratal architecture across temporal and spatial scales (e.g., Heller et al., 1993; Hampson, 2016). While understanding the controlling mechanisms on sequence development is crucial, this approach tends to divert the interpreter from the initial goal of sequence stratigraphic interpretation, which is to describe and divide strata into a chronostratigraphic framework before discussing the controls (Catuneanu and Zecchin, 2016).

Sequence stratigraphy initially focused on workflows to identify and map key stratigraphic surfaces and sequences (i.e., model-independent approach; Mitchum et al., 1977a, 1977b; Mitchum and Vail, 1977; Vail et al., 1977; Vail and Mitchum, 1977), whereas subsequent work focused on establishing conceptual sequence stratigraphic models (i.e., model-dependent approach; Posamentier et al., 1988; Posamentier and Vail, 1988; Galloway, 1989; Hunt and Tucker, 1992; Catuneanu, 2002). This resulted in competing school of thoughts in the way to interpret the stratigraphic record and determine the criteria for selecting sequence boundaries (Christie-Blick et al., 2007; Catuneanu et al., 2009; Bhattacharya and Abreu, 2016). Hence, during the last decade, new approaches have been developed in an attempt to return to the roots of sequence stratigraphy based on observation-based and data-driven (i.e., model-independent) workflows (e.g., Neal and Abreu, 2009; Neal et al., 2016). This was made possible by the development of the “trajectory analysis” concept that focuses on the dynamic evolution of strata and not only the bounding surfaces (Helland-Hansen and Martinsen, 1996; Helland-Hansen and Hampson, 2009). This concept brought a quantitative and practical method to the sequence stratigrapher's toolkit and helped standardize sequence stratigraphic workflows (Helland-Hansen, 2009).

Resolution of the temporal and spatial interpretation is directly linked to the resolution of the data and methods used. In sequence stratigraphy, this resolution is expressed through the concepts of stratigraphic orders and ranks that define the hierarchy of stratigraphic surfaces and sequences (Catuneanu, 2006). Thus, hierarchical orders reflect the cyclic changes in depositional trends and the processes that govern them at different temporal and spatial scales (Van Wagoner et al., 1990; Mitchum and Van Wagoner, 1991; Vail et al., 1991; Embry, 1995). In this paper, a sequence hierarchy based on duration (*sensu* Vail et al., 1991) was chosen to give an empirical approach to the discussion, with the caveat that rates and periodicity of

mechanisms generating the sequences may have changed through geological times, hence the validity of a hierarchy based on the duration of the sequences remains an on-going debate (e.g., Carter et al., 1991; Drummond and Wilkinson, 1996; Catuneanu, 2006; Miall, 2010, 2016; Madof et al., 2019). Each stratigraphic order mentioned in this paper refers to a specific duration: e.g., 3<sup>rd</sup> order ranges from 0.5 to 3 Myr; 4<sup>th</sup> order ranges from 0.08 to 0.5 Myr; and 5<sup>th</sup> order ranges from 0.03 to 0.08 Myr (*sensu* Vail et al., 1991).

The Barrow Group was deposited in the Northern Carnarvon Basin (NCB; North West Shelf, Australia) from the latest Tithonian to the Late Valanginian (Figs. 1a and 2). This shelf margin (~100–500 m high clinoforms) prograded during a syn-rift (Lower Barrow Group; LBG) to post-rift (Upper Barrow Group; UBG) transition, and it constitutes a natural laboratory to study the linkages between tectonics and sedimentation in extensional basins under supply-dominated conditions (Paumard et al., 2018). In the Investigator Depocentre (study area for this paper; Fig. 1), lateral variations in rates of accommodation changes and rates of sediment supply strongly impacted the 3D stratigraphic architecture of the LBG margin, as well as the distribution of shallow- and deep-marine reservoirs (Paumard, 2018). Therefore, the LBG constitutes an ideal case study to discuss the creation of a sequence stratigraphic framework in a complex setting and the various methods available to integrate the variability of shelf-margin depositional systems in sequence stratigraphic workflows.

In general, limitations on the vertical resolution of conventional seismic data make it an unsuitable tool for the identification and mapping of high-frequency (4<sup>th</sup>, 5<sup>th</sup> order) stratigraphic sequences (Catuneanu et al., 2009; Zecchin and Catuneanu, 2013). However, the increasing quality and resolution of 3D seismic surveys, combined with modern interpretation tools, now allow to define high-resolution seismic sequences (Paumard et al., 2019). This paper uses the high-resolution seismic stratigraphic framework defined by Paumard et al. (2019) in combination with a dynamic stratigraphic approach (Helland-Hansen and Hampson, 2009; Henriksen et al., 2009) in order to: (1) quantitatively characterize the evolution of the LBG shelf margin (e.g., shelf-edge trajectory angle, progradation rates) at high resolution; (2) establish a sequence stratigraphic framework at both high frequency and low frequency based on the accommodation succession method (Neal and Abreu, 2009; Neal et al., 2016) and the concepts of trajectory analysis (Helland-Hansen and Hampson, 2009); and (3) evaluate the relative importance of allogenic and autogenic controls on the generation of stratigraphic sequences at 3<sup>rd</sup>, 4<sup>th</sup> and 5<sup>th</sup> stratigraphic orders (*sensu* Vail et al., 1991). This observation-based and data-driven approach is compared to a traditional sequence stratigraphic workflow (i.e., depositional sequence model; Catuneanu et al., 2009) to consider the advantages and limitations of each approach.

Thus, the main scientific objective of this paper is to test the relevance of different sequence stratigraphic approaches to characterize the evolution of the LBG, and to discuss the significance of allogenic and autogenic controls on sequence development through time and space. This paper aims to show that quantitative 3D seismic stratigraphy can be a first step towards the establishment of a 3D sequence stratigraphic paradigm, where the integration of 4D depositional heterogeneity in siliciclastic systems could ultimately be applied to petroleum exploration, namely in the prediction of source, reservoir and seal distribution.

## 2. Regional setting

### 2.1. Geological setting and Barrow Group stratigraphy

The NCB, which covers an area of ~535,000 km<sup>2</sup> (Hocking, 1988), comprises NE-trending deep, elongate and en-echelon Mesozoic depocentres (e.g., Exmouth, Barrow, Dampier), and an extensive plateau (i.e., the Exmouth Plateau; Fig. 1). The NCB was formed through a complex tectono-stratigraphic history, including several phases of rifting and structural inversion (Audley-Charles et al., 1988; Driscoll and Karner, 1998; Borel and Stampfli, 2002; Metcalfe, 2013). Onset of Mesozoic rifting occurred during the Late Triassic and culminated during the Middle Jurassic (Bradshaw et al., 1998; Longley et al., 2002; Jitmahantakul and McClay, 2013; Marshall and Lang, 2013; Gartrell et al., 2016). Onset of a renewed phase of rifting activity took place in the latest Tithonian and continued until the final break-up between Australia and Greater India during the Valanginian (Fig. 2; Reeve et al., 2016; Paumard et al., 2018). Following break-up, the basin evolved into a carbonate-dominated passive margin perturbed by

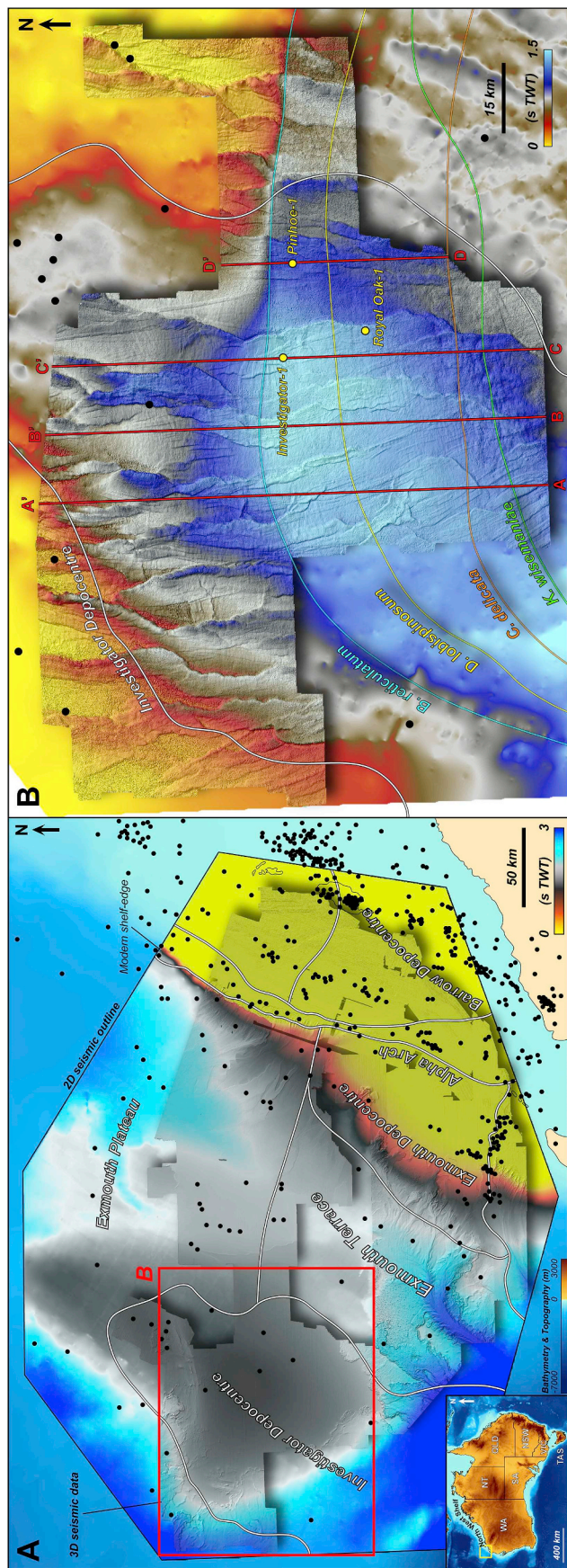


**Fig. 1.** (A) Location map of the study area. The background map, and the inset of Australia, corresponds to bathymetry (m below modern sea-level) and topography (m above modern sea-level) data (250 m resolution) obtained from the Geoscience Australia database. Map within 2D seismic outline corresponds to the seafloor horizon interpreted and gridded on 2D seismic data; and overlying high-resolution horizon (shaded outline) corresponds to the seafloor horizon interpreted on 3D seismic data. White outlines define geological provinces (i.e., Investigator Depocentre, Exmouth Terrace, Exmouth Depocentre, Barrow Depocentre) where the Lower Barrow Group (LBG) was deposited during the Late Jurassic–Early Cretaceous (Paumard et al., 2018). Note that the black dots indicate the presence of wells. (B) LBG sediment thickness map (s TWT) between BB and KV seismic unconformities (see Fig. 2), showing the location of dip-oriented seismic lines (AA' to DD'; see Figs. 3–6); used for quantitative analysis of LBG clinothems (see Fig. 2). The thickest part in blue corresponds to the Investigator Depocentre. Wells Investigator-1, Royal Oak-1 and Pinhoe-1 are used for calibration. Note the location of the final shelf edge of each 3<sup>rd</sup> seismic sequence (see Fig. 2) and the outline of the Investigator Depocentre. Data courtesy of TGS and Spectrum. (For interpretation of the references to color in this figure legend, the reader is referred to the Web version of this article.)

periods of tectonic inversion shaping the structural landscape of the NCB (Apthorpe, 1988; Barber, 1988; Hocking, 1988; Bradshaw et al., 1998; Tindale et al., 1998).

The Barrow Group was firstly described as a large progradational delta and is typically referred to in the literature as the “Barrow Delta” (e.g., Tait, 1985; Hocking, 1985; Kirk, 1985; Kopsen and McGann, 1985; Reeve et al., 2016). However, seismic analysis showed that the Barrow Group constitutes a moderately deep-water shelf margin, with a shelf-to-basin profile of a few hundred meters (Paumard et al., 2018). This shelf margin prograded

continuously from the latest Tithonian to the Late Valanginian across four distinct regional depocentres, namely the: Investigator Depocentre, Exmouth Terrace, Exmouth Depocentre and Barrow Depocentre (Figs. 1 and 2). Seven 3<sup>rd</sup> order seismic sequences of 1.2–3.1 Myr duration were identified. Their ages were constrained using dinocysts and regional correlation of their bounding seismic unconformities (Fig. 2). The LBG was deposited during the late syn-rift phase of basin extension from the Late Tithonian (base of the *P. iehiense* sequence; 148 Ma) to the Early Valanginian (top of the *E. torynum* sequence; 138.2 Ma). In contrast, the UBG was deposited during an early

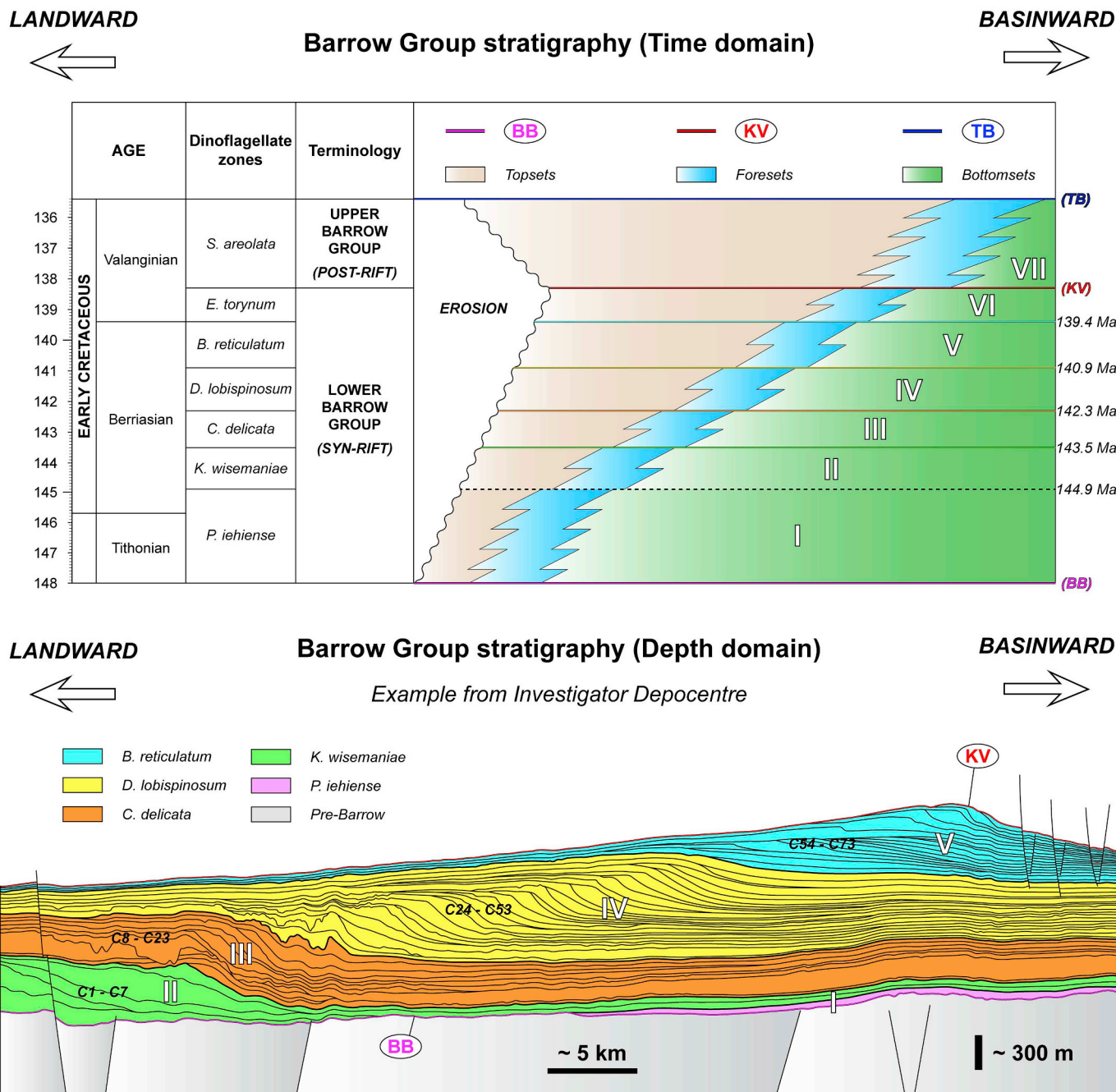


**Fig. 2.** Stratigraphic framework of the Barrow Group based on the Investigator Depocentre in time and depth domains. Late Jurassic–Early Cretaceous dinoflagellate zones, defined by Helby et al. (1987, 2004), constrain the age of seismic unconformities. Age data for each biozone and calibration with standard chronostratigraphy are based on Geoscience Australia Biostratigraphy and Regional Lithostratigraphy datapack integrated in the Time Scale Creator© software. The LBG represents a long-term regressive megasequence developed during the late syn-rift phase before break-up, followed by the Upper Barrow Group (UBG) deposited during the early post-rift phase (Paumard et al., 2018). Interpretation of shelf-edge trajectories was done for 73 clinothems from the *K. wisemaniae* to *B. reticulatum* sequences in the Investigator Depocentre, (~4.6 Myr; 144–139.4 Ma), which represents an average duration of ~63,000 years for each clinothem. A detailed quantitative analysis was conducted on the *D. lobisposum* sequence (142.3–140.9 Ma), which presents 30 clinothems developed during a period 1.4 Myr with an average duration of ~47,000 yrs each. Note that the workflow for very high resolution interpretation of the seismic stratigraphy of the LBG to identify these clinothems was described in Paumard et al. (2019).

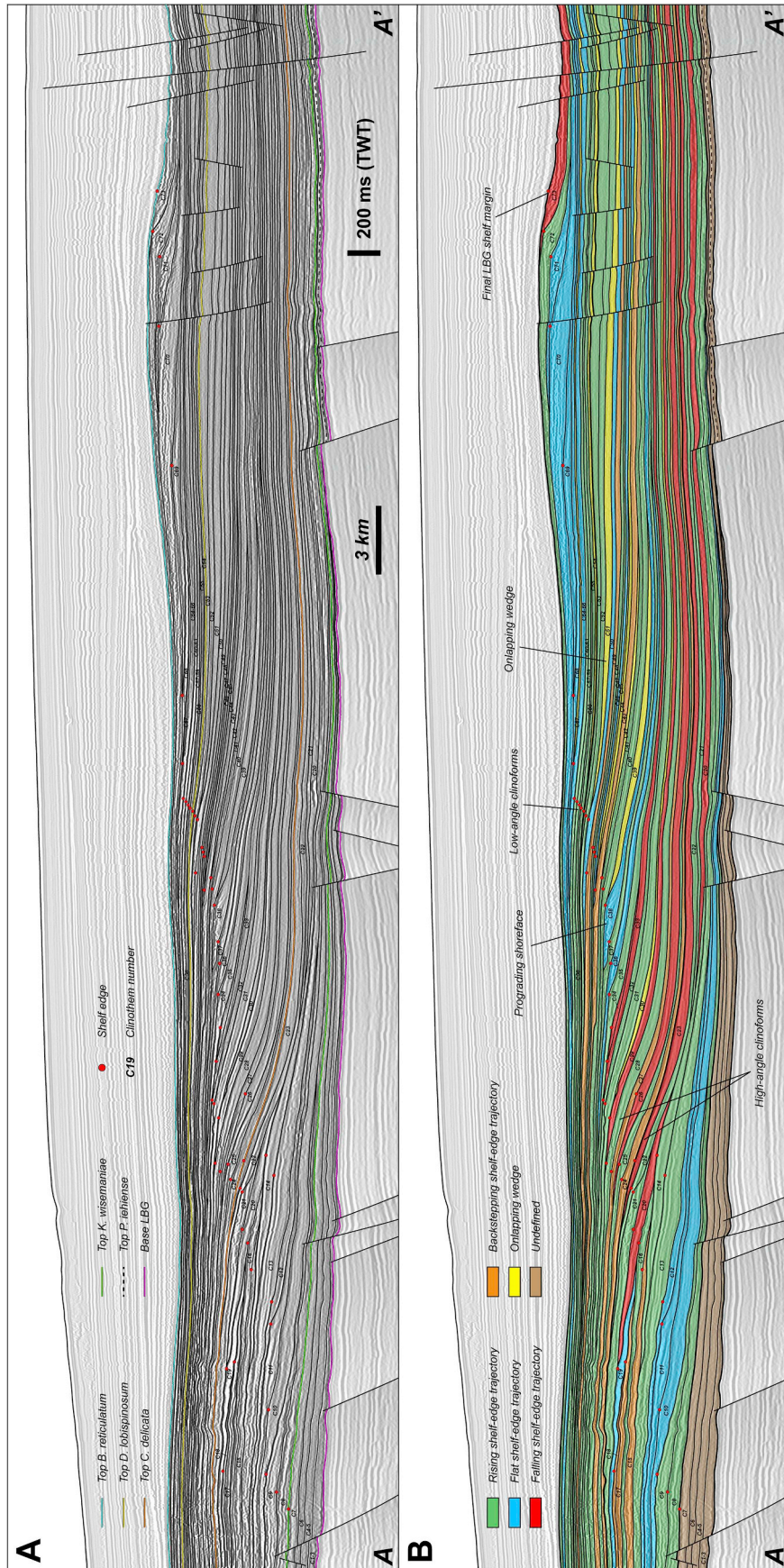


**Fig. 3.** Un-interpreted (A) and interpreted (B) regional 2D seismic profile (A-A'); see location on Fig. 1b) showing the main seismic unconformities and their downslope correlative conformities, bounding clinothems C1 to C73. Identification of the shelf edge and lower rollover point for each clinothem helped to characterize internal stratal stacking patterns and types of shelf-margin architecture (B). Note that the quantitative data extracted from the *D. lobispinosum* interval along this seismic profile is presented in Table 1. Data courtesy of TGS.

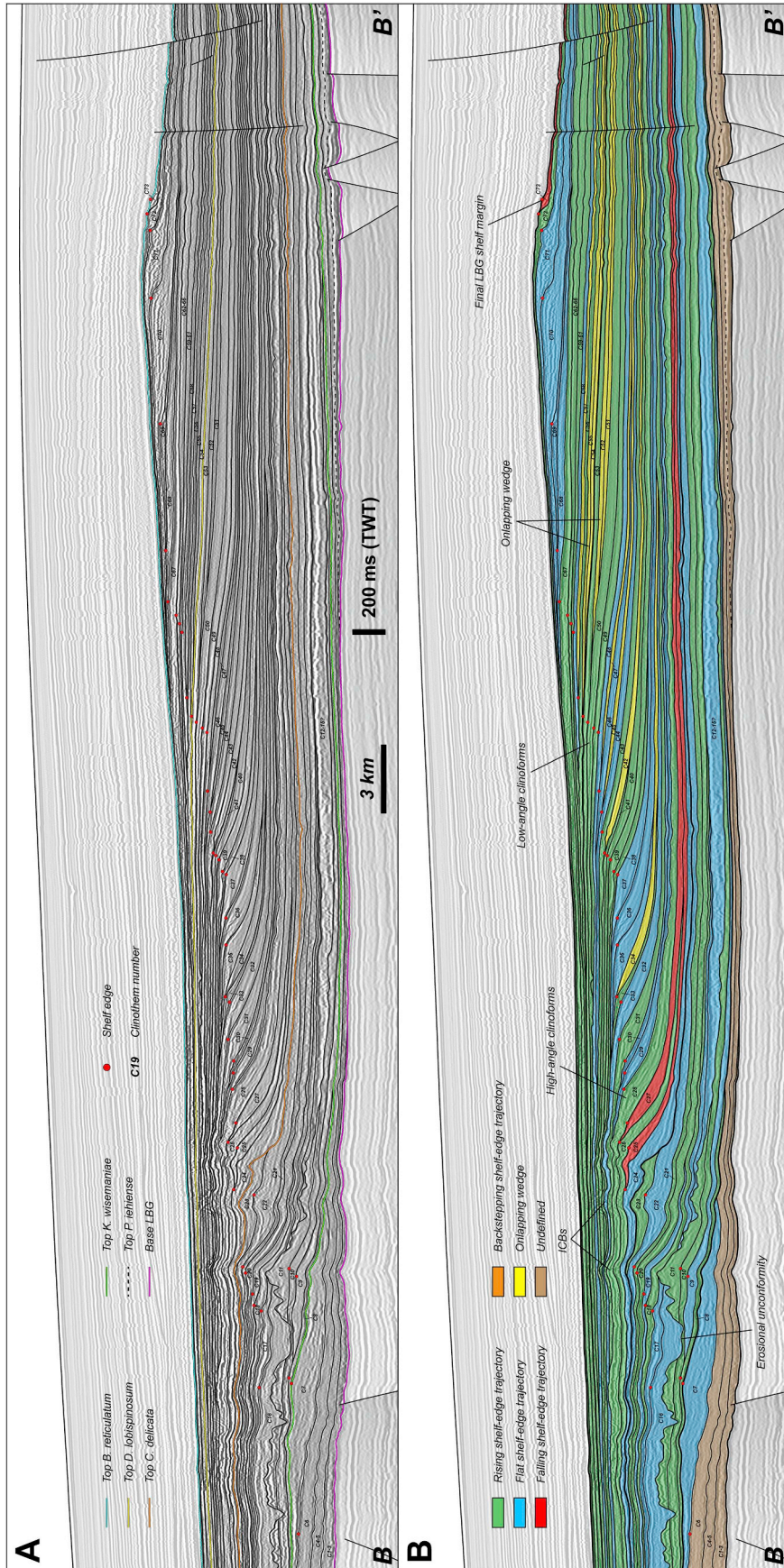
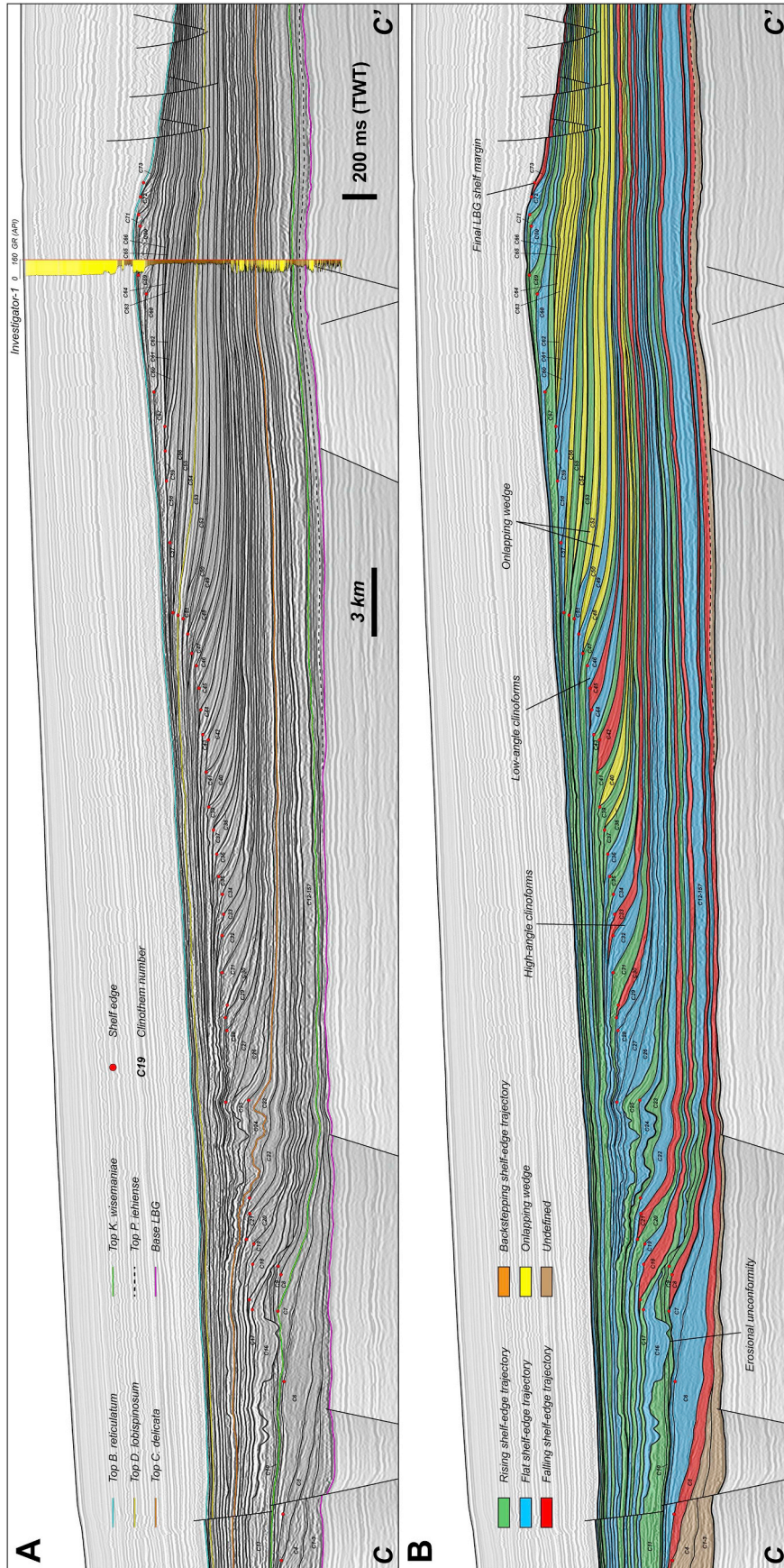


Fig. 4. Un-interpreted (A) and interpreted (B) regional 2D seismic profile (B-B’; see location on Fig. 1b) showing the main seismic unconformities and their downslope correlative conformities, bounding clinothems C1 to C73. Identification of the shelf edge and lower rollover point for each clinothem helped to characterize internal stratal stacking patterns and types of shelf-margin architecture (B). Note that the quantitative data extracted from the *D. lobispinosum* interval along this seismic profile is presented in Table 2. Data courtesy of TGS.



**Fig. 5.** Un-interpreted (A) and interpreted (B) regional 2D seismic profile (C–C’; see location on Fig. 1b) showing the main seismic unconformities and their downslope correlative conformities, bounding clinothems C1 to C73. Identification of the shelf edge and lower rollover point for each clinothem helped to characterize internal stratal stacking patterns and types of shelf-margin architecture (B). Note that the quantitative data extracted from the *D. lobispososum* interval along this seismic profile is presented in Table 3. Data courtesy of TGS.

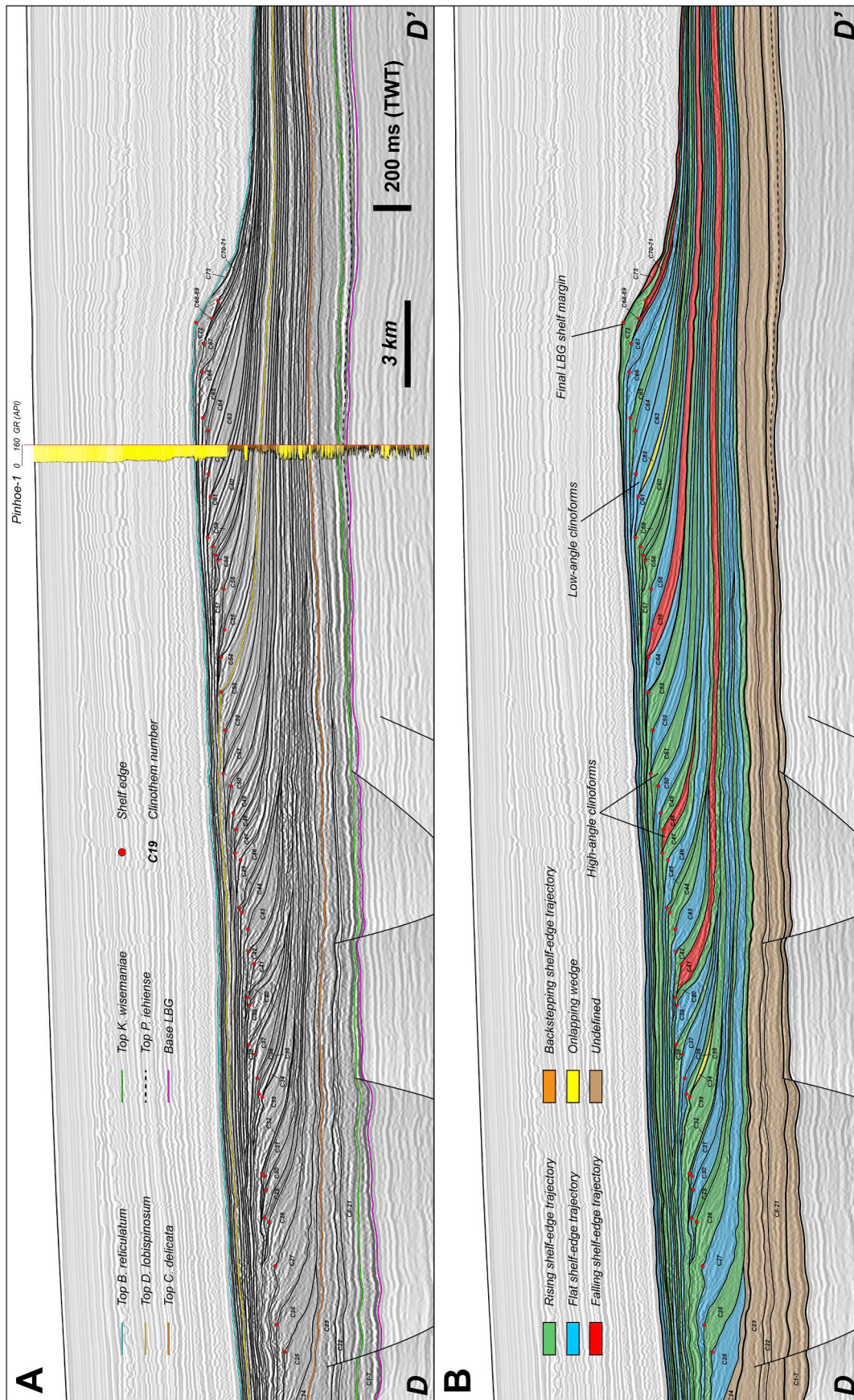


Fig. 6. Un-interpreted (A) and interpreted (B) regional 2D seismic profile (D-D’; see location on Fig. 1b) showing the main seismic unconformities and their downslope correlative conformities, bounding clinothems C1 to C73. Identification of the shelf edge and lower rollover point for each clinothem helped to characterize internal stratal stacking patterns and types of shelf-margin architecture (B). Note that the quantitative data extracted from the *D. lobispinosum* interval along this seismic profile is presented in Table 4. Data courtesy of TGS.

**Table 1**  
 Summary of the various measured and calculated parameters to describe the shelf-margin architecture in each clinothem of the *D. lobisiposum* interval (C24 to C53) along the dip-oriented seismic line A-A' (see Fig. 3 and see location on Fig. 1b). This table also includes the results and interpretations based on the  $T_{se}$  curve analysis to define stratigraphic sequences (see Fig. 15a) and composite stratigraphic sequences (see Fig. 16a). Parameters were measured in time (ms TWT) and converted in depth (m).

Clinothem number	STRATIGRAPHIC SEQUENCES										COMPOSITE STRATIGRAPHIC SEQUENCES			
	Shelf-edge trajectory type	Shelf-margin progradation $P_{se}$ (m)	Shelf-margin aggradation $A_{se}$ (ms TWT)	Shelf-margin aggradation $A_{se}$ (m)	Shelf-margin $A_{se}/P_{se}$ ratio	Shelf-edge trajectory angle $T_{se}$ (°)	Accommodation set	Stratigraphic sequence	Shelf-margin progradation $P_{se}$ (m)	Shelf-margin aggradation $A_{se}$ (m)	Shelf-margin $A_{se}/P_{se}$ ratio	Shelf-edge trajectory angle $T_{se}$ (°)	Composite accommodation set	Composite stratigraphic sequence
C24	Backstepping	-1310	100	155	-0.12	-6.75	R	S1	2520	15.5	0.01	0.35	?	?
C25	Rising	730	25	38.75	0.05	3.04	APD	(incomplete?)						
C26	Falling	3100	-115	-178.25	-0.06	-3.29	APD							
C27	Backstepping	-3270	150	232.5	-0.07	-4.07	R	S2	-220	240.25	-1.09	-47.52	R	CS1
C28	Rising	540	35	54.25	0.10	5.74	APD							(incomplete?)
C29	Falling	2510	-30	-46.5	-0.02	-1.06	APD							
C30	Onlapping wedge	0	0	0	0.00	0.00	PA	S3	2700	23.25	0.01	0.49	APD	
C31	Rising	850	35	54.25	0.06	3.65	PA							
C32	Rising	280	15	23.25	0.08	4.75	PA							
C33	Falling	1570	-35	-54.25	-0.03	-1.98	APD							
C34	Falling	1520	-25	-38.75	-0.03	-1.46	PA	S4	4440	0	0.00	0.00	APD	
C35	Rising	1750	20	31	0.02	1.01	PA							
C36	Flat	1170	5	7.75	0.01	0.38	APD							
C37	Rising	940	15	23.25	0.02	1.42	PA	S5	2860	54.25	0.02	1.09	PA	CS2
C38	Flat "SED"	1920	20	31	0.02	0.93	APD							(incomplete?)
C39	Onlapping wedge	0	0	0	0.00	0.00	APD							
C40	Rising	810	20	31	0.04	2.19	PA	S6	1190	54.25	0.05	2.61	PA	
C41	Rising	380	15	23.25	0.06	3.50	PA							
C42	Onlapping wedge	0	0	0	0.00	0.00	APD							
C43	Backstepping	-560	50	77.5	-0.14	-7.88	R	S7	-560	77.5	-0.14	-7.88	R	
C44	Onlapping wedge	0	0	0	0.00	0.00	APD							
C45	Onlapping wedge	0	0	0	0.00	0.00	APD							
C46	Flat	1360	10	15.5	0.01	0.65	PA	S8	2890	139.5	0.05	2.76	APD	
C47	Rising	270	15	23.25	0.09	4.92	PA							
C48	Rising	250	15	23.25	0.09	5.31	PA							
C49	Backstepping	-1320	40	62	-0.05	-2.69	R							
C50	Flat	2330	10	15.5	0.01	0.38	APD							
C51	Onlapping wedge	0	0	0	0.00	0.00	APD							
C52	Rising	210	20	31	0.15	8.40	PA	S9	410	54.25	0.13	7.54	?	?
C53	Rising	200	15	23.25	0.12	6.63	APD	(incomplete?)						

**Table 2**  
 Summary of the various measured and calculated parameters to describe the shelf-margin architecture in each clinothem of the *D. lobispirosus* interval (C24 to C53) along the dip-oriented seismic line B-B' (see Fig. 4 and see location on Fig. 1 b). This table also includes the results and interpretations based on the  $T_{se}$  curve analysis to define stratigraphic sequences (see Fig. 15b) and composite stratigraphic sequences (see Fig. 16b). Parameters were measured in time (ms TWT) and converted in depth (m).

Clinothem number	CLINOTHEMS											STRATIGRAPHIC SEQUENCES											COMPOSITE STRATIGRAPHIC SEQUENCES		
	Shelf-edge trajectory type	Shelf-margin progradation $P_{se}$ (m)	Shelf-margin aggradation $A_{se}$ (ms TWT)	Shelf-margin aggradation $A_{se}$ (m)	Shelf-margin aggradation ratio $A_{se}/P_{se}$	Shelf-edge trajectory angle $T_{se}$ (°)	Accommodation set	Stratigraphic sequence	Shelf-margin progradation $P_{se}$ (m)	Shelf-margin aggradation $A_{se}$ (m)	Shelf-margin aggradation ratio $A_{se}/P_{se}$	Shelf-edge trajectory angle $T_{se}$ (°)	Composite accommodation set	Composite stratigraphic sequence											
C24	N/A	N/A	N/A	N/A	N/A	N/A	N/A	N/A	N/A	N/A	N/A	N/A	N/A	N/A											
C25	Falling	2100	-30	-46.5	-0.02	-1.27	APD	2100	-46.5	-0.02	-1.27	?	?												
C26	Rising	280	50	77.5	0.28	15.47	PA	1160	-7.75	-0.01	-0.38	?	CS1 (incomplete?)												
C27	Falling	880	-55	-85.25	-0.10	-5.53	APD	2300	31	0.02	1.08	PA	PA												
C28	Rising	1650	20	7.75	0.01	0.68	APD	3150	69.75	0.02	1.27	PA	PA												
C29	Flat	650	5	7.75	0.01	0.84	PA	420	31	0.07	4.22	PA	PA												
C30	Flat	530	5	7.75	0.01	0.84	PA	420	31	0.07	4.22	PA	PA												
C31	Rising	1220	30	46.5	0.04	2.18	PA	420	31	0.07	4.22	PA	PA												
C32	Flat	1400	10	15.5	0.01	0.63	APD	420	31	0.07	4.22	PA	PA												
C33	Rising	420	20	31	0.07	4.22	PA	420	31	0.07	4.22	PA	PA												
C34	Onlapping wedge	0	0	0	0.00	0.00	APD	5280	46.5	0.01	0.50	APD	?												
C35	Flat	2240	10	15.5	0.01	0.40	PA	640	69.75	0.11	6.22	PA	CS2												
C36	Flat	1100	10	15.5	0.01	0.81	PA	480	46.5	0.10	5.53	APD	?												
C37	Flat	1940	10	15.5	0.01	0.46	APD	1750	23.25	0.01	0.76	APD	?												
C38	Rising	210	15	23.25	0.11	6.32	PA	1300	15.5	0.01	0.68	APD	?												
C39	Rising	430	30	46.5	0.11	6.17	APD	2950	116.25	0.04	2.26	PA	CS3 (incomplete?)												
C40	Rising	270	20	31	0.11	6.55	PA	260	54.25	0.21	11.79	PA	?												
C41	Rising	210	10	15.5	0.07	4.22	APD	260	54.25	0.21	11.79	PA	?												
C42	Onlapping wedge	0	0	0	0.00	0.00	APD	260	54.25	0.21	11.79	PA	?												
C43	Flat	850	10	15.5	0.02	1.04	PA	260	54.25	0.21	11.79	PA	?												
C44	Flat	900	5	7.75	0.01	0.49	APD	260	54.25	0.21	11.79	PA	?												
C45	Onlapping wedge	0	0	0	0.00	0.00	APD	260	54.25	0.21	11.79	PA	?												
C46	Flat	1300	10	15.5	0.01	0.68	PA	260	54.25	0.21	11.79	PA	?												
C47	Onlapping wedge	0	0	0	0.00	0.00	APD	260	54.25	0.21	11.79	PA	?												
C48	Flat	2350	5	7.75	0.00	0.19	PA	260	54.25	0.21	11.79	PA	?												
C49	Rising	290	25	38.75	0.13	7.61	PA	260	54.25	0.21	11.79	PA	?												
C50	Rising	310	45	69.75	0.23	12.68	PA	260	54.25	0.21	11.79	PA	?												
C51	Onlapping wedge	0	0	0	0.00	0.00	APD	260	54.25	0.21	11.79	PA	?												
C52	Onlapping wedge	0	0	0	0.00	0.00	APD	260	54.25	0.21	11.79	PA	?												
C53	Rising	260	35	54.25	0.21	11.79	PA	260	54.25	0.21	11.79	PA	?												

**Table 3**  
 Summary of the various measured and calculated parameters to describe the shelf-margin architecture in each clinothem of the *D. lobispirosum* interval (C24 to C53) along the dip-oriented seismic line C-C' (see Fig. 5 and see location on Fig. 1b). This table also includes the results and interpretations based on the  $T_{se}$  curve analysis to define stratigraphic sequences (see Fig. 15c) and composite stratigraphic sequences (see Fig. 16c). Parameters were measured in time (ms TWT) and converted in depth (m).

Clinothem number	STRATIGRAPHIC SEQUENCES										COMPOSITE STRATIGRAPHIC SEQUENCES			
	Shelf-edge trajectory type	Shelf-margin progradation $P_{se}$ (m)	Shelf-margin aggradation $A_{se}$ (ms TWT)	Shelf-margin aggradation $A_{se}$ (m)	Shelf-margin ratio $A_{se}/P_{se}$	Shelf-edge trajectory angle $T_{se}$ (°)	Accommodation set	Stratigraphic sequence	Shelf-margin progradation $P_{se}$ (m)	Shelf-margin aggradation $A_{se}$ (m)	Shelf-margin ratio $A_{se}/P_{se}$	Shelf-edge trajectory angle $T_{se}$ (°)	Composite accommodation set	Composite stratigraphic sequence
C24	N/A	N/A	N/A	N/A	N/A	N/A	N/A	N/A	N/A	N/A	N/A	N/A	N/A	N/A
C25	N/A	N/A	N/A	N/A	N/A	N/A	N/A	N/A	N/A	N/A	N/A	N/A	N/A	N/A
C26	N/A	N/A	N/A	N/A	N/A	N/A	N/A	N/A	N/A	N/A	N/A	N/A	N/A	N/A
C27	N/A	N/A	N/A	N/A	N/A	N/A	N/A	N/A	N/A	N/A	N/A	N/A	N/A	N/A
C28	Flat	3200	5	7.75	0.00	0.14	APD	SI (incomplete?)	3200	7.75	0.00	0.14	?	?
C29	Flat	890	10	15.5	0.02	1.00	PA	S2	1490	-15.5	-0.01	-0.60	?	CS1 (incomplete?)
C30	Falling	600	-20	-31	-0.05	-2.96	APD	S3	5130	46.5	0.01	0.52	PA	
C31	Rising	2370	35	54.25	0.02	1.31	PA							
C32	Flat	1570	10	15.5	0.01	0.57	APD							
C33	Falling	1190	-15	-23.25	-0.02	-1.12	APD	S4	2860	69.75	0.02	1.40	PA	
C34	Flat	750	5	7.75	0.01	0.59	PA							
C35	Rising	880	35	54.25	0.06	3.53	PA							
C36	Flat	1230	5	7.75	0.01	0.36	APD							
C37	Rising	1230	15	23.25	0.02	1.08	PA	S5	1230	23.25	0.02	1.08	APD	
C38	Onlapping wedge	0	0	0	0.00	0.00	APD	S6	980	38.75	0.04	2.26	PA	CS2
C39	Rising	980	25	38.75	0.04	2.26	PA							
C40	Onlapping wedge	0	0	0	0.00	0.00	APD							
C41	Flat	1650	10	15.5	0.01	0.54	PA	S7	3320	-15.5	0.00	-0.27	APD	
C42	Falling	1670	-20	-31	-0.02	-1.06	APD	S8	2610	46.5	0.02	1.02	PA	CS3 (incomplete?)
C43	Rising	380	30	46.5	0.12	6.98	PA							
C44	Flat	1130	10	15.5	0.01	0.79	APD							
C45	Falling	1100	-10	-15.5	-0.01	-0.81	APD	S9	1690	54.25	0.03	1.84	PA	
C46	Flat	1020	10	15.5	0.02	0.87	PA							
C47	Rising	670	25	38.75	0.06	3.31	PA							
C48	Onlapping wedge	0	0	0	0.00	0.00	APD	SI10	920	15.5	0.02	0.97	APD	
C49	Flat	920	10	15.5	0.02	0.97	PA							
C50	Onlapping wedge	0	0	0	0.00	0.00	APD	SI11	1820	7.75	0.00	0.24	APD	
C51	Flat	1820	5	7.75	0.00	0.24	PA							
C52	Onlapping wedge	0	0	0	0.00	0.00	APD	SI12 (incomplete?)	670	77.5	0.12	6.60	?	?
C53	Rising	670	50	77.5	0.12	6.60	PA							

**Table 4**  
 Summary of the various measured and calculated parameters to describe the shelf-margin architecture in each clinothem of the *D. lobisinosum* interval (C24 to C53) along the dip-oriented seismic line D-D' (see Fig. 6 and see location on Fig. 1 b). This table also includes the results and interpretations based on the  $T_{se}$  curve analysis to define stratigraphic sequences (see Fig. 15d) and composite stratigraphic sequences (see Fig. 16d). Parameters were measured in time (ms TWT) and converted in depth (m).

Clinothem number	CLINOTHEMS										STRATIGRAPHIC SEQUENCES										COMPOSITE STRATIGRAPHIC SEQUENCES		
	Shelf-edge trajectory type	Shelf-margin progradation $P_{se}$ (m)	Shelf-margin aggradation $A_{se}$ (ms TWT)	Shelf-margin aggradation $A_{se}$ (m)	Shelf-margin aggradation ratio $A_{se}/P_{se}$	Shelf-edge trajectory angle $T_{se}$ (°)	Accommodation set	Stratigraphic sequence	Shelf-margin progradation $P_{se}$ (m)	Shelf-margin aggradation $A_{se}$ (m)	Shelf-margin aggradation ratio $A_{se}/P_{se}$	Shelf-edge trajectory angle $T_{se}$ (°)	Composite accommodation set	Composite accommodation set	Composite stratigraphic sequence								
C24	N/A	N/A	N/A	N/A	N/A	N/A	N/A	N/A	N/A	N/A	N/A	N/A	N/A	N/A	N/A								
C25	N/A	N/A	N/A	N/A	N/A	N/A	N/A	N/A	N/A	N/A	N/A	N/A	N/A	N/A	N/A								
C26	Rising	1000	40	62	0.06	3.55	PA	S1	2980	85.25	1.64	?	?	?									
C27	Flat	1980	15	23.25	0.01	0.67	APD	(incomplete?)															
C28	Rising	1580	40	62	0.04	2.25	PA	S2	3430	131.75	2.20	?	?	CSI									
C29	Rising	170	30	46.5	0.27	15.30	PA							(incomplete?)									
C30	Flat	1010	10	15.5	0.02	0.88	APD																
C31	Flat	670	5	7.75	0.01	0.66	APD																
C32	Rising	135	10	15.5	0.11	6.55	PA	S3	2765	62	1.28	APD	APD										
C33	Rising	2630	30	46.5	0.02	1.01	APD																
C34	Overlapping wedge	0	0	0	0.00	0.00	APD																
C35	Rising	170	15	23.25	0.14	7.79	PA	S4	770	31	2.31	PA	PA	CS2									
C36	Flat	600	5	7.75	0.01	0.74	APD																
C37	Flat	1050	10	15.5	0.01	0.85	PA	S5	2830	83.7	1.69	APD	APD										
C38	Rising	450	40	62	0.14	7.84	PA																
C39	Flat	1330	4	6.2	0.00	0.27	APD																
C40	Rising	360	5	7.75	0.02	1.23	PA	S6	1500	-38.75	-0.03	APD	APD										
C41	Falling	1140	-30	-46.5	-0.04	-2.34	APD																
C42	Rising	450	35	54.25	0.12	6.87	PA	S7	1330	62	2.67	PA	PA	CS3									
C43	Flat	880	5	7.75	0.01	0.50	APD																
C44	Rising	620	30	46.5	0.08	4.29	PA	S8	2640	74.4	1.61	APD	APD										
C45	Rising	200	15	23.25	0.12	6.63	PA																
C46	Flat	1820	3	4.65	0.00	0.15	APD																
C47	Rising	630	25	38.75	0.06	3.52	PA	S9	1360	0	0.00	APD	APD										
C48	Falling	730	-25	-38.75	-0.05	-3.04	APD																
C49	Rising	580	30	46.5	0.08	4.58	PA	S10	1570	62	2.26	PA	PA	CS4									
C50	Flat	990	10	15.5	0.02	0.90	APD							(incomplete?)									
C51	Rising	660	40	62	0.09	5.37	PA	S11	1880	65.1	1.98	APD	APD										
C52	Flat	1220	2	3.1	0.00	0.15	APD							?									
C53	Rising	1370	30	46.5	0.03	1.94	PA	S12 (incomplete?)	1370	46.5	1.94	?	?	?									

post-rift phase in the Middle Valanginian (*S. areolata* sequence; 138.2–135.4 Ma), following continental break-up and the uplift of the Nin-galoo Arch that acted as a local source of sediment (Fig. 2; Arditto, 1993; Tindale et al., 1998; Paumard et al., 2018).

## 2.2. 3<sup>rd</sup> order controls on the shelf-margin architecture of the Lower Barrow Group

Paumard et al. (2018) discussed the controls affecting the stratigraphic evolution of the LBG through time and space and proposed a refined chronology of rifting events in the region. The early stages of the LBG (i.e., *P. iehiense* to *K. wisemaniae* intervals) represent periods of relative tectonic quiescence where the shelf margins were associated with regionally low subsidence rates. This period is distinguished from the rest of the LBG deposition and corresponds to the late syn-rift stage I (148–143.5 Ma). A regional pulse of subsidence at the beginning of the *C. delicata* interval was the direct result of a pulse of extension (late syn-rift stage II; 143.5–138.2 Ma), followed by a pulse of sediment supply during the *D. lobispinosum* interval. Stage II ends with the final break-up between Australia and Greater India at the end of the *E. torynum* interval (i.e., KV unconformity; Fig. 2). The successive shelf margins that developed during this syn-rift period were overall supply-dominated (i.e. conditions that usually promote sediment delivery to the slopes and basins; Carvajal et al., 2009). The complex interplay between lateral shifts in sediment supply and pulses of subsidence across the four depocentres resulted in a significant along-strike variability in shelf-margin architecture and sediment partitioning trends (Paumard et al., 2018).

## 3. Data and methods

Both the Mary Rose 3D seismic survey (provided by TGS) and the Sovereign 3D seismic survey (provided by Geoscience Australia) were used for this study (Fig. 1b). These surveys have a vertical sampling interval of 4 ms and a bin spacing of 25 X 18.75 m. With an average velocity of 3100 m/s and a dominant frequency of about 32 Hz, the maximum vertical resolution of the seismic data in the LBG interval is approximately 25 m. Seismic data were calibrated by three wells (Investigator-1, Royal Oak-1, Pinhoe-1) using velocity (check-shot) survey data available in well completion reports. For each well, publicly available well logs and biostratigraphic data were included to provide stratigraphic and lithological controls on seismic interpretation.

Seismic interpretation was conducted using Paleoscan™ and the workflow for high-resolution interpretation of the seismic stratigraphy of the LBG has been described by Paumard et al. (2019). This workflow is based on the use of full-volume seismic interpretation tools in combination with a standard seismic stratigraphic approach, where reflection terminations are used to identify seismic unconformities (*sensu* Mitchum et al., 1977a, 1977b). Within the LBG interval, this workflow was used to identify 74 key regional seismic unconformities bounding 73 seismic sequences, here defined as clinothems and referred as C1 to C73 (oldest to youngest; Fig. 2). In this paper, several seismic attributes were calculated (over a time window of ~12 ms TWT) along the multiple horizons extracted. The attributes presented in this paper include the: (1) *similarity* attribute; and (2) *spectral decomposition* attribute. Spectral decomposition maps presented here are color-blended from frequency maps of 10 Hz (R channel), 40 Hz (G channel) and 70 Hz (B channel).

Analysis of the seismic sequences from the LBG is complemented by quantitative analysis conducted on clinothems C24 to C53 within the *D. lobispinosum* interval (Fig. 2), where clinof orm geometries were described and measured on four dip-oriented sections at different along-strike locations (Figs. 1b and 3–6). Measurements were taken on the upper boundary of each clinothem (i.e., upper seismic unconformity). Shelf edges are defined as the point where the gradient of the shelf rapidly increase basinward (Wear et al., 1974; Southard and Stanley, 1976; Steel and Olsen, 2002). Clinof orm heights (i.e., slope relief) and length were also measured where the upper (i.e., shelf edge) and lower rollover points of the clinof orms (*sensu* Patruno et al., 2015) were used as reference points. Within each clinothem, the lateral and vertical displacements of the shelf edge between the bounding clinof orms were measured, representing the shelf-margin progradation ( $P_{se}$ ) and shelf-margin aggradation ( $A_{se}$ ), respectively. We calculated the apparent shelf-edge trajectory angle ( $T_{se}$ ), as well as the aggradation/progradation ratio ( $A_{se}/P_{se}$ ), to help characterize the dynamic evolution of the LBG through time and space. All values were first measured in time and

converted to depth using an average velocity of 3100 m/s. Measurements were not corrected for compaction. All measured and calculated parameters are presented in Tables 1–4.

In this paper, the shelf-edge trajectory angles  $T_{se}$  (Table 5) and shelf-margin progradation rates  $R_p$  (Table 6) of clinothems C24 to C53 are compared between several cross-sections extracted from the 3D seismic surveys in order to quantify the vertical and lateral variability in stratal architecture within the *D. lobispinosum* interval (Fig. 2).

## 4. Results from quantitative seismic stratigraphy

### 4.1. 3<sup>rd</sup> to 5<sup>th</sup> order seismic stratigraphy of the LBG

Six 3<sup>rd</sup> order seismic sequences within the LBG were identified (Fig. 2; Paumard et al., 2018). Progradation of the LBG began in the Exmouth Depocentre with deposition of the *P. iehiense* (148–144.9 Ma) interval (Fig. 1a). From the Exmouth Depocentre, the LBG shelf margin continuously prograded towards the north (i.e., *K. wisemaniae* interval; 144.9–143.5 Ma) and finally reached the Investigator Depocentre (Figs. 3–6 and 7a). The shelf margin then continued to prograde and aggrade during the *C. delicata* (143.5–142.3 Ma; Fig. 7b), *D. lobispinosum* (142.3–140.9 Ma; Fig. 7c) and *B. reticulatum* (140.9–139.4 Ma; Fig. 7d) intervals (Figs. 3–6). The *E. torynum* interval is not developed in the Investigator Depocentre because the shelf margin retrograded towards the Exmouth Terrace (Fig. 1b). Thus, the top of the *B. reticulatum* interval corresponds to the KV seismic unconformity (regional break-up unconformity; Figs. 2–6).

Among the 73 seismic sequences or (clinothems) identified, four main types of shelf-margin architecture were recognized: (1) *falling* (progradational pattern); (2) *flat* (progradational pattern); (3) *rising* (progradational and aggradational pattern); and (4) *backstepping* (retrogradational pattern) *shelf-edge trajectories* (Figs. 3–6). Within the *D. lobispinosum* interval (C24–C53; Fig. 2), this interpretation is complemented by the analysis of the shelf-edge trajectory angles  $T_{se}$ , and shelf-margin progradation/aggradation ratio ( $P_{se}/A_{se}$  ratio) parameters, thus allowing quantification of the range of geometric values associated with each type of shelf-edge trajectory (Figs. 3–6 and Tables 1–4): (1) *falling* ( $T_{se} < 0^\circ$  and  $P_{se}/A_{se} < 0$ ); (2) *flat* ( $0^\circ < T_{se} < 1^\circ$  and  $P_{se}/A_{se} > 55$ ); (3) *rising* ( $T_{se} > 1^\circ$  and  $0 < P_{se}/A_{se} < 55$ ) and (4) *backstepping* ( $T_{se} < 0^\circ$  and  $P_{se}/A_{se} < 0$ ) *shelf-edge trajectories*. Based on biostratigraphic data, each clinothem represents an estimate average time interval of ~63,000 yrs. Therefore, these clinothems represent a 5<sup>th</sup> stratigraphic order (*sensu* Vail et al., 1991).

### 4.2. Three-dimensional architecture and evolution of the margin

Calculation of isopach maps of the *K. wisemaniae* to *B. reticulatum* intervals shows how depocentres (at 3<sup>rd</sup> order) of the LBG margin have migrated in the study area (Fig. 7). The data show that the gross depositional history of the LBG during the Early Cretaceous consists of a four-step depocentre evolution. Overall, the LBG shelf margin migrated from south to north but lateral (i.e., along-strike) thickness variations are observed (Fig. 7). Similarly, isopach maps were calculated for each clinothem to show the depositional evolution of the margin at higher frequency (e.g., Figs. 8 and 9).

#### 4.2.1. *K. wisemaniae* interval (C1 to C7)

Deposition of the *K. wisemaniae* seismic sequence ranged from 144.9 to 143.5 Ma (Fig. 2). However, only the latest progradational stages of this sequence are observed in the study area (Figs. 3–6 and 7a). Thus, the interval of deposition was estimated to be between ~144 and 143.5 Ma in the study area (Figs. 3–6). During this period, the locus of sedimentation was in the eastern part of the shelf (Fig. 7a). Sediment thickness reaches 400 ms TWT (~620 m) in the east (Fig. 5), with a maximum thickness of about 200 ms TWT (~310 m) in the west (Fig. 3). Down-dip, the thickness of the sequence locally increases up to 150 ms TWT (230 m) in the distal parts (Figs. 3–6 and 7a). This observation can be linked to active syn-rift tectonics at that time (Fig. 2), where paleotopography and faulting locally increased accommodation space (e.g., Figs. 4 and 7a). In the shelf area, the uppermost clinof orm (i.e., top of clinothem C7) corresponds to a toplap surface of underlying reflections landward and a downlap surface of overlying reflections basinward (Figs. 3–6).

Overall, the clinothems associated with the *K. wisemaniae* interval

**Table 5**  
 Shelf-edge trajectory angles  $T_{se}$  calculated in each clinothem of the *D. lobispinosum* interval (C24 to C53) along the four dip-oriented seismic lines A-A' to D-D' (see Figs. 3–6 and see location on Fig. 1b). This table also includes the calculation of a standard deviation parameter  $D_t$  showing the lateral variability of the  $T_{se}$  values in a single clinothem.  $D_t$  values were plotted in Fig. 10a. Note that the parameters used for the calculation of  $T_{se}$  are presented in Tables 1–4

Clinothem number	Shelf-edge trajectory angle $T_{se}$ (°) along seismic line AA' (Fig. 3)	Shelf-edge trajectory angle $T_{se}$ (°) along seismic line BB' (Fig. 4)	Shelf-edge trajectory angle $T_{se}$ (°) along seismic line CC' (Fig. 5)	Shelf-edge trajectory angle $T_{se}$ (°) along seismic line DD' (Fig. 6)	Standard deviation of shelf-edge trajectory angle $D_t$ (°)
C24	-6.75	N/A	N/A	N/A	N/A
C25	3.04	-1.27	N/A	N/A	3.05
C26	-3.29	15.47	N/A	3.55	9.50
C27	-4.07	-5.53	N/A	0.67	3.24
C28	5.74	1.08	0.14	2.25	2.45
C29	-1.06	0.68	1.00	15.30	7.60
C30	0.00	0.84	-2.96	0.88	1.81
C31	3.65	2.18	1.31	0.66	1.29
C32	4.75	0.63	0.57	6.55	3.01
C33	-1.98	4.22	-1.12	1.01	2.76
C34	-1.46	0.00	0.59	0.00	0.87
C35	1.01	0.40	3.53	7.79	3.36
C36	0.38	0.81	0.36	0.74	0.23
C37	1.42	0.46	1.08	0.85	0.40
C38	0.93	6.32	0.00	7.84	3.89
C39	0.00	6.17	2.26	0.27	2.85
C40	2.19	6.55	0.00	1.23	2.85
C41	3.50	4.22	0.54	-2.34	3.00
C42	0.00	0.00	-1.06	6.87	3.65
C43	-7.88	1.04	6.98	0.50	6.11
C44	0.00	0.49	0.79	4.29	1.96
C45	0.00	0.00	-0.81	6.63	3.47
C46	0.65	0.68	0.87	0.15	0.31
C47	4.92	0.00	3.31	3.52	2.09
C48	5.31	0.19	0.00	-3.04	3.46
C49	-2.69	7.61	0.97	4.58	4.46
C50	0.38	12.68	0.00	0.90	6.14
C51	0.00	0.00	0.24	5.37	2.65
C52	8.40	0.00	0.00	0.15	4.17
C53	6.63	11.79	6.60	1.94	4.02

**Table 6**  
 Shelf-margin progradation rate  $R_p$  calculated in each clinothem of the *D. lobispirosus* interval (C24 to C53) along the four dip-oriented seismic lines A-A' to D-D' (see Figs. 3–6 and see location on Fig. 1b). This table also includes the calculation of a standard deviation parameter  $D_p$  showing the lateral variability of the  $R_p$  values in a single clinothem.  $D_p$  values were plotted in Fig. 10b. Note that the parameters used for the calculation of  $R_p$  are presented in Tables 1–4

Clinothem number	Shelf-margin progradation rate $R_p$ (km/Myr) along seismic line AA' (Fig. 3)	Shelf-margin progradation rate $R_p$ (km/Myr) along seismic line BB' (Fig. 4)	Shelf-margin progradation rate $R_p$ (km/Myr) along seismic line CC' (Fig. 5)	Shelf-margin progradation rate $R_p$ (km/Myr) along seismic line DD' (Fig. 6)	Standard deviation of shelf-margin progradation rates $D_p$ (°)
C24	-27.87	N/A	N/A	N/A	N/A
C25	15.53	44.68	N/A	N/A	20.61
C26	65.96	5.96	N/A	21.28	31.17
C27	-69.57	18.72	N/A	42.13	58.91
C28	11.49	35.11	68.09	33.62	23.32
C29	53.40	13.83	18.94	3.62	21.60
C30	0.00	11.28	12.77	21.49	8.82
C31	18.09	25.96	50.43	14.26	16.24
C32	5.96	29.79	33.40	2.87	15.81
C33	33.40	8.94	25.32	55.96	19.56
C34	32.34	0.00	15.96	0.00	15.46
C35	37.23	47.66	18.72	3.62	19.55
C36	24.89	23.40	26.17	12.77	6.13
C37	20.00	41.28	26.17	22.34	9.56
C38	40.85	4.47	0.00	9.57	18.50
C39	0.00	9.15	20.85	28.30	12.51
C40	17.23	5.74	0.00	7.66	7.16
C41	8.09	4.47	35.11	24.26	14.30
C42	0.00	0.00	35.53	9.57	16.79
C43	-11.91	18.09	8.09	18.72	14.30
C44	0.00	19.15	24.04	13.19	10.39
C45	0.00	0.00	23.40	4.26	11.17
C46	28.94	27.66	21.70	38.72	7.06
C47	5.74	0.00	14.26	13.40	6.76
C48	5.32	50.00	0.00	15.53	22.47
C49	-28.09	6.17	19.57	12.34	21.11
C50	49.57	6.60	0.00	21.06	22.01
C51	0.00	N/A	38.72	14.04	19.60
C52	4.47	0.00	0.00	25.96	12.41
C53	4.26	5.53	14.26	29.15	11.46

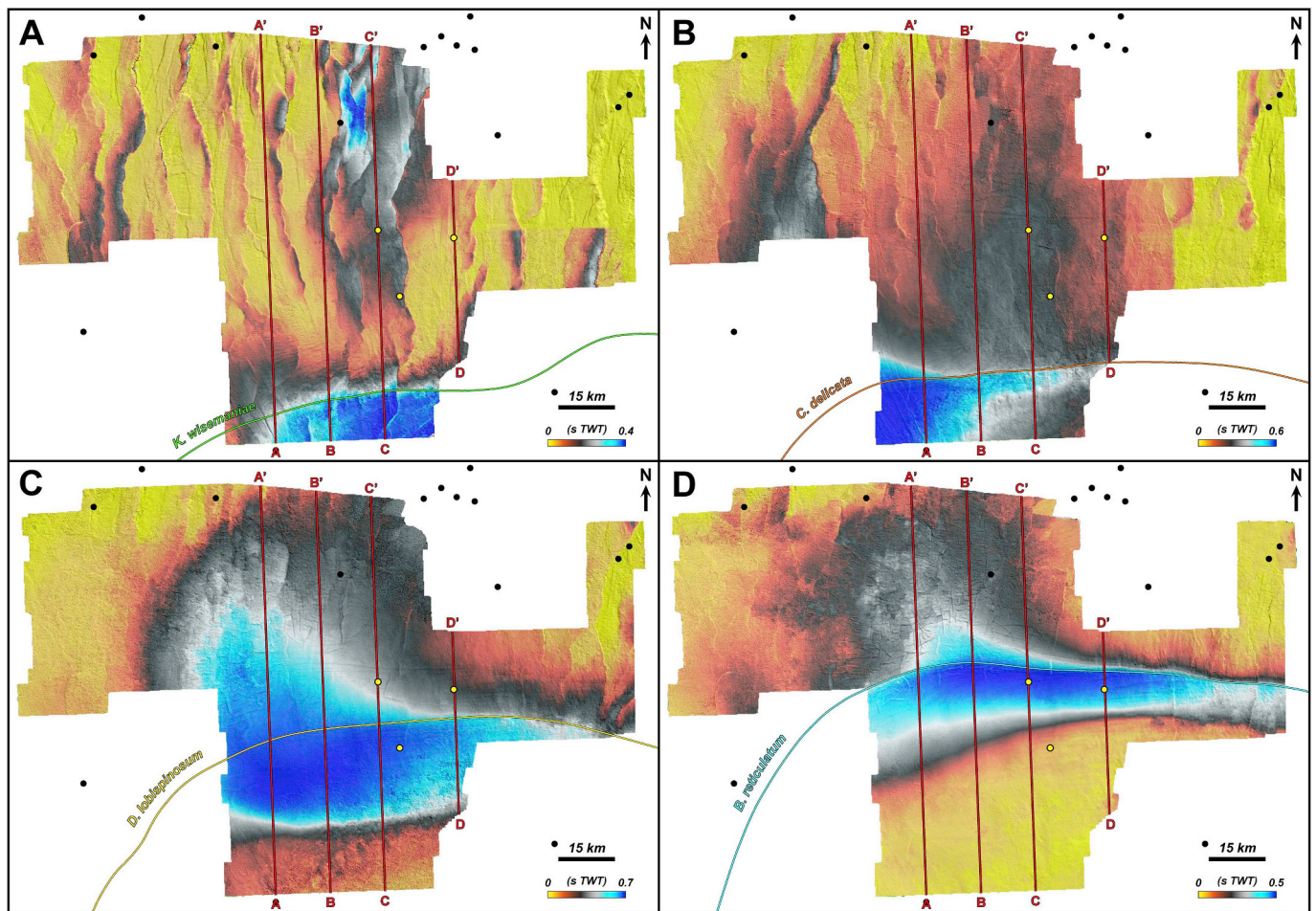


Fig. 7. Sediment thickness maps (s TWT) of the *K. wisemaniae* interval (A), *C. delicata* interval (B), *D. lobispinosum* interval (C) and *B. reticulatum* interval (D). Note location of the final shelf edge of each 3rd order seismic sequence (i.e., the last clinoform associated with the seismic unconformity; see Figs. 3–6). Data courtesy of TGS.

presents a *flat shelf-edge trajectory* associated with high-angle shelf-margin clinoforms and a strong progradational pattern (e.g., C5–C7; Fig. 5). The lowermost clinothems are “undefined”, because the corresponding shelf edges are not visible and what appear on the cross-section correspond to the distal component (i.e., bottomsets) of the clinoforms (Figs. 3–6).

#### 4.2.2. *C. delicata* interval (C8 to C23)

The *C. delicata* seismic sequence (143.5–142.3 Ma) represents a significant change in the stratigraphic architecture of the LBG. The locus of sedimentation is in the western part of the study area. Within the topsets, maximum sediment thickness reaches 600 ms TWT (~930 m) compared to 310 ms TWT (~480 m) in the east (Figs. 3, 5 and 7b). Thicker bottomsets are also accumulated in the west with a maximum sediment thickness of 290 ms TWT (~450 m; Figs. 3–6 and 7b). An erosional unconformity marks the top of the *C. delicata* interval (i.e., top of the clinothem C23) in the east part of the study area, associated with erosional truncation below and downlap reflection terminations above (e.g., Figs. 4 and 5). Toward the west, this horizon corresponds to a toplap surface locally associated with erosional truncation (Fig. 3). During this period, the shelf margin prograded over a distance of about 7 km (Figs. 3–6 and 7b).

Overall, the clinothems of this seismic sequence present a more aggradational pattern compared to the previous sequence (Figs. 3–5). However, the associated shelf-margin architecture varies along strike (Figs. 3–5). To the west, where the sequence is the thickest (Fig. 7b), the clinoforms are mostly low-angle, whereas they show progressively higher angles towards the east and are organized in all shelf-margin stacking patterns, except the *backstepping shelf-edge trajectory* (e.g., Figs. 4 and 5). A major erosional seismic unconformity is also observed at the base of C16 (Figs. 4 and 5). This surface incised up to 200 ms TWT (~310 m) of the underlying clinothems, almost completely eroding clinothems C12 to C15 (Figs. 4 and 5).

#### 4.2.3. *D. lobispinosum* interval (C24 to C53)

The *D. lobispinosum* seismic sequence (142.3–140.9 Ma) prograded over a distance of about 25 km in the study area (Figs. 3–6 and 7c). The isopach map shows that the interval is thicker in the west (700 ms TWT; 1080 m) than in the east (530 ms TWT; 820 m) in the shelf area (Figs. 3–6 and 7c). Downdip, the maximum sediment thickness of the bottomsets is more significant in the west (600 ms TWT; 930 m) than in the east (330 ms TWT; 510 m), suggesting that more sediments were delivered to the basin on the western edge of the study area (Figs. 3–6 and 7c). This seismic sequence is overlain by an unconformable surface that locally shows erosional truncation of underlying reflections (e.g., Fig. 5) or preserved toplap terminations (e.g., Fig. 6). This interval, which includes the highest number of clinothems (i.e., 30), displays the full spectrum of shelf-margin types across the entire study area (Figs. 3–6). However, *backstepping shelf-edge trajectories* are only observed at the western edge of the study area (Fig. 3).

Overall, the clinothems are bounded by high-angle shelf-margin clinoforms at the base of the sequence, which progressively pass up into low-angle shelf-margin clinoforms towards the top (Figs. 3–5), except on the eastern edge of the study area where the clinoforms display consistently high angles throughout the sequence (Fig. 6). Onlapping wedges are observed throughout and become more common towards the top of the *D. lobispinosum* interval (Figs. 3–6). High-gradient and low-relief clinoforms, interpreted as a prograding shoreface, are also observed within clinothem C38 in the western part of the study area (Fig. 3).

#### 4.2.4. *B. reticulatum* interval (C54 to C73)

The youngest seismic sequence of the LBG (i.e., *B. reticulatum* interval; 140.9–139.4 Ma) prograded over a distance of about 17 km (Figs. 3–6 and 7d). The locus of deposition was in the central part of the study area where

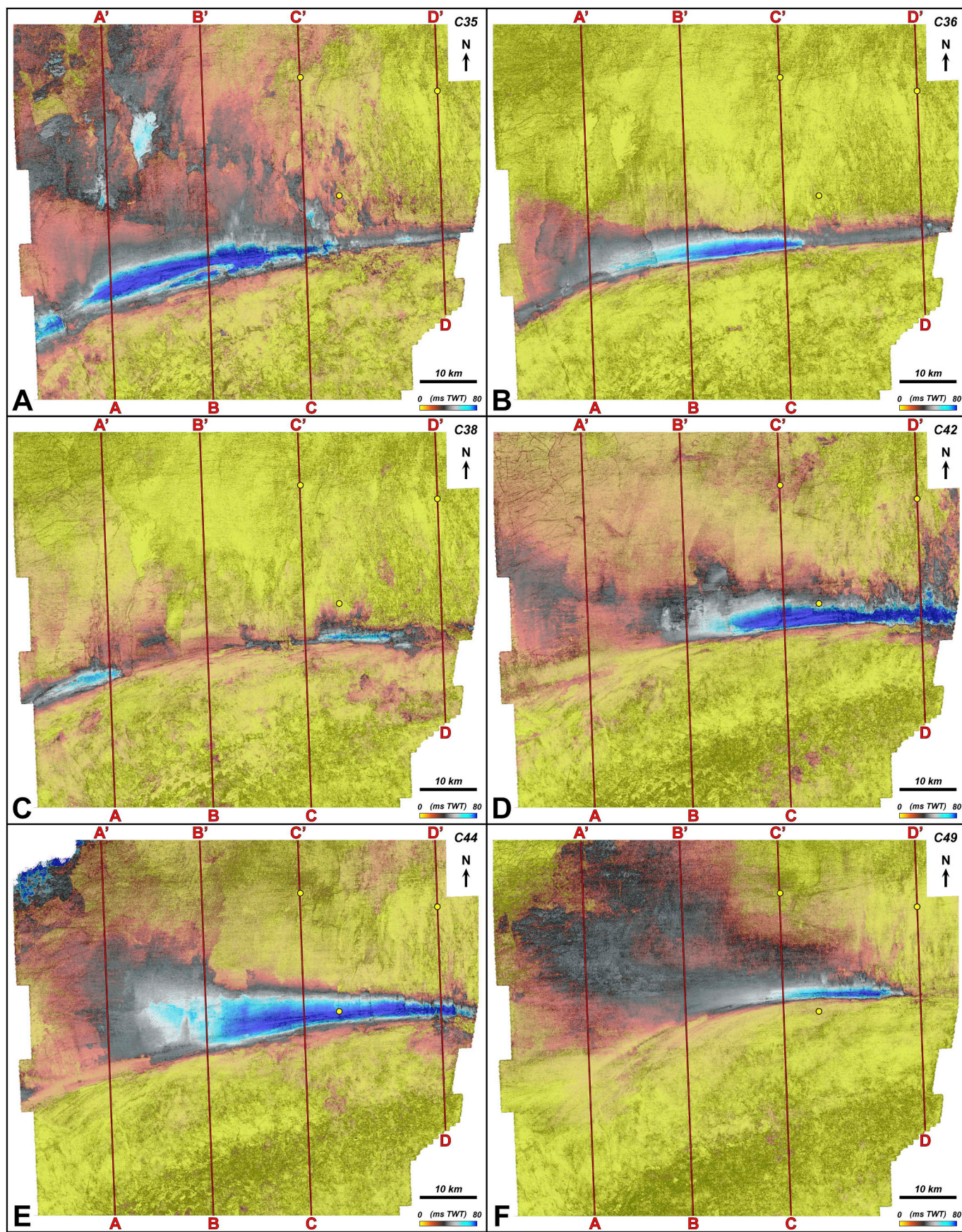
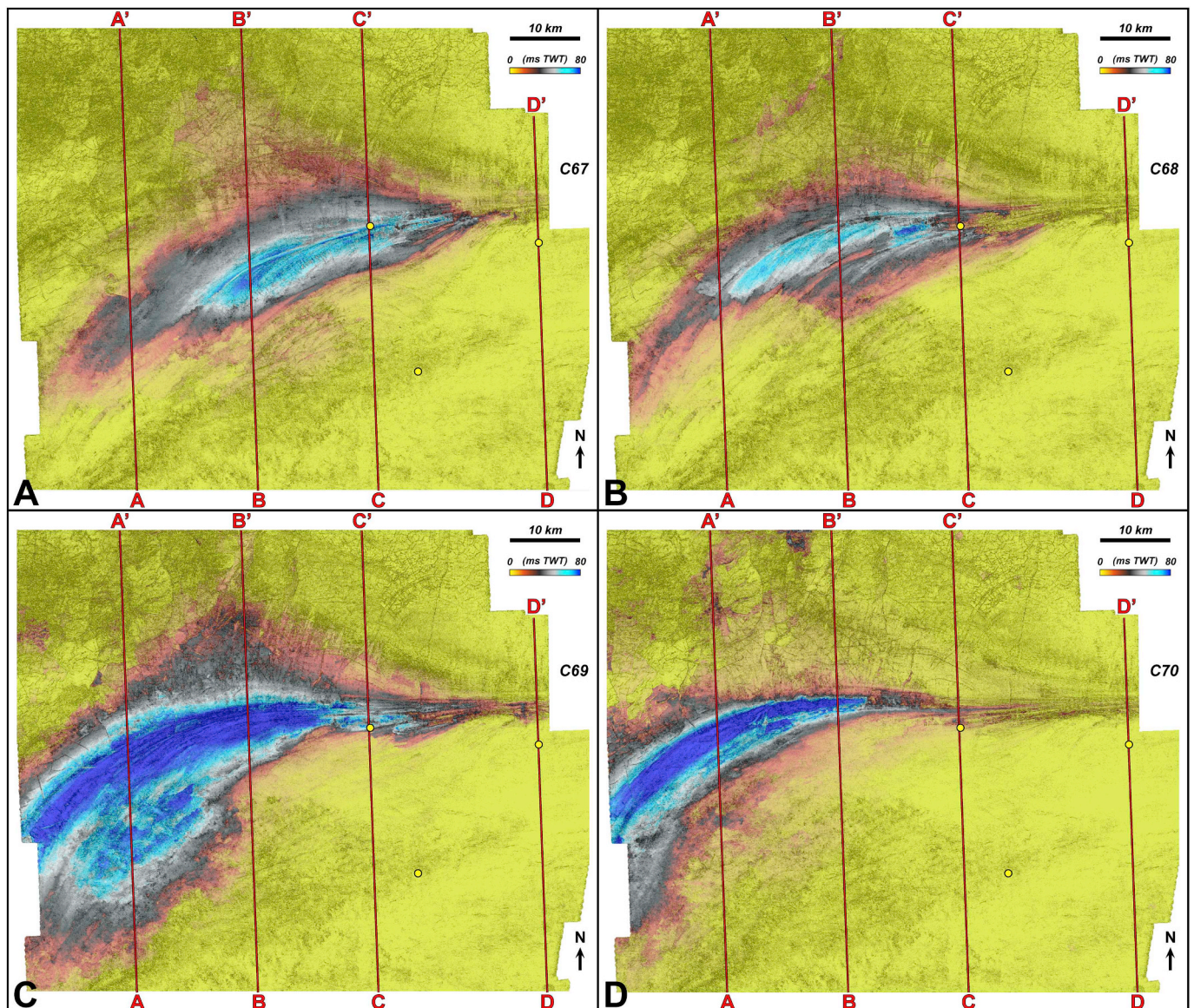


Fig. 8. Similarity attribute overlain by sediment thickness maps (ms TWT) of the clinothems C35 (A), C36 (B), C38 (C), C42 (D), C44 (E) and C49 (F). Note the switching of depocenters in the shelf-edge area across the clinothems. For instance, the locus of sedimentation switched from the west to the middle of the study area between the clinothems C35 and C36. Locally, sedimentation was partitioned across two different areas (e.g., clinothem C38). Data courtesy of TGS.



**Fig. 9.** Similarity attribute overlain by sediment thickness maps (ms TWT) of the clinothems C67 (A), C68 (B), C69 (C), and C70 (D). Note the gradual migration of the locus of sedimentation from east to west. Data courtesy of TGS.

the maximum sediment thickness reaches 500 ms TWT (775 m) in the shelf area (Figs. 3–6). Basinward, the maximum sediment thickness in the bottomset area is about 280 ms TWT (~430 m) where polygonal faulting is observed (Figs. 3–6 and 7d). The seismic unconformity at the top of the *B. reticulatum* seismic sequence (i.e., top of clinothem C73) is associated with toplap terminations below and onlap of overlying reflections in the shelf-margin area (Figs. 3–6).

The clinothems of this interval present mostly *flat* and *rising shelf-edge trajectories* (Figs. 3–6). *Backstepping shelf-edge trajectories* are not observed and *falling shelf-edge trajectories* are rare (e.g., clinothem C73; Figs. 3–5), except in the eastern edge of the study area where they are more commonly observed (C55, C68–72, C73; Fig. 6). At the base of the seismic sequence, the clinothems are mostly composed of low-angle clinoforms associated with overlapping wedges, except in the east where high-angle clinoforms are present (Fig. 6). Towards the top of the interval, the clinothems show high-angle shelf-margin geometries (Figs. 3–6).

#### 4.3. Lateral and vertical variability of clinothems

Examples of thickness maps of various clinothems from the *D. lobispinosum* and *B. reticulatum* intervals are presented in Figs. 8 and 9, respectively. Videos S1 and S2 present successive isopach maps of all the

clinothems from the *D. lobispinosum* and *B. reticulatum* intervals, respectively. These maps show that deposition at the shelf edge is switching at high frequency (Figs. 8 and 9). For example, the locus of sedimentation switched from the west to the central part of the study area between the clinothems C35 and C36, before becoming partitioned into two (a western and eastern) depocentre in C37, and back to a single eastern depocentre from C42 onward (Fig. 8). The depocentres of the clinothems C35 to C49 extended laterally (~10–40 km long; Fig. 8). In other cases, the locus of sedimentation is gradually evolving from the east to west in the *B. reticulatum* interval (e.g., clinothems C67 to C70; Fig. 9), where each depocentre presents a width varying between ~30 and 50 km (Fig. 9). While the locus of sedimentation in the shelf-edge area was focused in the eastern part of the study area for some clinothems, they also display bottomsets having a thickness of about 60 ms TWT (~90 m) that progressively decreases in thickness westward and basinward to about 10 ms TWT (~15 m) in the distal areas (e.g., clinothems C42, C44 and C49; Fig. 8). These thicker bottomsets are observed up to ~20–30 km downdip from the shelf edge (Fig. 8).

Supplementary video related to this article can be found at <https://doi.org/10.1016/j.marpetgeo.2019.07.007>.

Also, the results show that most of the 5<sup>th</sup> order clinothems show strong along-strike variability in stratal stacking patterns and shelf-edge trajectory types (Figs. 3–6). To demonstrate this variation quantitatively, a standard

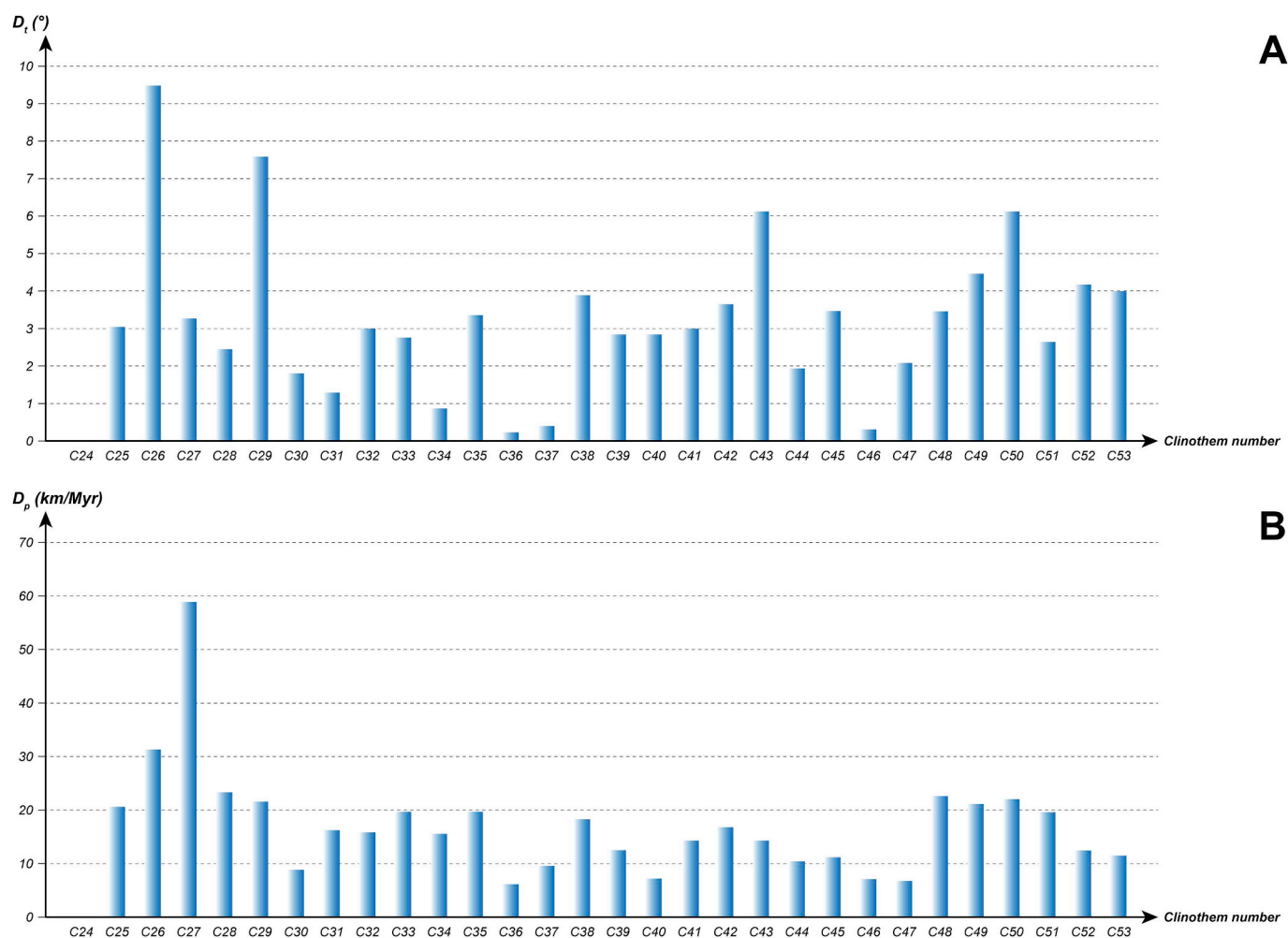


**Fig. 10.** Standard deviation parameters plotted against clinothem numbers of the (A) shelf-edge trajectory angles ( $D_s$ ) and (B) shelf-margin progradation rates ( $D_p$ ). These parameters were calculated for each clinothem from the *D. lobispinosum* interval by compiling the shelf-edge trajectory angles  $T_{se}$  (see Table 5) and shelf-margin progradation rates  $R_p$  (see Table 6) extracted along four-depositional dip-profiles (see Figs. 3–6 and location on Fig. 1b). For shelf-edge trajectory angles, most standard deviation values are between  $\sim 1$  and  $4^\circ$ , with some clinothems having values up to  $\sim 9^\circ$ , indicating highly variable shelf-edge trajectory angles along-strike in a single clinothem. Note that shelf-margin progradation rates are highly variable along-strike with most standard deviation values  $> 10$  km/Myr. Thus, accommodation and sediment supply ( $\delta A/\delta S$ ) ratios were highly variable along strike and strongly influenced the 3D stratigraphic architecture of each clinothem.

deviation parameter ( $D_s$ ) of the shelf-edge trajectory angle  $T_{se}$  (Fig. 10a and Table 5) is calculated for each clinothem along four dip-oriented seismic cross-sections (AA', BB', CC' and DD'; Fig. 1b). Most standard deviations are between  $\sim 1$  and  $4^\circ$ , whereas some clinothems have higher-angle values up to  $\sim 9^\circ$  (Fig. 10a and Table 5). These values indicate that overall, the shelf-edge trajectory angles of single clinothems (reflecting local  $\delta A/\delta S$  conditions along the shelf margin) are highly variable along strike. For example, clinothem C43 displays a *backstepping shelf-edge trajectory* in the west and a *flat shelf-edge trajectory* in the east of the study area (Figs. 3 and 6, respectively). As a result, clinothem C43 has a standard deviation of  $\sim 6^\circ$  (Fig. 10a and Table 5). Only few clinothems show consistent stacking patterns across the Investigator Depocentre and are associated with standard deviations up to  $1^\circ$  (e.g., clinothem C46; Figs. 3–6 and Fig. 10a).

Therefore, the high-frequency shelf-margin lobe switching pattern illustrated on isopach maps (Figs. 8 and 9; Videos S1 and S2) is the reflection of the vertical and lateral variability in stratal stacking patterns and shelf-edge trajectory types previously observed on seismic cross-sections. This depocentre migration explains why the stratal architecture and thickness of each individual clinothem is so variable along-strike (Figs. 3–6). This pattern is also seen when analyzing shelf-margin progradation rates  $R_p$  (Table 6). Vertically (i.e., through time),  $R_p$  fluctuated rapidly from one clinothem to the next (e.g., from  $\sim 3$  to  $55$  km/Myr between the clinothems C32 and C33 on the seismic line DD'; Fig. 6; Table 6). However, significant variations in  $R_p$  are also observed along-strike (e.g., from  $\sim 4$  to  $53$  km/Myr between the seismic lines AA' and DD' for the clinothem C29; Figs. 3 and 6; Table 6). To

highlight this lateral variability quantitatively, a standard deviation parameter ( $D_p$ ) of the shelf-margin progradation rate  $R_p$  is calculated for each clinothem (Fig. 10b and Table 6). Results show that most standard deviations are between  $\sim 10$  and  $30$  km/Myr, whereas some clinothems present higher values up to  $\sim 60$  km/Myr (e.g., clinothem C27; Fig. 10b and Table 6). These values are overall indicative of highly variable shelf-margin progradation rates along-strike in a single clinothem.

## 5. Sequence stratigraphic framework

This part aims to establish a sequence stratigraphic framework for the LBG. Firstly, a classical sequence stratigraphic approach based on the observation of both the internal stacking patterns of each clinothem and the stratal terminations above and below high-order seismic unconformities is applied (e.g., Catuneanu et al., 2009, 2011). Secondly, a dynamic stratigraphic approach based on shelf-edge trajectory angles within each clinothem is used (e.g., Helland-Hansen and Hampson, 2009; Neal et al., 2016).

### 5.1. Depositional sequence model

The depositional sequence model is widely used by sequence stratigraphers, with some variations relating to the position of the correlative conformities (e.g., Posamentier et al., 1988; Van Wagoner et al., 1988, 1990; Christie-Blick, 1991; Hunt and Tucker, 1992; Posamentier and Allen, 1999). A depositional sequence is bounded by a *Sequence Boundary (SB)* that

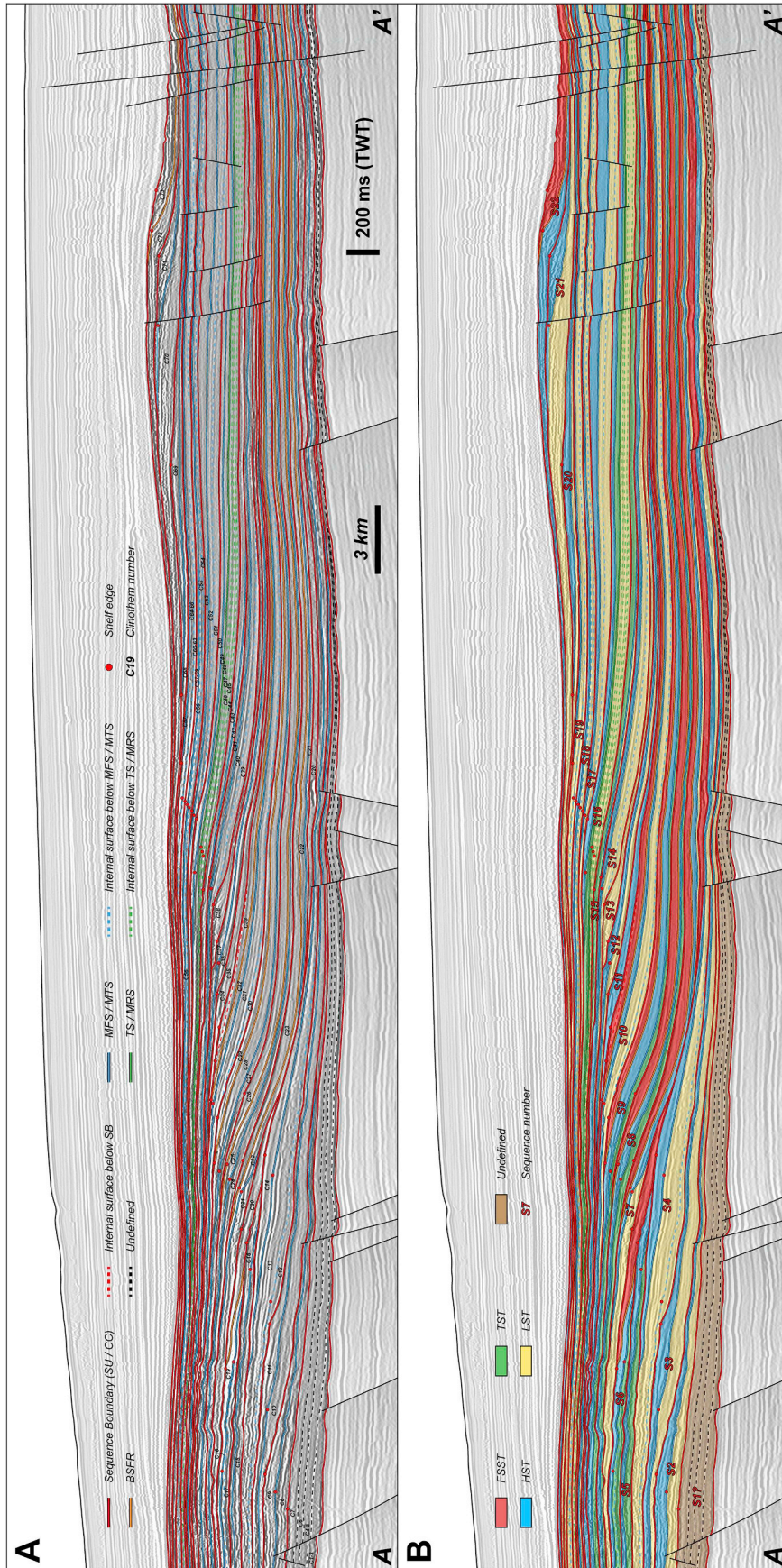


**Fig. 11.** Interpretation of the regional 2D seismic profile A-A' (see location on Fig. 1b) within a sequence stratigraphic framework based on the depositional sequence model (Catuneanu et al., 2009). Seismic unconformities bounding the clinothems in the LBG are interpreted as sequence stratigraphic surfaces based on stratal terminations of the reflector below and above (A), and used to define depositional sequences and systems tracts (B). Note that considering a time interval of ~4.6 Myr for the LBG in this area, the cyclicity of the stratigraphic sequences interpreted is ~210,000 years, representing a 4<sup>th</sup> stratigraphic order (i.e., 0.08–0.5 Myr; *sensu* [Vail et al., 1991](#)). SB = Sequence Boundary; SU = Subaerial Unconformity; CC = Correlative Conformity; BSFR = Basal Surface of Forced Regression; MFS = Maximum Flooding Surface; MTS = Maximum Transgressive Surface; TS = Transgressive Surface; MRS = Maximum Regressive Surface; FSST = Falling-Stage Systems Tract; HST = Highstand Systems Tract; TST = Transgressive Systems Tract; LST = Lowstand Systems Tract. Data courtesy of TGS.

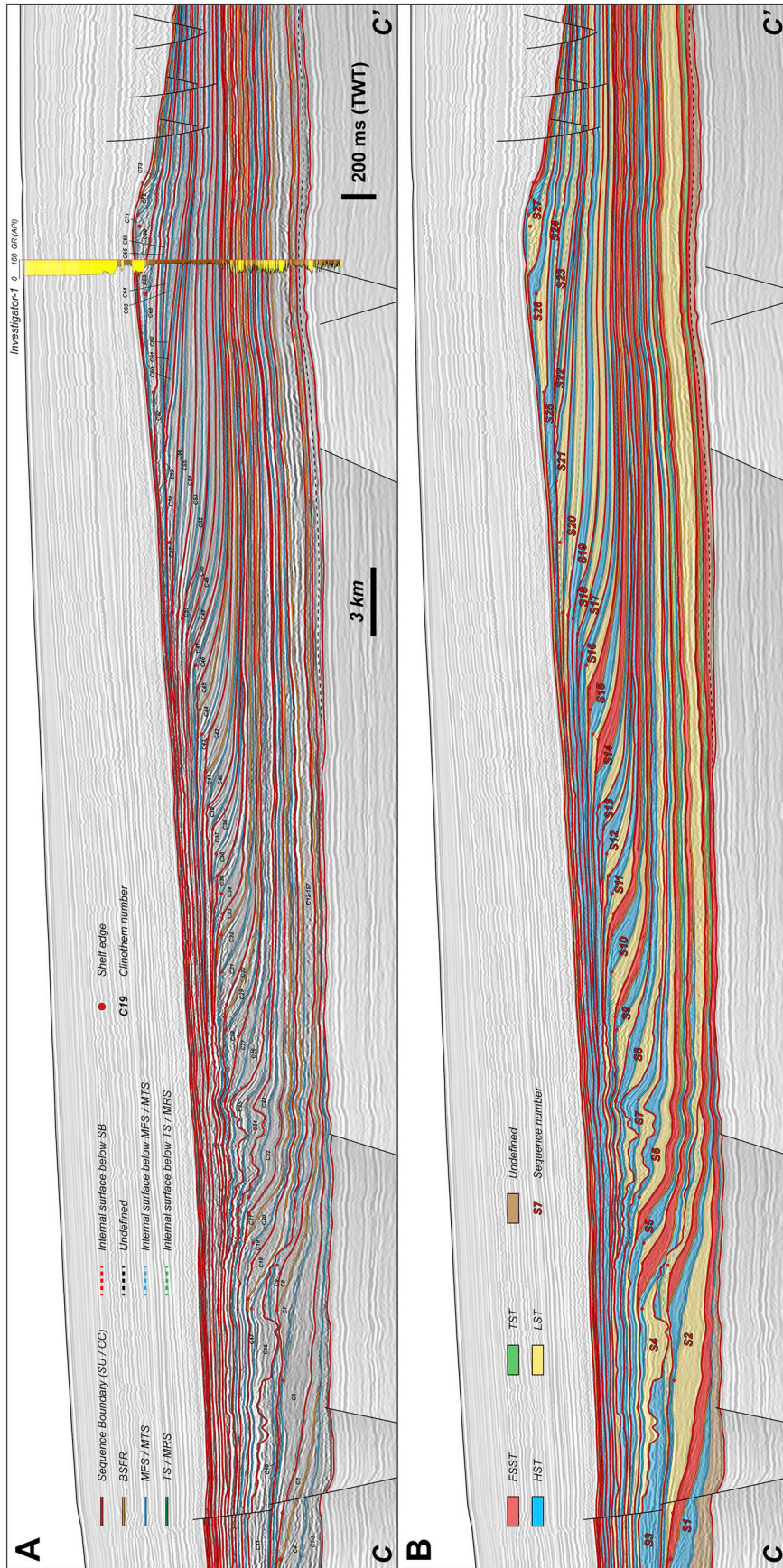


Fig. 12. Interpretation of the regional 2D seismic profile C–C' (see location on Fig. 1b) within a sequence stratigraphic framework based on the depositional sequence model (Catuneanu et al., 2009). Seismic unconformities bounding the clinohems in the LBG are interpreted as sequence stratigraphic surfaces based on stratal terminations of the reflector below and above (A), and used to define depositional sequences and systems tracts (B). Note that considering a time interval of ~4.6 Myr for the LBG in this area, the cyclicity of the stratigraphic sequences interpreted is ~170,000 years, representing a 4<sup>th</sup> stratigraphic order (i.e., 0.08–0.5 Myr; *sensu* [Vail et al., 1991](#)). SB = Sequence Boundary; SU = Subaerial Unconformity; CC = Correlative Conformity; BSFR = Basal Surface of Forced Regression; MFS = Maximum Flooding Surface; MTS = Maximum Transgressive Surface; TS = Transgressive Surface; MRS = Maximum Regressive Surface; FSST = Falling-Stage Systems Tract; HST = Highstand Systems Tract; TST = Transgressive Systems Tract; LST = Lowstand Systems Tract. Data courtesy of TGS.

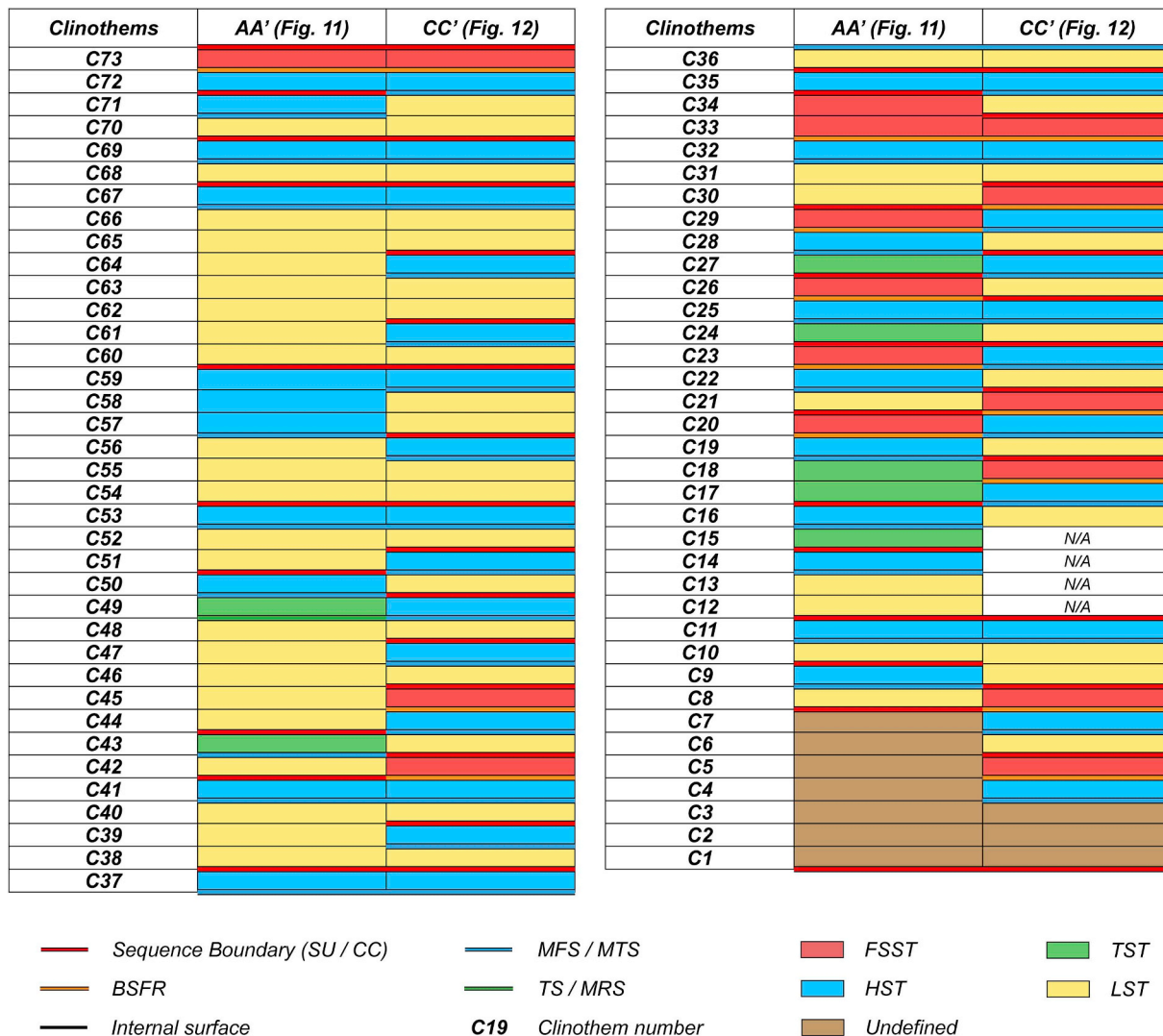


Fig. 13. Comparison chart of sequence stratigraphic surfaces, systems tracts and depositional sequences interpreted on seismic profiles AA' and CC' (see Figs. 12 and 13, respectively) using a standard sequence stratigraphic approach (i.e., depositional sequence model; sensu Catuneanu et al., 2009). Note the significant lateral variability between the two examples where a seismic unconformity interpreted as a sequence boundary on one seismic line can pass laterally to a maximum flooding surface, thus resulting in lateral variations of the systems tracts interpreted below. SB = Sequence Boundary; CC = Correlative Conformity; SU = Subaerial Unconformity; BSFR = Basal Surface of Forced Regression; MFS = Maximum Flooding Surface; MTS = Maximum Transgressive Surface; TS = Transgressive Surface; MRS = Maximum Regressive Surface; FSST = Falling-Stage Systems Tract; HST = Highstand Systems Tract; TST = Transgressive Systems Tract; LST = Lowstand Systems Tract.

corresponds to a *Subaerial Unconformity (SU)* (i.e., presence of erosional truncations) and a *Correlative Conformity (CC)* bounding a depositional sequence (sensu Catuneanu et al., 2009). On seismic data, subaerial unconformities are evidenced by several key features related to stratal terminations (Catuneanu, 2006): (1) erosional truncation of the strata below; (2) toplap of underlying reflections; (3) offlap along the unconformity; (4) onlap of reflections above. On the other hand, correlative conformities are defined only as a downlap surface of the reflections above (Catuneanu, 2006). Each depositional sequence can be subdivided into several systems tracts that link contemporaneous depositional systems (sensu Brown and Fisher, 1977) and form during different phases of the depositional cycle that include (Van Wagoner et al., 1987; Posamentier and Vail, 1988; Catuneanu et al., 2009): (1) a *Falling-Stage Systems Tract (FSST)*; (2) a *Highstand Systems Tract (HST)*; (3) a *Transgressive Systems Tract (TST)*; and (4) a *Lowstand Systems Tract (LST)*. Each systems tract is bounded by a specific sequence stratigraphic surface. One of the key surfaces often easily recognizable on seismic data is the *Maximum Flooding Surface (MFS)* that separates the *TST* (i.e., retrogradation) below from the *HST* (i.e., progradation) above and that is commonly expressed as a downlap surface (Posamentier et al., 1988; Van Wagoner et al., 1988; Galloway, 1989). Another surface corresponds to the *Transgressive Surface (TS)* that separates the *LST* (i.e., progradation) below

from the *TST* (i.e., retrogradation) above (Posamentier and Vail, 1988). Finally, when forced regressive packages are present, a *Basal Surface of Forced Regression (BSFR)* can be identified, thus separating the *HST* (i.e., progradational and normal regressive) below from the *FSST* (i.e., progradational and forced regressive) above (Hunt and Tucker, 1992). Alternative names commonly found in the literature for *MFS* and *TS* is the *Maximum Transgressive Surface (MTS)* and the *Maximum Regressive Surface (MRS)* (sensu Helland-Hansen and Martinsen, 1996).

Each clinothem mapped in this study corresponds to a relatively conformable succession of genetically related strata bounded by seismic unconformities and their correlative conformities (sensu Mitchum et al., 1977b). Clinothems represent stratal packages deposited during relatively stable  $\delta A/\delta S$  conditions and separated by surfaces marking a change in those  $\delta A/\delta S$  conditions. The depositional sequence model is here applied within the LBG on the seismic lines AA' (western part of the study area; Fig. 1b) and CC' (east part of the study area; Fig. 1b) where *Sequence Boundaries (SB)*, *Transgressive Surfaces (TS)*, *Maximum Flooding Surfaces (MFS)* and *Basal Surfaces of Forced Regression (BSFR)* were identified based on the criteria defined above (Figs. 11 and 12).

Where no transgressive packages (i.e., *Transgressive Systems Tracts TST*) are observed, the *TS* is combined with the *MFS* forming a composing surface,

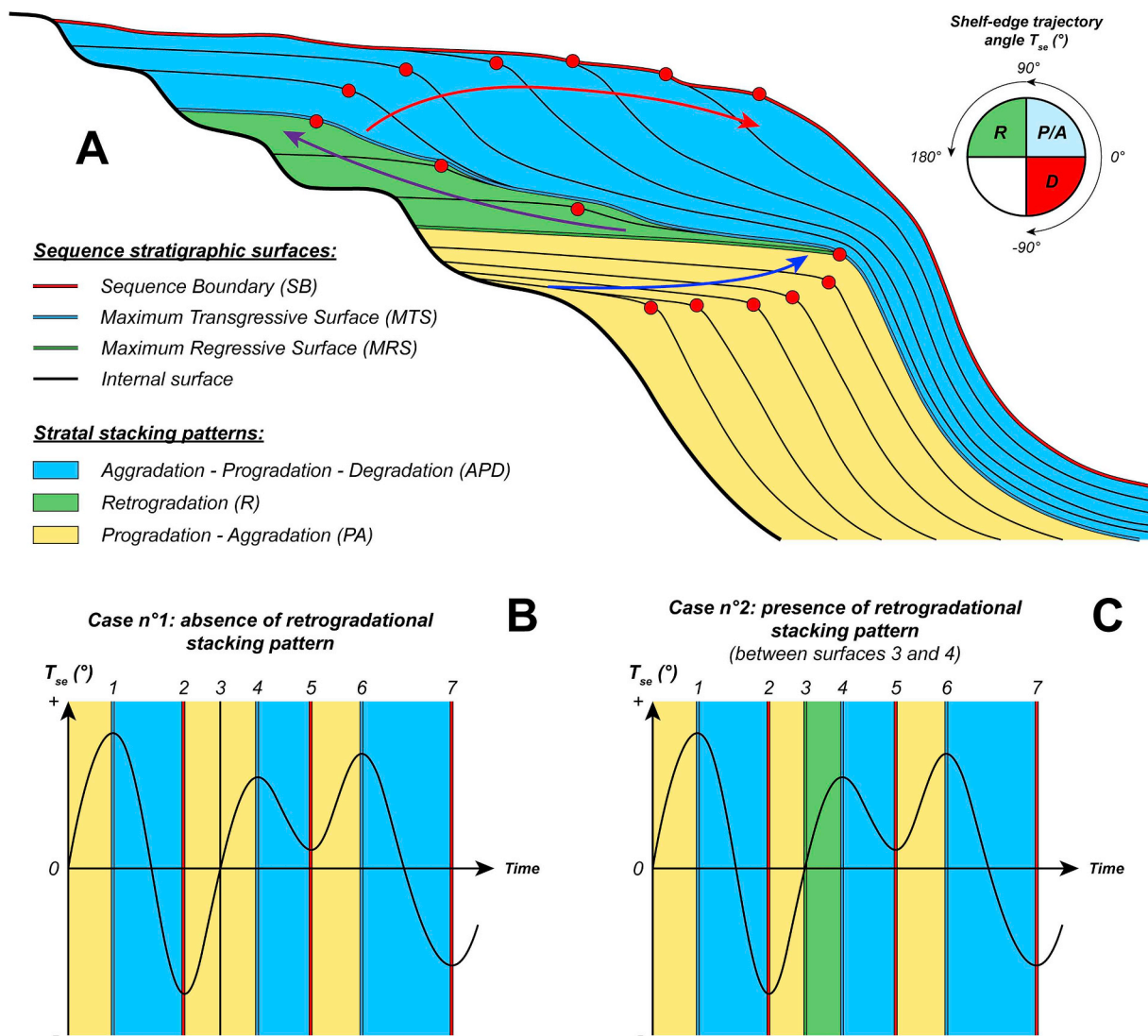
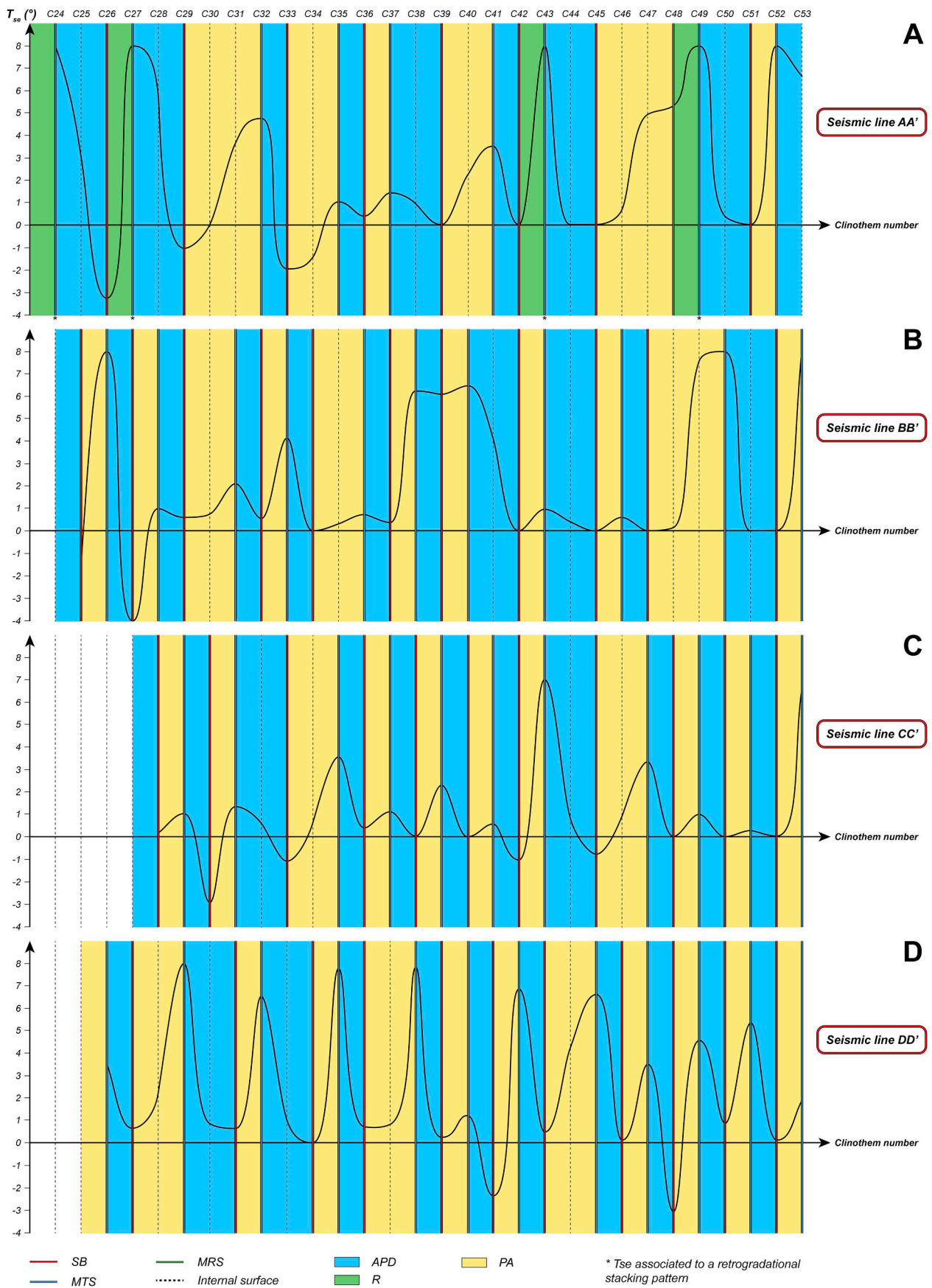


**Fig. 14.** Workflow used in this paper to interpret the high-resolution clinostems within a sequence stratigraphic framework using a dynamic stratigraphic approach, employing a combination of the accommodation succession method (Neal et al., 2016) and trajectory analysis (Helland-Hansen and Hampson, 2009). (A) Accommodation succession method showing the main stratal stacking patterns (APD, R, PA) and associated sequence stratigraphic surfaces (SB, MTS, MRS), based on the geometric relationship of the strata (modified after Neal et al., 2016). Shelf-edge trajectory angles  $T_{se}$  calculated within individual clinostems at high resolution are used to generate shelf-edge trajectory curves to determine accommodation succession sets whereby: (1) decreasing  $T_{se}$  (potentially becoming negative) with aggradation to progradational (potentially degradational) stacking patterns corresponds to an APD set; (2) positive  $T_{se}$  with retrogradational stacking pattern corresponds to a R set; and (3) increasing  $T_{se}$  with progradational to aggradational stacking patterns corresponds to a PA set. If no retrogradational stacking pattern is present, only APD and PA sets associated with SB and MRS at their top, respectively, are interpreted (B); whereas if present, a R set is interpreted with a MRS surface at its base (C). Note that to facilitate visualization of the  $T_{se}$  curve and its interpretation, negative values of  $T_{se}$  associated with a retrogradational pattern are shifted to a positive value  $> 90^{\circ}$  and are marked by \*. Note that the  $T_{se}$  curves presented in B and C are for illustrative purposes only and do not refer to any cross-section interpreted from the LBG. SB = Sequence Boundary; MTS = Maximum Transgressive Surface; MRS = Maximum Regressive Surface; APD = Aggradation-Progradation-Degradation; R = Retrogradation; PA = Progradation-Aggradation.

and thus separating a *Lowstand Systems Tract (LST)* from a *Highstand Systems Tract (HST)* (Figs. 11 and 12). Similarly, where no forced regressive packages (i.e., *Falling-Stage Systems Tracts FSST*) are observed, the *BSFR* is combined with the *SB* to separate a *HST* from a *LST* (Figs. 11 and 12). Fig. 13 presents the sequence stratigraphic surfaces and systems tracts identified for each seismic line. Based on the depositional sequence model, the interpretation from seismic data suggests that the LBG would mostly consist of normal regressive and forced regressive prograding sequences (Figs. 11 and 12).

The types of sequence stratigraphic surfaces and the number of depositional sequences identified varies significantly between the two interpreted seismic lines (Figs. 11–13). Along cross-section AA', 23 SB encompassing 22 depositional sequences were identified (Fig. 11); whereas along the cross-section CC', 28 SB encompassing 27 depositional sequences were interpreted (Fig. 12). Differences are observed between the

two seismic lines in terms of the numbers of depositional sequences developed. For instance, several depositional sequences can be identified along the depositional-dip profile CC', whereas a single depositional sequence or a single systems tract can be observed along the profile AA' for the same time interval (e.g., clinostems C44 to C48; Fig. 13). In contrast, some systems tracts and depositional sequences are fully preserved along the seismic line AA', whereas significant erosion occurred along the seismic line CC' (e.g., clinostem C12 to C15; Fig. 13). Both of these observations may explain the differences in the along-strike interpretation. However, the results also show that a single seismic unconformity bounding a clinostem can pass laterally from a SB to a MFS, thus resulting in systems tracts passing laterally from HST or FSST to LST, and vice versa (e.g., top of clinostem C34; Fig. 13). Similarly, where transgressive and forced regressive packages are observed, interpretation of TS and BSFR, respectively, adds a degree of variability to the sequence stratigraphic



(caption on next page)

**Fig. 15.** Interpretation of stratigraphic sequences and sequence stratigraphic surfaces from application of the  $T_{se}$  curve analysis (see Fig. 14) to the *D. lobispinosum* interval along four depositional dip-profiles (see location on Fig. 1b): seismic line A–A' (A; see Fig. 3); seismic line B–B' (B; see Fig. 4); seismic line C–C' (C; see Fig. 5); and seismic line D–D' (D; see Fig. 6). Note that to facilitate visualization of the  $T_{se}$  curve and its interpretation,  $T_{se}$  values  $< -4^\circ$  and  $> 8^\circ$  were limited to these values on the curve. Quantitative data extracted from this interval along these seismic profiles are presented in Tables 1–4. SB = Sequence Boundary; MTS = Maximum Transgressive Surface; MRS = Maximum Regressive Surface; APD = Aggradation-Progradation-Degradation; R = Retrogradation; PA = Progradation-Aggradation.

framework if these surfaces are not interpreted along both profiles (e.g., top of clinothems C22 and C48; Fig. 13). Overall, it appears that less than 50% of the interpreted sequence stratigraphic surfaces and systems tracts are the same on both the AA' and CC' cross-sections (Fig. 13).

Considering a time interval of  $\sim 4.6$  Myr for the LBG in this area, the cyclicity of the depositional sequences is  $\sim 210,000$  yrs on average along the seismic profile AA' and  $\sim 170,000$  yrs on average along the seismic profile CC'. Thus, in both cases, stratigraphic surfaces and depositional sequences interpreted within the LBG are approximately 4<sup>th</sup> order (i.e., 0.08–0.5 Myr; *sensu* Vail et al., 1991).

## 5.2. Accommodation succession method and trajectory analysis

The accommodation succession method was initially defined by Neal and Abreu (2009), and later refined by Neal et al. (2016). This approach is based on the geometric relationship of the strata resulting from repeated phases of accommodation creation and sediment fill, referred to as the “accommodation succession” (Neal and Abreu, 2009; Neal et al., 2016). Therefore, a framework built using this approach is composed of regional packages resulting from changes in rates of accommodation creation and sediment supply (i.e.,  $\delta A/\delta S$  ratio; Swift and Thorne, 1991; Schlager, 1993; Shanley and McCabe, 1994; Muto and Steel, 1997). Three types of accommodation succession sets (i.e., stacking patterns) are defined (Fig. 14a; Neal and Abreu, 2009; Neal et al., 2016): (1) *Aggradation-Progradation-Degradation* (APD), where  $\delta A/\delta S < 1$  and decreasing; (2) *Retrogradation* (R), where  $\delta A/\delta S > 1$  (i.e., backstepping); and (3) *Progradation-Aggradation*, where  $\delta A/\delta S < 1$  and increasing. In this framework, sequence boundaries are located at the top of the APD. Surfaces at the top of the R and PA accommodation succession sets are recognized as *Maximum Transgressive Surface* (MTS) and *Maximum Regressive Surfaces* (MRS), respectively (*sensu* Helland-Hansen and Martinsen, 1996). The MTS is equivalent to the MFS and the MRS is equivalent to the TS. The accommodation succession method is an observation-based approach where the sequence stratigraphic interpretation is based on the genetic relationships between stratigraphic packages without any *a priori* knowledge of sea-level fluctuations (Neal and Abreu, 2009; Neal et al., 2016). In other words, this approach is based on the evolution of the shelf-edge trajectory through time, which reflects the evolution of the  $\delta A/\delta S$  ratio, allowing recognition of different types of shelf-edge trajectories having specific stratal stacking patterns (i.e., PA, R and APD). A fundamental aspect that underpins this method is the analysis of shelf-edge (or shoreline) trajectories within individual stratal packages (Helland-Hansen and Martinsen, 1996; Helland-Hansen and Hampson, 2009; Henriksen et al., 2009).

Shelf-edge trajectory angles  $T_{se}$  were calculated within individual clinothems from the *D. lobispinosum* interval. Using these data,  $T_{se}$  curves can be generated to visualize shelf-edge trajectory trends (Fig. 14). Thus, following the accommodation succession method (Fig. 14), accommodation succession sets and sequence stratigraphic surfaces can be directly picked on the curve whereby: (1) a decreasing  $T_{se}$  (potentially becoming negative) with aggradational to progradational (potentially degradational) stacking patterns corresponds to an APD set and is bounded at its top by a SB; (2) a positive  $T_{se}$  with retrogradational stacking pattern corresponds to a R set and is bounded at its top by a *Maximum Transgressive Surface* (MTS); and (3) an increasing  $T_{se}$  with progradational to aggradational stacking patterns corresponds to a PA set and is bounded at its top by a *Maximum Regressive Surface* (MRS). If no retrogradational pattern is observed, the MTS is combined with the MRS (Fig. 14b).

The workflow of this approach is threefold: (1) identify the clinothems with a retrogradational stacking pattern (if present); (2) interpret the accommodation succession sets following the shelf-edge trajectory trends; and (3) identify the sequence stratigraphic surfaces bounding the accommodation succession sets (e.g., Fig. 14c). In this study, the shelf-edge trajectory angles  $T_{se}$  associated with a retrogradational stacking pattern are negative as the shelf-margin progradation  $P_{se}$  is negative (i.e., moving landward). However, shelf edges moving landward are commonly associated with a positive trajectory value between  $90^\circ$  and  $180^\circ$  (Helland-Hansen and Hampson, 2009). Hence,  $T_{se}$  values associated with a retrogradational pattern were

automatically shifted to a positive value on the  $T_{se}$  curves and marked with an asterisk (e.g., Fig. 14c).

Within the *D. lobispinosum* interval, shelf-edge trajectory angles  $T_{se}$  were calculated within each clinothem along the four dip-oriented cross-sections (Figs. 3–6 and Tables 1–4). By default, the overlapping wedges are associated with a  $T_{se}$  value of 0 as no lateral and/or vertical evolution of the shelf edge is observed (Tables 1–4).  $T_{se}$  curves for each seismic profile are compiled on Fig. 15. A stratigraphic sequence is here defined as being bounded at its base and top by sequence boundaries (Fig. 15). Overall, nine stratigraphic sequences (i.e., full cycle between two sequence boundaries) were identified along the cross-section AA' and 12 stratigraphic sequences identified along the cross-section BB', CC' and DD' (Fig. 15; Tables 1–4).

Although the number of sequences is similar for the seismic lines BB', CC' and DD', results show that the sequence stratigraphic surfaces and accommodation succession sets are highly variable across the four seismic lines, where a SB may pass laterally into a MTS (e.g., top of the clinothem C40; Fig. 15). As the time span of the *D. lobispinosum* interval is  $\sim 1.4$  Myr, the average cyclicity of the stratigraphic sequences is  $\sim 130,000$  years along the seismic profile AA' and  $\sim 100,000$  years along the seismic profiles BB', CC' and DD'. Therefore, the sequences identified are 4<sup>th</sup> order (i.e., 0.08–0.5 Myr; *sensu* Vail et al., 1991).

$T_{se}$  curves can also be generated to interpret composite accommodation succession sets and composite stratigraphic sequences (Fig. 16 and Tables 1–4). Shelf-margin progradation ( $P_{se}$ ) and aggradation ( $A_{se}$ ) values can be calculated within each 4<sup>th</sup> order sequence previously interpreted by adding the  $P_{se}$  and  $A_{se}$  values of each 5<sup>th</sup> order clinothem comprised between the sequence boundaries of the 4<sup>th</sup> order sequence, which are then used to calculate an overall shelf-edge trajectory angle  $T_{se}$  (Tables 1–4). Then, following the same approach of the  $T_{se}$  curve analysis, composite sequence stratigraphic surfaces and accommodation succession sets can be identified (Fig. 16). A composite stratigraphic sequence is interpreted as being bounded at its base and top by composite sequence boundaries (Fig. 16). Between two and four composite sequences were interpreted on the seismic profile AA', BB', CC' and DD', respectively (Fig. 16; Tables 1–4). The cyclicity of these sequences varies between  $\sim 350,000$  yrs (seismic profile DD') and 700,000 yrs (seismic profile AA'), thus representing 4<sup>th</sup> order to 3<sup>rd</sup> stratigraphic order, respectively (i.e.,  $\sim 0.08$ –3 Myr; *sensu* Vail et al., 1991). Fig. 17 shows an example of sequence and composite sequence interpretation for the cross-section CC'.

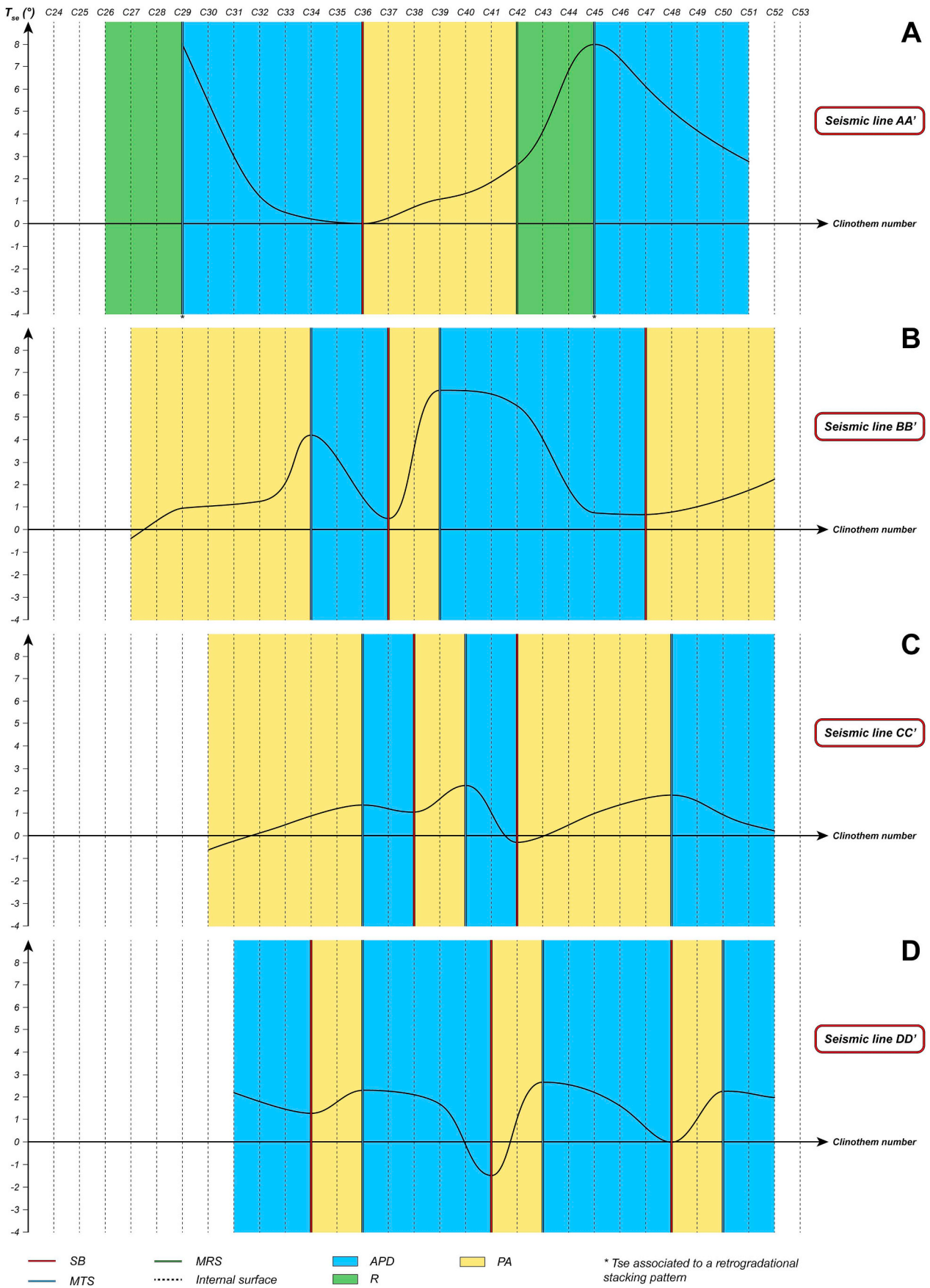
This workflow can be applied to any type of 3D seismic data (i.e., low to high quality), providing that the shelf edges are resolvable, allowing  $T_{se}$  calculation within individual clinothems. However, the resolution of the initial clinothems interpreted within the 3D volume is dependent of the data quality (Paumard et al., 2019), which will impact the resolution of the sequence stratigraphic framework interpreted with the  $T_{se}$  curve analysis. For instance, high-quality 3D seismic data will promote the interpretation of high-order to low-order stratigraphic sequences (e.g., Fig. 17). In contrast, if the initial clinothems interpreted present a lower resolution due to poorer data quality, the  $T_{se}$  curve analysis can still be applied but the stratigraphic sequences interpreted will be of lower order. Therefore, the quantitative seismic stratigraphy approach can be applied with any type of data but the maximum resolution of the interpretation will be dependent of the data quality.

## 6. Discussion

### 6.1. Building a sequence stratigraphic framework

#### 6.1.1. Model-dependent vs. model-independent approaches

The model-independent aspects of sequence stratigraphy are mostly relevant to the concepts of seismic stratigraphy through objective observation of stratal stacking patterns and stratal terminations to identify key seismic unconformities (Mitchum et al., 1977a, 1977b; Mitchum and Vail, 1977). In contrast, the definition of sequence boundaries (i.e., selection of a seismic unconformity elevated to the grade of sequence boundary) is model-dependent, following the criteria chosen for their selection (Catuneanu et al.,



(caption on next page)

**Fig. 16.** Interpretation of composite stratigraphic sequences and composite sequence stratigraphic surfaces from application of the  $T_{se}$  curve analysis (see Fig. 14) to 4<sup>th</sup> order stratigraphic sequences (see Fig. 16) along four depositional dip-profiles (see location on Fig. 1b): seismic line A-A' (A; see Fig. 3); seismic line B-B' (B; see Fig. 4); seismic line C-C' (C; see Fig. 5); and seismic line D-D' (D; see Fig. 6). Note that to facilitate the visualization of the  $T_{se}$  curve and its interpretation, the  $T_{se}$  values  $< -4^\circ$  and  $> 8^\circ$  were limited to these values on the curve. Quantitative data extracted from each 4<sup>th</sup> order stratigraphic sequence along these seismic profiles are presented in Tables 1–4. SB = Sequence Boundary; MTS = Maximum Transgressive Surface; MRS = Maximum Regressive Surface; APD = Aggradation-Progradation-Degradation; R = Retrogradation; PA = Progradation-Aggradation.

2009). In this study, two different approaches are compared to identify sequence boundaries within the LBG using previously interpreted high-frequency seismic unconformities (Figs. 3–6): (1) depositional sequence model (Catuneanu et al., 2009, 2011); and (2) accommodation succession method in combination with trajectory analysis (Helland-Hansen and Hampson, 2009; Neal and Abreu, 2009; Neal et al., 2016). Each approach has its own merits and pitfalls and show different levels of model-independent and model-dependent aspects (Fig. 18).

The depositional sequence approach is model-dependent for two main reasons (Catuneanu et al., 2009): (1) the identification of sequence boundaries is dependent on the interpreter's observations and decisions; and (2) the identification of sequences boundaries is dependent on base-level falls that generate a subaerial unconformity (Fig. 18). Large scale erosional truncations are typically evident on seismic data, indicative of a subaerial unconformity, hence the interpretation of a sequence boundary (e.g., base of the clinothem C16; Figs. 12a and 19). In contrast, erosional truncations may not be visible if they are below seismic resolution and/or formed during minor base-level falls, which decreases confidence in defining sequence boundaries (e.g., clinothems C30 to C53; Fig. 12a). In this latter scenario,

their selection will be based on the observation of toplaps of the reflections below and onlaps of the reflections above, and potentially on the presence of downstepping offlap breaks (i.e., FSST) below. This exercise, conducted on the seismic lines AA' and CC', proved to be particularly challenging where no significant erosional truncations are observed (Figs. 11 and 12).

If FSSTs and TSTs are not observed, another level of uncertainty is added because it becomes difficult to discriminate a SB from a MFS: (1) both can constitute downlap surfaces; and (2) a lowstand wedge (i.e., LST) can present apparent toplaps on its upper bounding surface if topsets are absent and/or below seismic resolution. Thus, the interpreter is confronted with a choice typically based on the 'ideal' succession of surfaces and systems tracts: if a MFS is identified, it is tempting to identify the next surface as a SB if uncertainty is high (Figs. 11 and 12). Despite those uncertainties and limitations, the depositional sequence model has the advantage of: (1) being an easy workflow to apply in a relatively short timeframe; and (2) being a model applicable even where shelf margins are deeply eroded (Fig. 18).

The accommodation succession method is based on evolution of the  $\delta S/\delta S$  ratio that influences the shelf-edge trajectory trends and is recognized as an observation-based approach (Schlager, 1993; Shanley and McCabe, 1994;

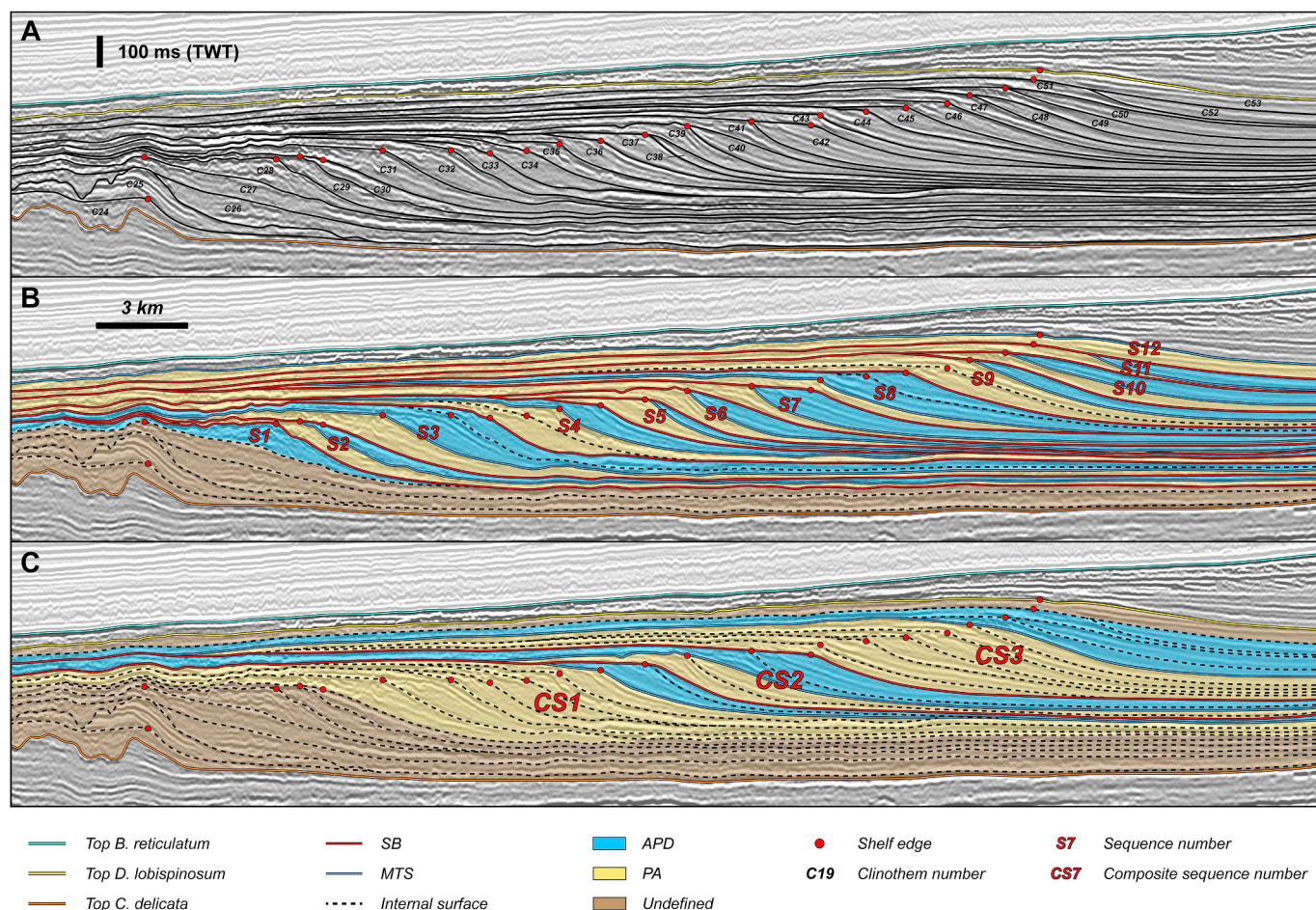


**Fig. 17.** Example of seismic and sequence stratigraphic interpretation applied to the seismic profile C-C' (see location on Fig. 1b) at different stratigraphic ranks. (A) High-resolution seismic stratigraphy from the *D. lobisposum* interval (see Fig. 5) showing the interpretation of high-frequency clinothems of 5<sup>th</sup> order. (B) Sequence stratigraphic interpretation based on the  $T_{se}$  curve analysis (see Fig. 15c) within individual clinothems highlighting the presence of 12 stratigraphic sequences. (C) Sequence stratigraphic interpretation based on the  $T_{se}$  curve analysis (see Fig. 16c) within individual stratigraphic sequences highlighting the presence of 3 composite stratigraphic sequences. Quantitative data extracted from the *D. lobisposum* interval along this seismic profile are presented in Table 3. SB = Sequence Boundary; MTS = Maximum Transgressive Surface; APD = Aggradation-Progradation-Degradation; PA = Progradation-Aggradation. Data courtesy of TGS.

	<b>Depositional sequence model</b> <i>Catuneanu et al., 2009, 2011</i>	<b>Trajectory analysis &amp; accommodation succession method</b> <i>Helland-Hansen and Hampson, 2009; Neal et al., 2016; This paper</i>
<b>Main focus of the approach</b>	Stratal terminations and stacking patterns	Stratal stacking patterns and shelf-edge trajectory angles $T_{se}$ Generation of $T_{se}$ curves
<b>Criteria to identify sequence boundaries</b>	Erosional truncation, toplap of reflectors below, onlap and downlap of reflectors above	Location at the top of an <i>Aggradational-Progradational-Degradational (APD)</i> accommodation succession set presenting a decreasing $T_{se}$ , potentially becoming negative if presence of a degradational stacking pattern
<b>Internal subdivisions of sequences</b>	Systems tracts	Accommodation succession sets
<b>Type of sequence stratigraphic approach</b>	Model-dependent (decision-based)	Model-independent (objective and observation-based)
<b>Highest stratigraphic order of sequences interpreted</b>	Fourth	Fourth
<b>Average cyclicity</b> <i>(sensu Vail et al., 1991)</i>	0.08 - 0.5 Myr	0.08 - 0.5 Myr
<b>Objective approach to identify surfaces and sequences of lower order</b>	No	Yes
<b>Results easily reproducible by different interpreters</b>	No	Yes
<b>Applicability of the approach for low- to high quality data</b>	Yes	Yes
<b>Dimensionality of the sequence stratigraphic framework</b>	Two-dimensional	Two-dimensional
<b>Control on the lateral variability of sequences</b>	No	No
<b>Advantages</b>	<ol style="list-style-type: none"> <li>1) Can be applied even if the shelf margins are highly eroded and not preserved</li> <li>2) A sequence stratigraphic framework can be established relatively rapidly</li> </ol>	<ol style="list-style-type: none"> <li>1) Even if erosional truncations are not present, the <math>T_{se}</math> curves will highlight the slight changes in trajectory trends</li> <li>2) Will provide a higher resolution sequence stratigraphic framework with reduced uncertainty</li> <li>3) Sequence stratigraphic interpretations are reproducible across interpreters based on the same quantitative data analysis</li> </ol>
<b>Pitfalls</b>	<ol style="list-style-type: none"> <li>1) Difficult to apply if subaerial exposures are not resolved on seismic data (i.e., lack of erosional truncations)</li> <li>2) Results difficult to reproduce following the interpreter's experience and decisions for the selection of sequence boundaries</li> </ol>	<ol style="list-style-type: none"> <li>1) Can not be applied if the shelf margins are eroded and not preserved</li> <li>2) Measurements of shelf-margin progradation and aggradation can be time consuming</li> <li>3) Uncertainty may arise from the positioning of the shelf edge and the lower rollover point</li> </ol>

**Fig. 18.** Comparison of the two methods used in this paper to interpret the high-resolution seismic stratigraphic framework of the LBG within a sequence stratigraphic framework. Note that the elements of comparison presented here are applicable only for 3D seismic data and shelf-margin to basin-margin settings.

Muto and Steel, 1997; Neal and Abreu, 2009; Neal et al., 2016). However, changes in trajectory trends can be very subtle and the definition of sequence stratigraphic surfaces can remain difficult, particularly where the strata are mostly composed of normal regressive seismic sequences (i.e., *flat* and *rising shelf-edge trajectories*) and forced and transgressive seismic sequences are absent (i.e., *falling* and *backstepping shelf-edge trajectories*). Thus, using a combination of high-resolution seismic stratigraphy and quantitative analysis, the calculation of shelf-edge trajectory angles  $T_{se}$  and the generation of  $T_{se}$  curves can facilitate the determination of sequence boundaries, based on the objective recognition criteria of the accommodation succession method (Figs. 14 and 18). Therefore,  $T_{se}$  curve analysis may constitute a model-independent approach in the creation of a sequence stratigraphic framework without any *a priori* assumptions of sea-level or base-level curve

in predicting systems tract succession (e.g., Jervey, 1988; Posamentier and Vail, 1998; Schumm, 1993; Helland-Hansen and Gjelberg, 1994; Posamentier and Allen, 1999; Catuneanu, 2006). In this sense, the term “accommodation set” is preferred to systems tract as it relies directly on the geometry of the strata and not the position on a base-level or sea-level curve (Neal et al., 2016). Indeed, as outlined by Burgess et al. (2016), the use of a specific terminology should be free from any terms relative to a driving mechanisms (e.g., eustatic sea-level) because stratal geometries are non-unique and can be generated by the interplay of various mechanisms (Burgess and Prince, 2015).

The quantitative seismic stratigraphy workflow offers valuable insights into the development of sequence stratigraphic frameworks in shelf-slope-basin systems with an uncertainty reduced by: (1) highlighting minor

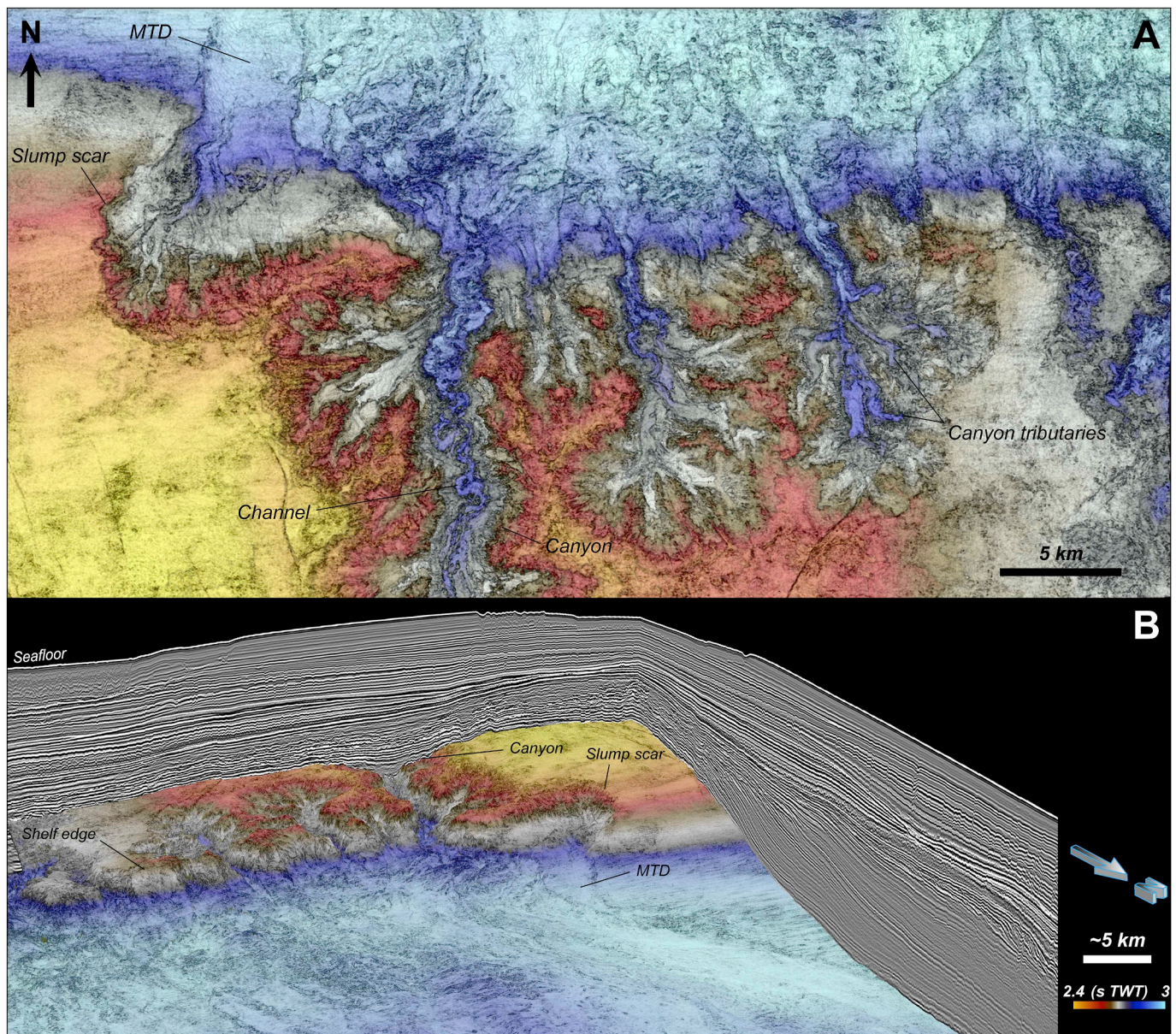


**Fig. 19.** Similarity attribute overlay by time-structure map (in s TWT) in map view (A) and three-dimensional view (B) showing the canyon at the base of the clinothem C16 of the *C. delicata* interval (see Figs. 3–6). This is the largest and deepest canyon developed within the LBG, feeding a mature, extensive and thick turbidite system. (B) shows the presence of numerous tributaries attached to the canyon and the presence along-strike of a large MTD associated with a slump scar on the shelf margin. Data courtesy of TGS.

changes in shelf-edge trajectory even though erosional truncations may not be present; (2) providing a higher resolution sequence stratigraphic framework; and (3) proposing a method reproducible by different interpreters using the same quantitative data analysis (Fig. 17). However, the main limitation of this method is the preservation of shelf margins (i.e., not eroded) as a prerequisite for the trajectory analysis (Fig. 18).

#### 6.1.2. Hierarchy of sequences: stratigraphic order and ranks

In establishing a sequence stratigraphic framework for a specific dataset, the key question is to determine which interpreted stratigraphic surfaces also have significance at a higher rank (i.e., lower order). The depositional sequence model does not allow the identification of lower-order sequence stratigraphic surfaces in an objective way, where any of the surfaces from the initial sequence stratigraphic framework could be a potential candidate (Fig. 18; Catuneanu et al., 2009). Only a few surfaces, based on the appreciation of the interpreter, can present characteristics facilitating their identification as regional sequence boundaries. For instance, the base of the clinothem C16 seems to constitute a major erosional unconformity that may

be interpreted as a regional event (i.e., regional sequence boundary) traceable across the basin (e.g., Fig. 12). In map view, the same horizon displays large-scale erosion and canyon development along the entire LBG margin, thus constituting a spatially and temporally significant event that could be linked to the accumulation of thick deep-water deposits, such as deep-water fans, in the basin (Figs. 12 and 19). This example highlights the predictive power of the depositional sequence model by identifying regional sequence boundaries likely associated with accumulation of thick sands in the basin (e.g., Posamentier et al., 1988; Posamentier and Vail, 1988).

The workflow proposed in this paper based on  $T_{se}$  curve analysis may provide a tool to objectively identify stratigraphic surfaces and sequences of lower order through recognition of patterns in the arrangement of higher order packages (Fig. 18). First, the clinothems represent the highest frequency, highest order (i.e., 5<sup>th</sup> order) and lowest rank packages identified (Figs. 3–6 and 17a). Trajectory analysis conducted for individual clinothems serve as a base for  $T_{se}$  curve analysis and definition of 4<sup>th</sup> order stratigraphic surfaces and sequences (Figs. 15 and 17b). Similarly, a trajectory analysis conducted for individual 4<sup>th</sup> order sequences may help identify 3<sup>rd</sup> order

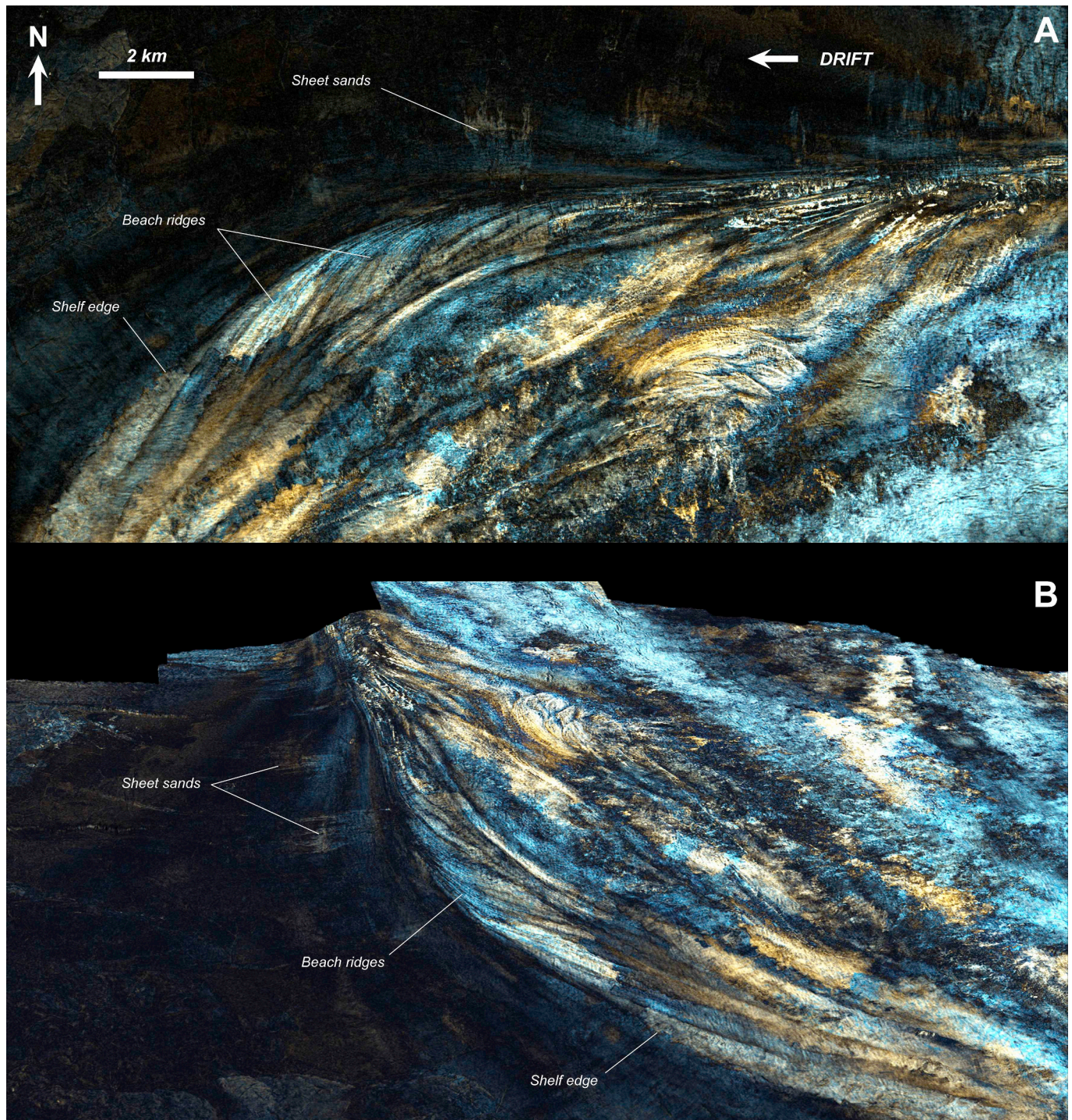


**Fig. 20.** Color-blended (RGB) spectral decomposition attribute in map view (A) and three-dimensional view (B) showing the LBG shelf margin within the clinothem C69 of the *B. reticulatum* sequence (see Figs. 3–6). Note the presence of extensive strandplains (i.e., stacked beach ridges) recording the activity of longshore currents drifting sediments from east to west along the paleoshoreline. Data courtesy of TGS. (For interpretation of the references to color in this figure legend, the reader is referred to the Web version of this article.)

stratigraphic surfaces and sequences (Figs. 16 and 17c).

Therefore, in a manner similar to the recent sequence stratigraphic approach of Ainsworth et al. (2018) for interpreting regressive-transgressive full or partial shelf transits (i.e., parasequences based on outcrop, well or core data), the clinothem, based on seismic data, represents the elementary building block of high-frequency sequences (*sensu* Zecchin and Catuneanu, 2013; Catuneanu and Zecchin, 2013) and constitutes the basis or anchor point for a quantitative-based workflow to develop sequence stratigraphic frameworks that include different orders and ranks of hierarchy (Fig. 18).

## 6.2. Controls on the high-frequency variability of stratigraphic sequences

The along-strike variability of the LBG stratigraphic sequences is expressed at high frequency through the: (1) lateral changes in shelf-edge trajectory types (Figs. 3–6 and Tables 1–4); (2) lateral variations in shelf-edge trajectory angles  $T_{se}$  in individual clinothems (Figs. 10a and 15; Table 5); (3) lateral switching of the locus of sedimentation at the shelf margin (Figs. 8 and 9); and (4) lateral variations in progradation rates  $R_p$  (Fig. 10b and Table 6). All these observations indicate that the rate of

accommodation creation and the rate of sediment supply (i.e.,  $\delta A/\delta S$  ratio) varied at high frequency, laterally and vertically, and strongly influenced the three-dimensional stratigraphic architecture of individual shelf-margin sequences.

### 6.2.1. Eustasy

Eustatic sea-level fluctuations and subsidence variations are the primary controls on the rate of accommodation creation (Jervey, 1988; Posamentier et al., 1988; Posamentier and Vail, 1988). The 4<sup>th</sup> order sequences interpreted from the trajectory analysis method give a cycle duration of ~100,000 yrs (seismic profiles BB', CC' and DD'), except for the seismic profile AA' where it is ~130,000 yrs (Fig. 15 and Tables 1–4). The predominance of the ~100,000 yrs periodicity suggests that the high-frequency sequences are climatically controlled (i.e., glacio-eustasy), because they match short-term Milankovitch cycle frequencies (i.e., short-term eccentricity cycles of ~100,000 yrs; Sames et al., 2016). Although the Cretaceous is known as a period of greenhouse climate (e.g., Huber et al., 2002; Littler et al., 2011), some studies have suggested that the Early Cretaceous had cooler greenhouse conditions with potentially small-scale glaciation events and ephemeral ice sheets developing at the poles (e.g., Stoll and Schrag, 1996; Bornemann et al., 2008; Price and Nunn, 2010; Sames et al., 2016; O'Brien et al., 2017).

Therefore, short-term glacio-eustatic sea-level variations (i.e., Milankovitch-type cycles) may have influenced the generation of high-frequency sequences within the LBG (Fig. 15 and Tables 1–4). Milankovitch-type short-term glacio-eustatic signals have been interpreted for Early Cretaceous strata around the world: e.g., the Maiolica Formation and Biancone Formation in Italy (Herbert, 1992; Mayer and Appel, 1999); lacustrine deposits of Bernissart in Belgium (Schnyder et al., 2009); the Vocontian Basin in France (Gréselle and Pittet, 2010); and the LHS carbonate system in Oman (Dujonquoy et al., 2018). Therefore, it is suggested here that climatically paced eustasy was the main driver of the changes in rates of accommodation creation at 4<sup>th</sup>–5<sup>th</sup> order in the LBG.

### 6.2.2. Sediment supply

Relative changes in sea level, driven by glacio-eustasy, homogeneously affected the shelf-margin sequences of the LBG, although the results show a significant along-strike variability in stratal architecture within each clinothem. This indicates that local changes in rates of sediment supply also played a key role in the high-frequency spatial variations, as highlighted in shelf-margin systems elsewhere (e.g., Schlager, 1993; Martinsen and Helland-Hansen, 1995; Madof et al., 2016). At high frequency, mechanisms that affect sediment supply may be allogenic and/or autogenic (e.g., Swift et al., 1991; Heller et al., 1993; Storms and Hampson, 2005; Kim et al., 2006; Catuneanu and Zecchin, 2013).

The main autogenic parameter to consider is the type of hydrodynamic processes at the shelf edge, specifically the relative importance of river, wave and tidal currents (Ainsworth et al., 2011; Olariu, 2014). Significant along-strike variability in the hydrodynamic regime along paleoshorelines within a single clinothem were identified in the LBG by Paumard et al. (accepted). It is inferred that the rate of sediment supply at any point along the shelf margin will directly relate to the controls exerted by the supply of sediment by rivers. For example, the western depocentre on the isopach map of the clinothem C38 (Figs. 3 and 8c) is interpreted as a shelf-edge delta (Paumard et al., accepted). In this case, a fluvial channel reached the shelf edge and led to high shelf-margin progradation rates  $R_p$  of ~40 km/Myr (seismic line AA'; Table 1). Considering shelf-margin progradation  $R_p$  as a proxy for the rates of sediment supply, fluvial processes are an important contributor to the variations in sediment supply at the shelf edge, and hence in the architecture of high-frequency sequences (e.g., Video S2).

A second significant autogenic parameter to consider is the activity of along-strike currents. In the LBG, coarse-grained sediments can be reworked along paleoshorelines by longshore drift currents (Paumard et al., accepted). Fig. 9 presents successive isopach maps from clinothems C67 to C70 showing the lateral accretion of the margin (Video S2). Moreover, attribute mapping within clinothem C69 displays extensive strandplains (i.e., stacked beach ridges) indicating that the lateral accretion of the margin in this case resulted from lateral transport of coarse-grained sediments (Fig. 20). Video S3 provides an overview of all the successive spectral decomposition attribute maps extracted from the HR 3D Geomodel of the *B. reticulatum* interval and show the westward development of the margin through beach ridges accretion.

Supplementary video related to this article can be found at <https://doi.org/10.1016/j.marpetgeo.2019.07.007>.

It is also inferred that fine-grained sediments may be transported offshore and reworked along the continental slope by along-slope and bottom currents in association with the longshore drift currents (Paumard et al., accepted). Both isopach maps from clinothems C42 and C44 display a zone of accumulation of sediments in the deep-water areas that seem “attached” to the depocentre in the east (Fig. 8d and e, respectively), consistent with the presence of mud belts (i.e., onlapping wedges) on the seismic cross-section (e.g., clinothem C42; Figs. 3 and 4).

Other autogenic controls can be considered to play a role in the lateral variations of sediment supply (e.g., Catuneanu and Zecchin, 2013; Hampson, 2016). However, discriminating allogenic from autogenic mechanisms remains difficult as both may operate contemporaneously (e.g., Muto et al., 2007, 2016; Ainsworth et al., 2017). Since the paleoshorelines of the LBG were typically located at the shelf edge, river avulsion and delta-lobe switching are two autogenic parameters that may have locally affected the distribution of sediments along the LBG margin (e.g., Coleman and Gagliano, 1964; Mohrig et al., 2000; Slingerland and Smith, 2004; Edmonds et al., 2009). Although these processes cannot be interpreted from seismic data in the LBG (i.e., resulting stratal stacking patterns below seismic resolution), autogenic processes were interpreted from wireline logs from the well Royal Oak-1 (Fig. 1b) in a recent study conducted by Ainsworth et al. (2018). Only shoreline autoretreat may be considered minor in the case of the LBG, which is a supply-dominated system, because the effectiveness of autoretreat diminishes under high sediment supply (Muto and Steel, 1997).

The location of fluvial feeder systems as a line source (e.g., clinothem C35; Fig. 8a) or point source (e.g., clinothem C38; Fig. 8c), the presence of longshore drift currents (e.g., clinothems C67 to C70; Fig. 9) and along-slope/bottom currents (e.g., clinothems C42 and C44; Figs. 7d and e, respectively), and the likely action of autogenic processes (e.g., fluvial channel avulsion), all represent controls on the local distribution and accumulation of sediments (Videos S1–S3). Even though high-frequency supply-driven cycles are recognized in the literature (e.g., Schwarz et al., 2016), it is suggested here that the lateral variability of the high-frequency stratigraphic sequences resulted from the complex interplay between sediment supply rates and eustatically-driven changes in rates of accommodation creation, coupled with lateral variations in subsidence rates in response to the active syn-rift tectonic setting (Paumard et al., 2018).

### 6.3. Controls on low-frequency variability of composite stratigraphic sequences

Within the *D. lobispinosum* interval, composite sequences identified display 4<sup>th</sup> to 3<sup>rd</sup> order cyclicity (~350,000 to 700,000 yrs; Fig. 16 and Tables 1–4). These scales of observation provide insight into low-frequency cycles and longer term  $\delta A/\delta S$  controls on development of shelf-margin composite sequences (Vail et al., 1991; Posamentier and Allen, 1999).

Composite sequences identified along seismic profile AA' present the longest duration cycles (i.e., ~700,000 yrs) and highest amplitude variations in shelf-edge trajectory angles  $T_{se}$  (from ~0 to 8° and *backstepping shelf-edge trajectories*; Fig. 16a and Table 1). Towards the east, amplitude and frequency of  $T_{se}$  variations show minor decreases and increases, respectively (Fig. 16b–d and Tables 2–4). For example, composite sequences identified along seismic profile DD' have the shortest duration cyclicity (i.e., ~350,000 yrs) and lowest amplitude variations in shelf-edge trajectory angles  $T_{se}$  (from ~–2 to 2°; Fig. 16d and Table 4).

Interestingly, cyclicity of the composite sequences identified along seismic profile DD' fits the long-term Milankovitch band cycle frequencies (i.e., long-term eccentricity cycles of ~400,000 yrs; Boullia et al., 2011; Wendler et al., 2014; Sames et al., 2016). During the Early Cretaceous, most of the depositional systems interpreted to record Milankovitch-type short-term cyclicity have also recorded the long-term Milankovitch eccentricity cycles of ~400,000 yrs (e.g., Schnyder et al., 2009; Gréselle and Pittet, 2010; Dujonquoy et al., 2018).

Studies commonly highlight an asymmetrically shaped sea-level curve with rapid sea-level rise, due to rapid ice-sheet melting, and slow sea-level fall, due to long ice-sheet waxing (e.g., Gréselle and Pittet, 2010; Dujonquoy et al., 2018). The shape of the  $T_{se}$  curve for composite sequences along seismic profile DD' display the same asymmetry with short PA accommodation sets followed by longer APD accommodation sets (Fig. 16d and Table 4). This observation suggests that rapid sea-level rises controlled



**Fig. 21.** Proposed idealized workflow towards 3D sequence stratigraphy using 3D seismic data in shelf-margin to basin-margin settings. Quantitative 3D seismic stratigraphy may represent the first opportunity in this direction because seismic data are interpreted in a 3D environment taking into account the full lateral and vertical variability of the data when defining seismic unconformities and sequences (Paumard et al., 2019). However, quantitative analysis and definition of sequence stratigraphic surfaces are conducted on 2D depositional-dip profiles, hence the need to develop of new tools and methods to consider the 3D variability of the data, based on quantitative analysis, when assigning a sequence stratigraphic significance to a surface.

increased rates of accommodation creation (i.e., progradational to aggradational trend), overprinting the subsidence signal, whereas slow sea-level falls were associated with decreasing rates of accommodation creation (i.e., aggradational to progradational, possibly degradational trend; Fig. 16d and Table 4). Therefore, it is argued that at this scale of observation, eustatic sea-level fluctuations strongly influenced the stratigraphic architecture of shelf-margin sequences in the eastern part of the Investigator Depocentre (Fig. 1b). In contrast, towards the western part of the Investigator Depocentre (i.e., seismic line AA'; Fig. 1b), no long-term Milankovitch-type cycle is visible, suggesting that tectonically-controlled subsidence overprinted the eustatic signal and controlled the rates of accommodation creation, which is consistent with the high amplitude variations in  $T_{se}$  observed (Fig. 16a and Table 1) and with a much higher thickness of sediments observed in the western part of the Investigator Depocentre (Fig. 7c). Similar trends can be observed in the Upper Campanian Cozzette Sandstone (Book Cliffs) where tectonic drivers are interpreted to be responsible for lateral changes in thicknesses and stratal stacking patterns due to periods of tilting and renewed accommodation creation, which directly impacted nearshore sediment accumulation and stratigraphic architecture (Madof et al., 2015).

Overall, these results are consistent with the interpretations of 3<sup>rd</sup> order packages from Paumard et al. (2018). Indeed, the LBG development during the *D. lobispinosum* interval is associated with high rates of sediment supply across the entire basin, whereas a pulse of subsidence is recognized in the Investigator Depocentre and the Exmouth Depocentres (Paumard et al., 2018). This pulse of subsidence may explain the higher rates of accommodation creation towards the western part of the study area, located in the middle of the Investigator Depocentre, consistent with an overall aggradational stratal stacking pattern of the LBG during this period (e.g., seismic profile AA'; Figs. 1b and 3). In the eastern part of the study area located on the border of the Investigator Depocentre and Exmouth Terrace, subsidence did not overprint the eustatic signal, consistent with an overall progradational stratal stacking pattern of the LBG during this time (e.g., seismic profile DD'; Figs. 1b and 6).

#### 6.4. Towards 3D sequence stratigraphy?

Despite more than 30 years of development, integration of lateral variability in siliciclastic systems remains a problematic aspect of sequence stratigraphy applied to shelf-margin settings (e.g., Martinsen and Helland-Hansen, 1995; Madof et al., 2016). For example, none of the sequence stratigraphic approaches used in this paper considers the along-strike variability of the clinothems in establishing a sequence stratigraphic framework (Fig. 18). Indeed, interplay between allocyclic and autocyclic controls strongly influenced the high-frequency stratigraphic architecture of the LBG, resulting in the identification of “local” sequence boundaries (i.e., cannot be tracked extensively laterally) along individual dip-oriented depositional profiles (e.g., Fig. 15). The problem highlighted here relates to the observation that sequence stratigraphic analyses are usually conducted on 2D cross-sections, that may lead to highly variable sequence stratigraphic interpretations along strike in the same system (e.g., Figs. 11 and 12). Therefore, the main challenge in further improving sequence stratigraphy will be the integration of a third dimension to fully consider the variability of depositional systems, not only in time, but as well in space (Burgess, 2016; Burgess et al., 2016).

The focus of this paper is on the application of observation-based, data-driven approaches, supported by quantitative analysis, and their application to sequence stratigraphic analysis (Figs. 17 and 18). Usually, the quantitative elements of sequence stratigraphy take the form of either numerical forward modelling (e.g., Burgess et al., 2006; Burgess and Prince, 2015; Muto et al., 2016) or physical modelling experiments (e.g., Kim et al., 2006; Muto et al., 2007), and typically focus on the controls on stratal architecture across temporal and spatial scales (e.g., Burgess and Steel, 2017).

The recent TSF sequence stratigraphic analysis method developed by Ainsworth et al. (2018) is an early attempt to integrate a quantitative component in building a sequence stratigraphic framework. This approach is based on the study of parasequence thicknesses and sandstone fractions based on vertical 1D data (e.g., core and well logs) and lacking integration of lateral information to define sequence boundaries, unless the results can be correlated laterally with several data points. However, this method provides an interesting calibration tool if well data can be integrated with seismic data and/or constitutes a standalone quantitative method in cases of poor seismic resolution (Ainsworth et al., 2018).

As highlighted in recent studies (e.g., Dujoncquoy et al., 2018), the accommodation succession method is the best practical and descriptive tool to conduct sequence stratigraphic analysis by considering the dynamic evolution of the strata in a physical stratigraphic framework (Neal and Abreu, 2009; Neal et al., 2016). Adding the trajectory analysis component of Helland-Hansen and Hampson (2009) enables the interpreter to add a degree of objectivity to define sequence boundaries with reduced uncertainty (Figs. 14 and 18). With the resolution of seismic datasets enabling interpretation of high-resolution seismic sequences, conducting a quantitative analysis in 3D, rather than on 2D dip-oriented depositional profiles, may well be the key to unlocking the application of 3D sequence stratigraphy in shelf-slope-basin systems (Fig. 21).

Quantitative 3D seismic stratigraphy may be a first step in this direction, among others (e.g., Madof et al., 2016; Burgess and Steel, 2017; Ainsworth et al., 2018), as the identification of key stratigraphic surfaces is conducted in a 3D environment, thus taking into account the variability of the data in a more objective way (Paumard et al., 2019). However, new tools and methods will need to be developed to conduct 3D quantitative and trajectory analysis in order to select seismic unconformities that could be upgraded to the rank of sequence boundary across the different levels of sequence stratigraphy hierarchy (Fig. 21).

## 7. Conclusion

This paper presents the results of comparing two approaches to developing a sequence stratigraphic framework and their potential to highlight the controls on the variability of shelf-margin systems through space and time. An inherent problem in sequence stratigraphy is the limitations in having objective ways to establish sequence stratigraphic frameworks that are not solely based on the decisions of stratigraphers. Thus, most interpretations are likely to include some interpreter bias to select key sequence stratigraphic surfaces (e.g., sequence boundaries).

In contrast to more classical approaches, quantitative 3D seismic stratigraphy helps define high-resolution seismic sequences (i.e., clinothems) that may be used for quantitative analysis and, particularly, for the calculation of shelf-edge trajectory angles  $T_{se}$  in individual clinothems. Using clinothems that represent the highest order (i.e., lowest rank) resolvable on seismic data, high-frequency  $T_{se}$  curves can be generated. Following the accommodation succession method, sequence stratigraphic surfaces can be picked directly on the curve based on trajectory trends and stratal stacking patterns to define accommodation succession sets. Thus, this approach offers a data-driven and more objective workflow to define sequence stratigraphic frameworks in shelf-slope-basin systems with reduced uncertainty by: (1) highlighting subtle changes in trajectory trends even though major erosional truncations (and related unconformities) are not present; (2) providing a higher resolution sequence stratigraphic framework; and (3) proposing a method that has high potential to be reproducible by interpreters based on quantitative data analysis. Moreover, conducting the same workflow within individual sequences results in the generation of lower-frequency  $T_{se}$  curves and definition of lower-order stratigraphic surfaces and sequences.

Quantitative 3D seismic stratigraphy constitutes the basis for a trajectory-based workflow to define high-resolution sequence stratigraphic

frameworks across different orders and hierarchical ranks. In contrast, a more traditional approach may be preferred where shelf margins are not preserved because of significant erosional truncations and/or limited time available for analysis given that quantitative analysis can be time-consuming.

Within the LBG, the along-strike variability of stratigraphic sequences has here been quantified through the measurement of the lateral: (1) changes in shelf-edge trajectory types and angles ( $T_{se}$ ) in individual sequences at 3<sup>rd</sup> to 5<sup>th</sup> stratigraphic orders; (2) switching of the locus of sedimentation at the shelf margin; and (3) variations in shelf-margin progradation rates  $R_p$ . This paper documents the high-frequency interplay between short-term glacio-eustasy (i.e., Milankovitch eccentricity cycles of ~100,000 yrs) and sediment supply (locus of fluvial sediment supply along the margin) as it has impacted the three-dimensional stratigraphic architecture of the LBG.

Local variations in sediment supply were generated by the: (1) distribution of fluvial feeder systems along shelf margins; (2) activity of long-shore drift currents; and (3) activity of along-slope and bottom currents. The composite sequences defined in this study reflect the impact of longer-term controls on the LBG depositional systems. During the *D. lobispinosum* interval (142.3–140.9 Ma), under supply-dominated conditions, tectonic subsidence controlled the stratigraphic architecture of the LBG in the Investigator Depocentre, whereas outside areas of active subsidence, long-term glacio-eustatic sea-level fluctuations (i.e., Milankovitch long-term eccentricity cycles of ~400,000 yrs) exerted more control.

Trajectory analysis represents the best observation-based, data-driven practical tool for seismic/sequence stratigraphic analysis that considers the dynamic evolution of the strata. Quantitative 3D seismic stratigraphy, including lateral variability when identifying seismic stratigraphic surfaces, is potentially capable of bridging the gap between 3D seismic stratigraphy and 3D sequence stratigraphy. However, as in any sequence stratigraphic approach, this workflow is limited by its dimensionality because both the quantitative analysis and definition of sequence stratigraphic surfaces are conducted on 2D seismic cross-sections. Thus, there is a step missing in establishing 3D sequence stratigraphic frameworks. One direction for future research is the creation of new tools for quantitative analysis of the strata at various orders in 3D.

This study emphasizes the combination of broad coverage, high-resolution 3D seismic data with the use of advanced interpretation software to provide unprecedented insights into the lateral and vertical variability of shelf-margin depositional systems through time. Thus, the development of more powerful tools to extract this information (i.e., quantitative 3D seismic stratigraphy) may help build sequence stratigraphic workflows that more fully exploit these data. The reliability of quantitative 3D seismic stratigraphy, which is observation-based and data-driven, promotes the opportunity for reproducible results by different stratigraphers. Therefore, one of the future challenges of sequence stratigraphy will be to fill the gap between quantitative 3D seismic stratigraphy and 3D sequence stratigraphy, that incorporates the variability of 3D seismic datasets located at shelf margins, with the aim of improving the prediction of facies relationships (i.e., source, reservoir, seal distribution) and stratal geometry of siliciclastic depositional systems in time and space.

## Acknowledgements

We thank Chevron Australia Pty. Ltd. for funding this research project. Victorien Paumard received a postgraduate scholarship from the University of Western Australia (UWA), and additional funding support from the AAPG Grant-in-Aid Program, ASEG Research Foundation and School of Earth Sciences (UWA). We are sincerely grateful to TGS for providing the Mary Rose 3D seismic dataset as well as giving permission to publish these results. We are also indebted to Eliis for providing the PaleoScan™ software. We wish to thank Ron Steel, Stephen Hubbard and Tor Somme for providing preliminary comments on this manuscript in Victorien Paumard's PhD thesis. We are thankful to the journal reviewers Andrew Madof and Boyan Vakarelov for their thoughtful comments on this manuscript. We are also grateful to Istvan Csato for handling the publication of this manuscript.

## References

Ainsworth, R.B., McArthur, J.B., Lang, S.C., Vonk, A.J., 2018. Quantitative sequence stratigraphy. *Am. Assoc. Petrol. Geol. Bull.* 102, 1913–1939.

- Ainsworth, R.B., Vakarelov, B.K., MacEachern, J.A., Rarity, F., Lane, T.I., Nanson, R.A., 2017. Anatomy of a shoreline regression: implication for the high-resolution stratigraphic architecture of deltas. *J. Sediment. Res.* 87, 425–459.
- Ainsworth, R.B., Vakarelov, B.K., Nanson, R.A., 2011. Dynamic spatial and temporal prediction of changes in depositional processes on clastic shorelines: toward improved subsurface uncertainty reduction and management. *Am. Assoc. Petrol. Geol. Bull.* 95, 267–297.
- Aporthe, M., 1988. Cenozoic depositional history of the North West shelf. In: Purcell, P.G., Purcell, R.R. (Eds.), *The North West Shelf, Australia. Proceedings of the Petroleum Exploration Society of Australia Symposium*, Perth, WA, pp. 55–84.
- Arditto, P.A., 1993. Depositional sequence model for the post-barrow Group neocomian succession, Barrow and Exmouth Sub-basins, western Australia. *APEA J.* 33, 151–160.
- Armitage, J.J., Duller, R.A., Whittaker, A.C., Allen, P.A., 2011. Transformation of tectonic and climatic signals from source to sedimentary archive. *Nat. Geosci.* 4, 231–235.
- Audley-Charles, M.G., Ballantyne, P.D., Hall, R., 1988. Mesozoic-Cenozoic rift-drift sequence of Asian fragments from Gondwanaland. *Tectonophysics* 155, 317–330.
- Barber, P.M., 1988. The Exmouth Plateau deep water frontier: a case history. In: Purcell, P.G., Purcell, R.R. (Eds.), *The North West Shelf, Australia. Proceedings of the Petroleum Exploration Society of Australia Symposium*, pp. 173–187.
- Bhattacharya, J.P., Abreu, V., 2016. Wheeler's confusion and the seismic revolution: how geophysics saved stratigraphy. *Sediment. Rec.* 14, 4–11.
- Borel, G.D., Stampfli, G.M., 2002. Geohistory of the North West shelf: a tool to assess the Palaeozoic and Mesozoic motion of the Australian plate. In: Keep, M., Moss, S.J. (Eds.), *The Sedimentary Basins of Western Australia 3. Proceedings of the Petroleum Exploration Society of Australia Symposium*, pp. 119–128.
- Bornemann, A., Norris, R.D., Friedrich, O., Beckmann, B., Schouten, S., Sinninghe Damste, J.S., Vogel, J., Hofmann, P., Wagner, T., 2008. Isotopic evidence for glaciation during the Cretaceous supergreenhouse. *Science* 319, 189–193.
- Boullia, S., Galbrun, B., Miller, K.G., Pekar, S.F., Browning, J.V., Laskar, J., Wright, J.D., 2011. On the origin of Cenozoic and Mesozoic “third-order” eustatic sequences. *Earth Sci. Rev.* 109, 94–112.
- Bradshaw, J., Sayers, J., Bradshaw, M., Kneale, R., Ford, C., Spencer, L., Lisk, M., 1998. Palaeogeography and its impact on the petroleum systems of the North West shelf, Australia. In: Purcell, P.G., Purcell, R.R. (Eds.), *The Sedimentary Basins of Western Australia 2. Proceedings of the Petroleum Exploration Society of Australia Symposium*, pp. 95–121.
- Brown, L.F., Fisher, W.L., 1977. Seismic stratigraphic interpretation of depositional systems: examples from Brazilian rift and pull apart basins. In: Payton, C.E. (Ed.), *Seismic Stratigraphy - Applications to Hydrocarbon Exploration*, vol. 26. AAPG Memoir, pp. 213–248.
- Burgess, P.M., 2016. The future of the sequence stratigraphy paradigm: dealing with a variable third dimension. *Geology* 44, 335–336.
- Burgess, P.M., Allen, P.A., Steel, R.J., 2016. Introduction to the future of sequence stratigraphy: evolution or revolution? *J. Geol. Soc. Lond.* 173, 801–802.
- Burgess, P.M., Lammers, H., Van Oosterhout, C., Granjeon, D., 2006. Multivariate sequence stratigraphy: tackling complexity and uncertainty with stratigraphic forward modeling, multiple scenarios, and conditional frequency maps. *Am. Assoc. Petrol. Geol. Bull.* 90, 1883–1901.
- Burgess, P.M., Prince, G.D., 2015. Non-unique stratal geometries: implications for sequence stratigraphic interpretations. *Basin Res.* 27, 351–365.
- Burgess, P.M., Steel, R.J., 2017. How to interpret, understand, and predict stratal geometries using stratal-control spaces and stratal-control-space trajectories. *J. Sediment. Res.* 87, 325–337.
- Carter, R.M., Abbott, S.T., Fulthorpe, C.S., Heywick, D.W., Henderson, R.A., 1991. Application of global sea-level and sequence-stratigraphic models in southern hemisphere Neogene strata. In: Macdonald, D.I.M. (Ed.), *Sedimentation, Tectonics and Eustasy: Sea-Level Changes at Active Margins*, vol. 12. IAS Special Publication, pp. 41–65.
- Castelltort, S., Van Den Driessche, J., 2003. How plausible are high-frequency sediment supply-driven cycles in the stratigraphic record? *Sediment. Geol.* 157, 3–13.
- Catuneanu, O., 2006. Principles of Sequence Stratigraphy. Elsevier, Amsterdam.
- Catuneanu, O., 2002. Sequence stratigraphy of clastic systems: concepts, merits, and pitfalls. *J. Afr. Earth Sci.* 35, 1–43.
- Catuneanu, O., 2019. Model-independent sequence stratigraphy. *Earth Sci. Rev.* 188, 312–388.
- Catuneanu, O., Abreu, V., Bhattacharya, J.P., Blum, M.D., Dalrymple, R.W., Eriksson, P.G., Fielding, C.R., Fisher, W.L., Galloway, W.E., Gibling, M.R., Giles, K. a., Holbrook, J.M., Jordan, R., Kendall, C.G.S.C., Macurda, B., Martinsen, O.J., Miall, A.D., Neal, J.E., Nummedal, D., Pomar, L., Posamentier, H.W., Pratt, B.R., Sarg, J.F., Shanley, K.W., Steel, R.J., Strasser, A., Tucker, M.E., Winker, C., 2009. Towards the standardization of sequence stratigraphy. *Earth Sci. Rev.* 92, 1–33.
- Catuneanu, O., Galloway, W.E., Kendall, C.G.S.C., Miall, A.D., Posamentier, H.W., Strasser, A., Tucker, M.E., 2011. Sequence stratigraphy: methodology and nomenclature. *Newslett. Stratigr.* 44, 173–245.
- Catuneanu, O., Zecchin, M., 2013. High-resolution sequence stratigraphy of clastic shelves II: controls on sequence development. *Mar. Pet. Geol.* 39, 26–38.
- Catuneanu, O., Zecchin, M., 2016. Unique vs. non-unique stratal geometries: relevance to sequence stratigraphy. *Mar. Pet. Geol.* 78, 184–195.
- Christie-Blick, N., 1991. Onlap, offlap, and the origin of unconformity-bounded depositional sequences. *Mar. Geol.* 97, 35–56.
- Christie-Blick, N., Pekar, S.F., Madof, A.S., 2007. Is there a role for sequence stratigraphy in chronostratigraphy? *Stratigraphy* 4, 217–229.
- Coleman, J.M., Gagliano, S.M., 1964. Cyclic sedimentation in the Mississippi River delta plain. *Trans. Gulf Coast Assoc. Geol. Soc.* 14, 67–80.
- Driscoll, N.W., Karner, G.D., 1998. Lower crustal extension across the Norther Carnarvon

- Basin, Australia: evidence for an eastward dipping detachment. *J. Geophys. Res.* 103, 4975–4991.
- Drummond, C.N., Wilkinson, B.H., 1996. Stratal thickness frequencies and the prevalence of orderedness in stratigraphic sequences. *J. Geol.* 104, 1–18.
- Dujoncqoy, E., Grelaud, C., Razin, P., Imbert, P., Buchem, F., Van, Dupont, G., Le Bec, A., 2018. Seismic stratigraphy of a Lower Cretaceous prograding carbonate platform (Oman) and implications for the eustatic sea-level curve. *Am. Assoc. Petrol. Geol. Bull.* 102, 509–543.
- Edmonds, D.A., Hoyal, D.C.J.D., Sheets, B.A., Slingerland, R.L., 2009. Predicting delta avulsions: implications for coastal wetland restoration. *Geology* 37, 759–762.
- Embry, A.F., 1995. Sequence boundaries and sequence hierarchies: problems and proposals. In: In: Steel, R.J., Felt, V.L., Johannessen, E.P., Mathieu, C. (Eds.), *Sequence Stratigraphy on the Northwest European Margin*, vol. 5. Norwegian Petroleum Society Special Publication, pp. 1–11.
- Galloway, W.E., 1989. Genetic stratigraphic sequences in basin analysis I: architecture and genesis of flooding-surface bounded depositional units. *Am. Assoc. Petrol. Geol. Bull.* 73, 125–142.
- Gartrell, A., Torres, J., Dixon, M., Keep, M., 2016. Mesozoic rift onset and its impact on the sequence stratigraphic architecture of the Northern Carnarvon Basin. *APPEA J.* 56, 143–158.
- Gréselle, B., Pittet, B., 2010. sea-level reconstructions from the Peri-Vocontian zone (South-east France) point to Valanginian glacio-eustasy. *Sedimentology* 57, 1640–1684.
- Hampson, G.J., 2016. Towards a sequence stratigraphic solution set for autogenic processes and allogenic controls: upper Cretaceous strata, Book Cliffs, Utah, USA. *J. Geol. Soc. Lond.* 173, 817–836.
- Helland-Hansen, W., 2009. Towards the standardization of sequence stratigraphy. *Earth Sci. Rev.* 94, 95–97.
- Helland-Hansen, W., Gjelberg, J.G., 1994. Conceptual basis and variability in sequence stratigraphy: a different perspective. *Sediment. Geol.* 92, 31–52.
- Helland-Hansen, W., Hampson, G.J., 2009. Trajectory analysis: concepts and applications. *Basin Res.* 21, 454–483.
- Helland-Hansen, W., Martinsen, O.J., 1996. Shoreline trajectories and sequences: description of variable depositional-dip scenarios. *J. Sediment. Res.* 66, 670–688.
- Heller, P.L., Burns, B.A., Marzo, M., 1993. Stratigraphic solution sets for determining the roles of sediment supply, subsidence, and sea level on transgressions and regressions. *Geology* 21, 747–750.
- Henriksen, S., Hampson, G.J., Helland-Hansen, W., Johannessen, E.P., Steel, R.J., 2009. Shelf edge and shoreline trajectories, a dynamic approach to stratigraphic analysis. *Basin Res.* 21, 445–453.
- Herbert, T.D., 1992. Paleomagnetic calibration of Milankovitch cyclicity in lower cretaceous sediments. *Earth Planet. Sci. Lett.* 112, 15–28.
- Hocking, R.M., 1988. Regional geology of the northern Carnarvon Basin. In: Purcell, P.G., Purcell, R.R. (Eds.), *The North West Shelf, Australia*. Proceedings of the Petroleum Exploration Society of Australia Symposium, pp. 97–114.
- Hocking, R.M., 1985. Revised Stratigraphic Nomenclature in the Carnarvon Basin. W.A. Geological Survey of Western Australia.
- Huber, B.T., Norris, R.D., Macleod, K.G., 2002. Deep-sea paleotemperature record of extreme warmth during the Cretaceous. *Geology* 30, 123–126.
- Hunt, D., Tucker, M.E., 1992. Stranded parasequences and the forced regressive wedge systems tract: deposition during base-level fall. *Sediment. Geol.* 81, 1–9.
- Jervey, M.T., 1988. Quantitative geological modeling of siliciclastic rock sequences and their seismic expression. In: In: Wilgus, C.K., Hastings, B.S., Kendall, C.G.S.C., Posamentier, H.W., Ross, C.A., Van Wagoner, J.C. (Eds.), *Sea-Level Changes - an Integrated Approach*, vol. 42. SEPM Special Publication, pp. 47–69.
- Jitmahantakul, S., McClay, K., 2013. Late triassic – Mid-Jurassic to neogene extensional fault systems in the Exmouth Sub-basin, northern Carnarvon Basin, North West shelf, western Australia. In: Keep, M., Moss, S.J. (Eds.), *The Sedimentary Basins of Western Australia 4*. Proceedings of the Petroleum Exploration Society of Australia Symposium, pp. 1–22.
- Jones, G.E.D., Hodgson, D.M., Flint, S.S., 2015. Lateral variability in clinoform trajectory, process regime, and sediment dispersal patterns beyond the shelf-edge rollover in exhumed basin margin-scale clinoforms. *Basin Res.* 27, 657–680.
- Kim, W., Paola, C., Voller, V.R., Swenson, J.B., 2006. Experimental measurement of the relative importance of controls on shoreline migration. *J. Sediment. Res.* 76, 270–283.
- Kirk, R.B., 1985. A seismic stratigraphic case history in the eastern Barrow Subbasin, North West Shelf, Australia: chapter 11. In: In: Berg, O.R., Woolverton, D.G. (Eds.), *Seismic Stratigraphy II: an Integrated Approach to Hydrocarbon Exploration*, vol. 39. AAPG Memoir, pp. 183–207.
- Kopsen, E., McGann, G., 1985. A review of the hydrocarbon habitat of the eastern and central Barrow - Dampier Sub-basin, Western Australia. *APEA J.* 25, 154–176.
- Laugier, F.J., Plink-Björklund, P., 2016. Defining the shelf edge and the three-dimensional shelf edge to slope facies variability in shelf-edge deltas. *Sedimentology* 63, 1280–1320.
- Littler, K., Robinson, S.A., Bown, P.R., Nederbragt, A.J., Pancost, R.D., 2011. High sea-surface temperatures during the early cretaceous epoch. *Nat. Geosci.* 4, 169–172.
- Longley, I.M., Buessenschuett, C., Clydsdale, L., Cubitt, C.J., Davis, R.C., Johnson, M.K., Marshall, N.M., Murray, A.P., Somerville, R., Spry, T.B., Thompson, N.B., 2002. The North West shelf of Australia – a worldwide perspective. In: Keep, M., Moss, S. (Eds.), *The Sedimentary Basins of Western Australia 3*. Proceedings of the Petroleum Exploration Society of Australia Symposium, pp. 27–88.
- Madof, A.S., Christie-Blick, N., Anders, M.H., 2015. Tectonically controlled nearshore deposition: cozzette sandstone, book Cliffs, Colorado. U.S.A. *J. Sediment. Res.* 85, 459–488.
- Madof, A.S., Harris, A.D., Connell, S.D., 2016. Nearshore along-strike variability: is the concept of the systems tract unhinged? *Geology* 44, 315–318.
- Madof, A.S., Harris, A.D., Baumgardner, S.E., Sadler, P.M., Laugier, F., Christie-Blick, N., 2019. Stratigraphic aliasing and the transient nature of deep-water depositional sequences: revisiting the Mississippi Fan. *Geology* 47, 545–549.
- Marin, D., Escalona, A., Sliwi, K.K., Nohr-hansen, H., Mordasova, A., 2017. Sequence stratigraphy and lateral variability of Lower Cretaceous clinoforms in the south-western Barents Sea. *Am. Assoc. Petrol. Geol. Bull.* 101, 1487–1517.
- Marshall, N.G., Lang, S.C., 2013. A new sequence stratigraphic framework for the North West Shelf, Australia. In: Keep, M., Moss, S.J. (Eds.), *The Sedimentary Basins of Western Australia 4*. Proceedings of the Petroleum Exploration Society of Australia Symposium, pp. 1–32.
- Martinsen, O.J., Helland-Hansen, W., 1995. Strike variability of clastic depositional systems: does it matter for sequence-stratigraphic analysis? *Geology* 23, 439–442.
- Martins-Neto, M.A., Catuneanu, O., 2010. Rift sequence stratigraphy. *Mar. Pet. Geol.* 27, 247–253.
- Mayer, H., Appel, E., 1999. Milankovitch cyclicity and rock-magnetic signatures of palaeoclimatic change in the early cretaceous Biancone Formation of the southern Alps, Italy. *Cretac. Res.* 20, 189–214.
- Metcalfe, I., 2013. Gondwana dispersion and Asian accretion: tectonic and palaeogeographic evolution of eastern Tethys. *J. Asian Earth Sci.* 66, 1–33.
- Miall, A.D., 2010. *The Geology of Stratigraphic Sequences*, second ed. Springer-Verlag, Berlin.
- Miall, A.D., 2016. The valuation of unconformities. *Earth Sci. Rev.* 163, 22–71.
- Mitchum, R.M., Vail, P.R., 1977. Seismic stratigraphy and global changes of sea level, part 7: seismic stratigraphic interpretation procedure. In: In: Payton, C.E. (Ed.), *Seismic Stratigraphy - Applications to Hydrocarbon Exploration*, vol. 26. AAPG Memoir, pp. 135–143.
- Mitchum, R.M., Vail, P.R., Sangree, J.B., 1977a. Seismic stratigraphy and global changes of sea level, part 6: stratigraphic interpretation of seismic reflection patterns in depositional sequences. In: In: Payton, C.E. (Ed.), *Seismic Stratigraphy - Applications to Hydrocarbon Exploration*, vol. 26. AAPG Memoir, pp. 117–133.
- Mitchum, R.M., Vail, P.R., Thompson, S., 1977b. Seismic stratigraphy and global changes of sea level, part 2: the depositional sequence as a basic unit for stratigraphic analysis. In: In: Payton, C.E. (Ed.), *Seismic Stratigraphy - Applications to Hydrocarbon Exploration*, vol. 26. AAPG Memoir, pp. 53–62.
- Mitchum, R.M., Van Wagoner, J.C., 1991. High-frequency sequences and their stacking patterns: sequence-stratigraphic evidence of high-frequency eustatic cycles. *Sediment. Geol.* 70, 131–160.
- Mohrig, D., Heller, P.L., Paola, C., Lyons, W.J., 2000. Interpreting avulsion process from ancient alluvial sequences: Guadalope-Matarranya system (northern Spain) and Wasatch Formation (western Colorado). *Geol. Soc. Am. Bull.* 112, 1787–1803.
- Muto, T., Steel, R.J., 1997. Principles of regression and transgression: the nature of the interplay between accommodation and sediment supply. *J. Sediment. Res.* 67, 994–1000.
- Muto, T., Steel, R.J., 1992. Retreat of the front in a prograding delta. *Geology* 20, 967–970.
- Muto, T., Steel, R.J., 2002. Role of autoretreat and A/S changes in the understanding of deltaic shoreline trajectory: a semi-quantitative approach. *Basin Res.* 14, 303–318.
- Muto, T., Steel, R.J., Burgess, P.M., 2016. Contributions to sequence stratigraphy from analogue and numerical experiments. *J. Geol. Soc. Lond.* 173, 837–844.
- Muto, T., Steel, R.J., Swenson, J.B., 2007. Autostratigraphy: a framework norm for genetic stratigraphy. *J. Sediment. Res.* 77, 2–12.
- Neal, J.E., Abreu, V., Bohacs, K.M., Feldman, H.R., Pederson, K.H., 2016. Accommodation succession ( $\delta A/\delta S$ ) sequence stratigraphy: observational method, utility and insights into sequence boundary formation. *J. Geol. Soc. Lond.* 173, 803–816.
- Neal, J., Abreu, V., 2009. Sequence stratigraphy hierarchy and the accommodation succession method. *Geology* 37, 779–782.
- O'Brien, C.L., Robinson, S.A., Pancost, R.D., Sinnighe Damste, J.S., Schouten, S., Lunt, D.J., Alsenz, H., Bornemann, A., Bottini, C., Brassell, S.C., Farnsworth, A., Forster, A., Huber, B.T., Inglis, G.N., Jenkyns, H.C., Linnert, C., Littler, K., Markwick, P., Mcanena, A., Mutterlose, J., Naafs, B.D.A., Püttmann, W., Sluijs, A., van Helmond, N.A.G.M., Vellekoop, J., Wagner, T., Wrobel, N.E., 2017. Cretaceous sea-surface temperature evolution: constraints from TEX86 and planktonic foraminiferal oxygen isotopes. *Earth Sci. Rev.* 172, 224–247.
- Olariu, C., 2014. Autogenic process change in modern deltas. In: Martinus, A.W., Ravnas, R., Howell, J.A., Steel, R.J., Wonham, J.P. (Eds.), *Lessons from Depositional Systems to Sedimentary Successions on the Norwegian Continental Margin*. John Wiley, Chichester, United Kingdom, pp. 149–166.
- Patruno, S., Hampson, G.J., Jackson, C.A.-L., 2015. Quantitative characterisation of deltaic and subaqueous clinoforms. *Earth Sci. Rev.* 142, 79–119.
- Paumard, V., 2018. Shelf-margin Architecture, Sediment Partitioning and Shallow- to Deep-Water Reservoir Distribution in the Barrow Group (Northern Carnarvon Basin, North West Shelf, Australia): Insights from Quantitative 3D Seismic Stratigraphy. PhD Thesis. The University of Western Australia, pp. 395.
- Paumard, V., Bourget, J., Payenberg, T., Ainsworth, R.B., George, A.D., Lang, S., Posamentier, H.W., Peyrot, D., 2018. Controls on shelf-margin architecture and sediment partitioning during a syn-rift to post-rift transition: insights from the Barrow Group (northern Carnarvon Basin, North West shelf, Australia). *Earth Sci. Rev.* 177, 643–677.
- Paumard, V., Bourget, J., Durot, B., Lacaze, S., Payenberg, T., George, A.D., Lang, S., 2019. Full-volume 3D Seismic Interpretation Methods: A New Step towards High-Resolution Seismic Stratigraphy. *Interpretation* 7, B33–B47.
- Paumard, V., Bourget, J., Payenberg, T., George, A.D., Ainsworth, R.B., Lang, S., Posamentier, H.W., n.d. Controls on deep-water sand delivery beyond the shelf edge: accommodation, sediment supply and deltaic process regime. Accepted in *J. Sediment. Res.* (Accepted).

- Porebski, S.J., Steel, R.J., 2006. Deltas and sea-level change. *J. Sediment. Res.* 76, 390–403.
- Posamentier, H.W., Allen, G.P., 1999. SEPM Concepts in Sedimentology and Paleontology. *Siliciclastic Sequence Stratigraphy: Concepts and Applications*, vol. 7. Posamentier, H.W., Allen, G.P., 1993. Variability of the sequence stratigraphic model: effects of local basin factors. *Sediment. Geol.* 86, 91–109.
- Posamentier, H.W., Jervy, M.T., Vail, P.R., 1988. Eustatic controls on clastic deposition I - Conceptual framework. In: In: Wilgus, C.K., Hastings, B.S., Kendall, C.G.S.C., Posamentier, H.W., Ross, C.A., Van Wagoner, J.C. (Eds.), *Sea-Level Changes - an Integrated Approach*, vol. 42. SEPM Special Publication, pp. 109–124.
- Posamentier, H.W., Vail, P.R., 1988. Eustatic controls on clastic deposition II - sequence and systems tract models. In: In: Wilgus, C.K., Hastings, B.S., Kendall, C.G.S.C., Posamentier, H.W., Ross, C.A., Van Wagoner, J.C. (Eds.), *Sea-Level Changes - an Integrated Approach*, vol. 42. SEPM Special Publication, pp. 125–154.
- Price, G.D., Nunn, E.V., 2010. Valanginian isotope variation in glendonites and belemnites from Arctic Svalbard: transient glacial temperatures during the Cretaceous greenhouse. *Geology* 38, 251–254.
- Reeve, M.T., Jackson, C.A.L., Bell, R.E., Magee, C., Bastow, I.D., 2016. The stratigraphic record of prebreakup geodynamics: evidence from the Barrow Delta, offshore Northwest Australia. *Tectonics* 35, 1935–1968.
- Sames, B., Wagreich, M., Wendler, J.E., Haq, B.U., Conrad, C.P., Melinte-Dobrinescu, M.C., Hu, X., Wendler, I., Wolfgring, E., Yilmaz, I., Zorina, S.O., 2016. Review: short-term sea-level changes in a greenhouse world — a view from the Cretaceous. *Palaeogeogr. Palaeoclimatol. Palaeoecol.* 441, 393–411.
- Sanchez, C.M., Fulthorpe, C.S., Steel, R.J., 2012. Middle Miocene-Pliocene siliciclastic influx across a carbonate shelf and influence of deltaic sedimentation on shelf construction, Northern Carnarvon Basin, Northwest Shelf of Australia. *Basin Res.* 24, 664–682.
- Schlager, W., 1993. Accommodation and supply - a dual control on stratigraphic sequences. *Sediment. Geol.* 86, 111–136.
- Schnyder, J., Dejax, J., Keppens, E., Thuy, T., Tu, N., Spagna, P., Boulija, S., Galbrun, B., Riboulleau, A., Tshibangu, J.-P., Yans, J., 2009. An Early Cretaceous lacustrine record: organic matter and organic carbon isotopes at Bernissart (Mons Basin, Belgium). *Palaeogeogr. Palaeoclimatol. Palaeoecol.* 281, 79–91.
- Schumm, S.A., 1993. River response to baselevel change: implications for sequence stratigraphy. *J. Geol.* 101, 279–294.
- Schwarz, E., Veiga, G., Álvarez Trentini, G., Spalletti, L.A., 2016. Climatically versus eustatically controlled, sediment-supply-driven cycles: carbonate-siliciclastic, high-frequency sequences in the Valanginian of the Neuquén Basin (Argentina). *J. Sediment. Res.* 86, 312–335.
- Shanley, K.W., McCabe, P.J., 1994. Perspectives on the sequence stratigraphy of continental strata. *Am. Assoc. Petrol. Geol. Bull.* 78, 544–568.
- Slingerland, R., Smith, N.D., 2004. River avulsions and their deposits. *Annu. Rev. Earth Planet Sci.* 32, 257–285.
- Southard, J.B., Stanley, D.J., 1976. Shelf-break processes and sedimentation. In: Stanley, D.J., Swift, D.J.P. (Eds.), *Marine Sediment Transport and Environmental Management*. John Wiley & Sons, New York, pp. 351–377.
- Steel, R., Olsen, T., 2002. Clinofolds, clinofold trajectories and deepwater Sands. In: Armentrout, J.M., Rosen, N.C. (Eds.), *Sequence Stratigraphic Models for Exploration and Production: Evolving Methodology, Emerging Models and Application Histories*. Proceedings of 22nd Annual Gulf Coast Section SEPM Foundation Bob F. Perkins Research Conference, Houston, Texas, pp. 367–380.
- Stoll, H.M., Schrag, P., 1996. Evidence for glacial control of rapid sea level changes in the Early Cretaceous. *Science* 272, 1771–1774.
- Storms, J.E.A., Hampson, G.J., 2005. Mechanisms for forming discontinuity surfaces within shoreface-shelf parasequences: sea level, sediment supply, or wave energy? *J. Sediment. Res.* 75, 67–81.
- Swift, D.J.P., Phillips, S., Thorne, J.A., 1991. Sedimentation on continental margins, V: parasequences. In: In: Swift, D.J.P., Oertel, G.F., Tillman, R.W., Thorne, J.A. (Eds.), *Shelf Sand and Sandstone Bodies: Geometry, Facies and Sequence Stratigraphy*, vol. 14. Special Publications International Association of Sedimentologists, pp. 153–187.
- Swift, D.J.P., Thorne, J.A., 1991. Sedimentation on continental margins I: a general model for shelf sedimentation. In: In: Swift, D.J.P., Oertel, G.F., Tillman, R.W., Thorne, J.A. (Eds.), *Shelf Sand and Sandstone Bodies: Geometry, Facies and Sequence Stratigraphy*, vol. 14. Special Publications International Association of Sedimentologists, pp. 3–31.
- Tait, A.M., 1985. A depositional model for the dupuy member and the Barrow Group in the Barrow Sub-basin, northwestern Australia. *APEA J.* 25, 282–290.
- Tindale, K., Newell, N., Keall, J., Smith, N., 1998. Structural evolution and charge history of the Exmouth Sub-basin, northern Carnarvon Basin, western Australia. In: Purcell, P.G., Purcell, R.R. (Eds.), *The Sedimentary Basins of Western Australia 2. Proceedings of the Petroleum Exploration Society of Australia Symposium*, pp. 447–472.
- Vail, P.R., Audemard, F., Bowman, S.A., Eisner, P.N., Perez-Cruz, C., 1991. The stratigraphic signatures of tectonics, eustasy and sedimentology - an overview. In: Einsele, G., Ricken, W., Seilacher, A. (Eds.), *Cycles and Events in Stratigraphy*. Springer-Verlag New York, Inc., pp. 617–659.
- Vail, P.R., Mitchum, R.M., 1977. Seismic stratigraphy and global changes of sea-level, part 1: Overview. In: In: Payton, C.E. (Ed.), *Seismic Stratigraphy - Applications to Hydrocarbon Exploration*, vol. 26. AAPG Memoir, pp. 51–52.
- Vail, P.R., Todd, R.G., Sangree, J.B., 1977. Seismic stratigraphy and global changes of sea level, part 5: chronostratigraphic significance of seismic reflections. In: Payton, C.E. (Ed.), *Seismic Stratigraphy - Applications to Hydrocarbon Exploration*. AAPG Memoir 26, pp. 99–116.
- Van Wagoner, J.C., Mitchum, R.M., Campion, K.M., Rahmanian, V.D., 1990. *Siliciclastic Sequence Stratigraphy in Well Logs, Core, and Outcrops: Concepts for High-Resolution Correlation of Time and Facies*, vol. 7. American Association of Petroleum Geologists Methods in Exploration Series.
- Van Wagoner, J.C., Mitchum, R.M., Posamentier, H.W., Vail, P.R., 1987. Seismic stratigraphy interpretation using sequence stratigraphy: Part 2, key definitions of sequence stratigraphy. In: In: Bally, A.W. (Ed.), *Atlas of Seismic Stratigraphy*, vol. 27. AAPG Studies in Geology, pp. 11–14.
- Van Wagoner, J.C., Posamentier, H.W., Mitchum, R.M., Vail, P.R., Sarg, J.F., Loutit, T.S., Hardenbol, J., 1988. An overview of the fundamentals of sequence stratigraphy and key definitions. In: In: Wilgus, C.K., Hastings, B.S., Kendall, C.G.S.C., Posamentier, H.W., Ross, C.A., Van Wagoner, J.C. (Eds.), *Sea-Level Changes - an Integrated Approach*, vol. 42. SEPM Special Publication, pp. 39–45.
- Wear, C.M., Stanley, D.J., Boula, J.E., 1974. Shelf break physiography between Wilmington and Norfolk canyons. *Mar. Technol. Soc. J.* 8, 37–48.
- Wendler, J.E., Meyers, S.R., Wendler, I., Kuss, J., 2014. A million-year-scale astronomical control on Late Cretaceous sea-level. *Newslett. Stratigr.* 47, 1–19.
- Zecchin, M., Catuneanu, O., 2013. High-resolution sequence stratigraphy of clastic shelves I: units and bounding surfaces. *Mar. Pet. Geol.* 39, 1–25.